ASSESSING CONNECTIVTY IN SIMULATED, IN-VITRO, AND IN-VIVO NEURAL NETWORKS USING GRANGER CAUSALITY

By

ALEX JOSEPH CADOTTE

A DISSERTATION PRESENTED TO THE GRADUATE SCHOOL
OF THE UNIVERSITY OF FLORIDA IN PARTIAL FULFILLMENT
OF THE REQUIREMENTS FOR THE DEGREE OF
DOCTOR OF PHILOSOPHY

UNIVERSITY OF FLORIDA

2007

To my Aunt Claire & Uncle Bill Parker.

ACKNOWLEDGMENTS

I thank Tom DeMarse for his guidance and patience for the past five years. I thank the other graduate students I have worked with in Neural Hybrid Computation Laboratory including, Ping He, Vinh Trin, Karl Dockendorf, Nicky Grimes, Pamela Douglas, Hany Elmariah, Crystal Stephens, Memming Park, and Amber Scarlatos for the many interesting conversations and collaborations. I specifically thank Ping He for the data provided from the Jimbo replicate experiment. Also, I specifically thank Amber Scarlatos, for the extensive collaborations we had during the past 2 years.

I thank Mingzhou Ding for his valuable teachings, time, and conversations and also members of his laboratory including Yonghong Chen, Anil Bollimunta, Yan Zhang, and Raj Rajagovindan. I thank Paul Carney, William Ditto, and all those associated with the Evolution into Epilepsy project for the work behind the data that was provided me for analysis. I thank all of the staff and faculty within the Biomedical Engineering department. I thank Yanni Constantinidis for his influence on my teaching style and for his career advice. His presence in the Biomedical Engineering department has been missed, may he rest in peace.

I thank my family and friends for their support over the past four years of graduate school. I thank my parents and my brothers for believing in me. Thanks to Shane Calfee and Courtney Calfee for suggesting UF for grad school, GO Gators! I'd also like to thank the many friends I have made here at the University of Florida including Cameron Siggs, John Azeke, Neel Bhatavadekar, Andres Argibay, Ning Jiang Argibay, John Quinlan, Amber Pouncy, and Lance Gardner. Finally, I'd like to thank Theresa McGuirk for her patience, love, and support while I was hard at work producing this document.

TABLE OF CONTENTS

page

LIST OF TABLES

LIST OF FIGURES

Abstract of Dissertation Presented to the Graduate School
of the University of Florida in Partial Fulfillment of the
Requirements for the Degree of Doctor of Philosophy

ASSESSING CONNECTIVTY IN SIMULATED, IN-VITRO, AND IN-VIVO NEURAL NETWORKS USING GRANGER CAUSALITY

By

Alex Joseph Cadotte

December 2007

Chair: Thomas DeMarse
Major: Biomedical Engineering

Since the early 1980s, interest in synchronization between regions in the brain has led to the adaptation of forecasting measures such as Granger Causality from fields like economics to neuroscience. The basic principle behind Granger Causality is that a directional causal relationship can be inferred from a time series X to a time series Y when the introduction of previous measurements of X reduces the variance of the error time series in the linear modeling of Y. Granger Causality methods are used in the Neural Hybrid Computing Laboratory to investigate functional relationships between neural units in simulation, in-vitro, and in-vivo.

Computer simulations using biologically plausible neural-network models have shown that the direct component of pairwise Granger Causality (PGC) scales linearly with synaptic efficacy within biologically relevant ranges. This suggests that the PGC values obtained from living neural networks may be useful in calculating the underlying connectivity of living networks. Thus, PGC was used in-vitro to identify connectivity within neural pathways in a living neural network of 50,000 neurons grown on a microelectrode array (MEA). An MEA is an 8x8 grid of electrodes embedded in a cell culture dish. Data recorded from two plastcity experiments using these MEA cultures was analyzed using PGC. The resulting difference in PGC connectivity

before and after the induction stage of this experiment reveals that PGC was able to describe plasticity within neural pathways in-vitro.

PGC was also applied in-vivo to spontaneous epileptic seizures recorded from a 32-electrode array implanted in a rat's hippocampus. These rats were electrically stimulated causing limbic status epilepticus and later began to develop spontaneous seizures consistent with Lothman's animal model of chronic limbic epilepsy. Results from the analysis of spontaneous limbic seizures reveal the dynamics of the directional causal influences during seizure. Interestingly, they indicate a sudden change in direction of causal influence between the CA1 and dentate gyrus regions of the hippocampus near the end of status epilepticus.

CHAPTER 1
INTRODUCTION AND BACKGROUND OF CAUSAL METHODS IN NEUROSCIENCE

Introduction

Multivariate time series analysis is increasingly used during the last 20 years in neuroscience to determine the relationships between simultaneously recorded signals. Granger Causality, a predictive forecasting tool originating from the field of economics (1), is one of the latest examples of multivariate time series analysis that has been adapted for use with neural systems (2). According to Granger Causality, a causal relationship is said to exist when, by introducing previous measurements of the first time series into the linear regression of the second time series, the error of the linear regression of the second time series is reduced. In essence, this says that the second time series is better predicted with information about the first time series because the second time series contains time delayed elements of the first time series when a causal relationship exists. This is the basic principle behind the calculation of Granger Causality. Expanding on this basic principle, the relationship between higher order multivariate systems can also be explored. However, reducing the multivariate system to pairwise relationships to determine causal relationships is often insufficient to sort out causal relations when those relations are mediated through another element rather than direct. While it is necessary to use Granger Causality to determine the interdependency and directionality of relationships (e.g., neural connections), Conditional Granger Causality is required to resolve whether relationships (e.g., neural pathways) are direct or mediated. Conditional Granger Causality does this by comparing error terms from bivariate and trivariate linear regressions. If the addition of a third time series to the linear regression that is already known to influence a first time series does not add to the prediction of a first, it can be inferred that its influence is already accounted for by mediation through the second time series.

This body of work focuses on the use of Granger Causality based methods as a tool to determine the effective connectivity in neural systems where the anatomical connectivity may be unknown or unclear. Included is a review of current causal methods, an explanation of the mathematical basis for Granger Causality, and four experiments where outputs from neural networks, both simulated and living, are analyzed using Granger Causality to determine effective connectivity. These include modeled, in-vitro, and in-vivo paradigms. First, a simple neural network model (3) will be used to determine the relationship between Granger Causality and synaptic weights used to drive the model. A modeled system is ideal because the synaptic weights are known and can be compared with those weights recovered using Granger Causality. Understanding this relationship is a prerequisite to experiments in living systems because it will define what kind of relationship between Granger Causality and the underlying anatomical synaptic efficacy underlying the living neural network.

Next, data from cortical cultures grown on microelectrode arrays will be the focus of two in-vitro experiments in Chapters 4 and 5. The first experiment based on the results from the modeling section determines the ability of using Granger methods to recover the effective connectivity of a dissociated neural network. Granger Causality was used to measure changes in effective connectivity observed after treatment with a protocol designed to induce plasticity (4). Granger's results are compared to estimates based on changes in firing rate. The second in-vitro experiment investigated Granger Causality's ability to provide information of effective connectivity prior to experimental manipulations. Using this effective connectivity sinks, where the balance of effective connectivity is directed inward, and sources, where the balance of effective connectivity is directed outward will be identified. Sinks and sources will be differentially subject to the same high frequency plasticity induction stimulation protocol, or tetanization, with the prediction that tetanization of sinks would yield depression while

tetanization of sources would yield potentiation. This prediction is based on the differential orientation of the connectivity of these pathways with the rest of the culture.

Finally, Chapter 6 examines the ability of Granger Causality to measure progressive changes in effective connectivity during epileptic seizures measured in a chronic limbic epileptic rat model. This data analysis will be conducted on in vivo 32-channel microelectrode arrays data in rat hippocampus originally recorded by the Evolution into Epilepsy project team to study the mechanisms of epileptigenesis. The goal of this work is to determine if Granger Causality methods can successfully be used to describe the changes in effective connectivity before and during seizures to learn more about in effective connectivity during seizure.

Review of Causal Methods in Neuroscience

Many experimental platforms are used in the neuroscience community to answer scientific and practical questions about the behavior and function of the nervous system. As these platforms have evolved over the last half a century, so to has the quality, content, and availability of data sets from these systems. These platforms have been adapted to better answer questions of causality and binding between various elements requiring multichannel data to be acquired. Subsequently, the methods used to analyze multichannel data have evolved alongside or even been borrowed from other disciplines, providing meaningful analysis of this data. Some examples of these methods are cross correlation, coherence, mutual information, partial directed coherence, the directed transfer function, and Granger causality. These methods fall into two broad categories, those that are non-parametric (calculated directly from data) and those that are parametric (the data is fit to a model and parameters from the model are used to calculate a result). The following sections will provide a brief background and examples using each of these methods.

Non-Parametric Methods

Cross Correlation

Cross correlation is one of the most basic and longest used algorithms that has been used to determine the interdependence between two time series. The cross correlation function measures the linear dependence between time series as a function of their time delay, τ. A significant value of the cross correlation function at a time delay τ may indicate a causal relationship. Consider two time series $x(t)$ and $y(t)$ that have been normalized to have a zero mean and unit variance. The cross correlation function of these two time series is shown in equation (1.1), where N is the length of the time series and τ is the time delay.

$$C_{xy}(\tau) = \frac{1}{N-\tau}\sum_{k=1}^{N-\tau} x(k+\tau)y(k) \qquad (1.1)$$

The output of the cross correlation function ranges from -1 to 1 for each value of τ, where -1 is complete inverse linear correlation and 1 is complete linear direct correlation. Values of τ where the cross correlation function is equal to zeros represent circumstances where there is no linear correlation. In practice, a statistical threshold is calculated around zero perhaps using a surrogate data set to determine when significant correlations exist.

The cross correlation function has been used in neuroscience for over 50 years, since it was used to measure correlation between EEG signals (5). Use of correlation based methods is widespread in neuroscience and a full elaboration of it use is beyond the scope of this research (see (6-9) for an excellent review). This measure has more recently been used to describe correlations among neurons (10-17) and specifically in studies of plasticity (4, 18-20). For example, Jimbo (4) found that neural activity that was highly correlated with a tetanic stimulation pulse train tended to be potentiated (an increase in effective connectivity). In contrast, neural activity that was weakly correlated with tetanic stimulation typically resulted in

depression (a decrease in effective connectivity). Jimbo suggests that the strength of correlation between these channels during tetanization may be representative of the total number of synapses in the pathway between the electrodes. Tateno and Jimbo (21) use a normalized cross correlation analysis for all neuron pairs during a similar plasticity experiment. The difference in cross correlation (post-tetanization correlation – pre-tetanus correlation) between all neuron pairs after tetanic stimulation highlighted changes in the correlation that was indicative of plasticity within a living neural network. Segev et al (14) has used cross correlation to describe connectivity patterns in multichannel data from similar living neural networks during synchronized spiking events known as bursts. Segev demonstrated that bursting activity contains statistically separable subgroups that he suggests may be a template for storage and retrieval of information.

Overall, cross correlation has been one of the primary methods used in neuroscience to demonstrate relationships especially in multichannel data. It has the advantage of being a widely understood, straightforward, and simple method. However, it does have some limitations. The results from cross correlation can often be subject to interpretation and be ambiguous (7). Additionally, for results to be statistically significant often a large amount of data is necessary. Directional information can be ascertained using cross correlation but this can become problematic and ambiguous over large data sets because manual interpretation is often required. Additionally, cross correlation, as presented here, is strictly a time domain measure. To examine correlations in the spectral domain known as coherence additional manipulations are required.

Coherence

Coherence is the linear correlation between two time series as a function of frequency. Also known as squared coherence or the coherence spectrum, this measure is simply the normalized Fourier transform of equation (1.1). Skipping several steps of this derivation, the resulting equation for squared coherence is shown in equation (1.2).

$$C(f) = \frac{\left|S_{xy}(f)\right|^2}{\left|S_{xx}(f)\right|\left|S_{yy}(f)\right|} \quad (1.2)$$

The spectral matrix *S,* used to calculate coherence, is non-parametric calculating using Welch's method to create a periodogram. An estimate of the average spectra can be estimated over several trials of event related data by averaging the resultant periodograms. However, this method only provides an estimate of coherence and significance would need to be established by calculating confidence intervals. The resulting coherence values for each frequency vary from 0 to 1, where 0 would indicate no correlation at that frequency and 1 would indicate maximum linear correlation at that frequency.

Like correlation, coherence is also widely used in neuroscience. Recent reviews detail the use of coherence in neuroscience (9) and in human epilepsy (22) over the past 40 years. While coherence shares many of the weaknesses of correlation, a critical weakness of this method is the lack of directionality. This specific weakness spurred the development (23) of a method called directed coherence also known as Gersch causality (24) that was initially used identify epileptic foci using three electrodes. Gersch stated "one channel is said to drive the other channels if the first channel explains or accounts for the linear relation between the two." This method has also found various neural applications (25) including EEG (26) (27, 28), fMRI (29) and spike trains (27, 30). Unfortunately this method has been shown to be sensitive to noise contamination (25), which can potentially lead to misidentification of directional influences. While coherence is often calculated directly from data (non parametrically) it can also be calculated using parameters from autoregressive models fit to the data (31). These parametric approaches will be elaborated later in this review. Mutual information, a non-parametric method that uses probabilistic estimates, is discussed next.

Mutual Information

This measure falls under the auspices of information theory and probability. The primary measure used in information theory is entropy. Entropy is defined for a variable X as the sum over all possible outcomes M of p_i (probability that an outcome occurs) multiplied by the base 2 logarithm of p_i as shown in equation (1.3) as Shannon entropy. Consequently, the Shannon entropy will be high for a uniform system where all states have an equal probability and lower for a system with a Poisson distribution where certain states have much higher probability.

$$I_x = -\sum_{i=1}^{M} p_i \log_2 p_i \tag{1.3}$$

It is this concept that is applied to the calculation of Mutual Information (MI) between two variables. MI is defined as:

$$MI_{xy} = \sum p_{ij} \log \frac{p_{ij}}{p_i p_j} \tag{1.4}$$

where p_{ij} is the joint probability that the outcomes for x and y occur. Essentially, this measure describes how much extra information is known about one signal by knowing the outcomes of the other one. MI will equal zero if the two variables are independent because p_{ij} would be equal to p_i p_j.

Mutual Information has been used to estimate the relationship between dynamic stimuli and the response in corresponding sensory areas in-vivo for various animals (32), including the response motion sensitive neurons in the visual cortex of primates to visual stimuli (33). It has also been used to estimate synaptic efficacy in vitro between pyramidal neurons in-vitro (34). Joint probability density can also be estimated between spike trains using Mutual Information (17, 35). Like cross correlation, Mutual Information also requires large amounts of data (9) in order to

produce a reliable representation of the probability distribution. Thus, the use of Mutual Information on experimental time-scales can sometimes be problematic.

Parametric Approaches

Likelihood Methods

Maximum Likelihood is a parametric approach that creates statistical models of a system for analysis. A parametric probability model is assumed for a process under study. Methods associated with Likelihood methods are very case dependent of the system being analyzed and the statistical model chosen (17) and cannot be elaborated on completely within this review. The likelihood is represented as joint probability density of the experimental data as a function of the unknown or free parameters in the model. Thus, the models parameters are estimated from the experimental data. If the experimental data fits the chosen model well, this is thought to be an optimal way of representing the experimental process (17). This method has been used to analyze the interactions of simultaneously recorded spike trains in the cat's auditory system (36, 37) and place cells within the hippocampus of rats (38). While this methods shows promise, extreme care must be taken in choosing an appropriate model to estimate the probability distribution. Similar to Mutual Information, this process often requires large amounts of data that can make analysis of experimental systems problematic.

Methods using Autoregressive Modeling

Several parametric methods make use of autoregressive modeling (AR) in order to assess a system's causality. These methods, including Partial Directed Coherence (PDC), the Directed Transfer Function (DTF), and Granger Causality (GC) each use different parameters from an AR model fit to the system in question. Additionally, it should be noted that the parameters of an AR model have been used on their own to assess changes in neural systems over time (39, 40). For example, Sanchez et. al. specifically highlights the changes in AR coefficients calculated

from a spiking time series over the development of spontaneous limbic seizures in-vivo. A general form for the AR model is shown in equation (1.5), where $\boldsymbol{X}$ is a vector consisting of p time series, $\boldsymbol{A}$ is a p x p coefficient matrix and $\boldsymbol{E}$ is the uncorrelated noise vector with a covariance matrix of Σ.

$$\boldsymbol{X}(t) + \sum_{m=1}^{p} \boldsymbol{A}(m)\boldsymbol{X}(t-m) = \boldsymbol{E}(t) \tag{1.5}$$

AR modeling makes use of the autocorrelation function to model the current value of a variable from past instances of that same variable (p=1). A multivariate AR (MVAR) model (p>1) uses this same framework to model the current value of a variable using not only past instances of that same variable, but past instances of the other variables in that multivariate system. It is easy to see why autoregressive modeling has become such a popular tool in neuroscience where multichannel recordings are common. A more comprehensive mathematical review of AR modeling will be expanded upon in Chapter 2.

Several more advanced methods collect information from the AR model and perform operations on them to determine a measure for causality or direction. Often these methods employ two or more AR models, which are calculated including and excluding a variable of interest. This methodology calculates a particular variable's effect on AR model coefficients and linear regression error that is used to calculate a measure of causality.

Partial Directed Coherence, the Directed Transfer Function, and Granger Causality

Three methods have emerged that use AR models to determine directional connectivity. Partial Directed Coherence (PDC), the Directed Transfer Function (DTF), and Granger Causality all use aspects of an AR model including and excluding a time series hypothesized to have a driving relationship with a second time series. This basic principle is common to all three methods. While these methods are often considered to be the same or similar, there are subtle

differences between these methods. For example, PDC and DTF are exclusively frequency domain measures that rely on the Fourier transform of the AR model resulting in new frequency domain coefficients. In contrast, Granger Causality has formulations in the time domain and the frequency domain. While PDC and DTF are closely related, both being derived from this new coefficient matrix, DTF differs from PDC in that the coefficient matrix is inversed, $H_{ij}(f) = A_{ij}^{-1}(f)$, and the DTF is squared when compared to the PDC. The equations for PDC and the DTF are shown below in equations (1.6) and (1.7) respectively. Notice the similar formulation for both equations.

$$\pi_{j\to i}(f) = \frac{\left|A_{ij}(f)\right|}{\sqrt{\Sigma_k \left|A_{kj}(f)\right|^2}} \tag{1.6}$$

$$\delta_{j\to i}(f) = \frac{\left|H_{ij}(f)\right|^2}{\Sigma_t \left|H_{il}(f)\right|^2} \tag{1.7}$$

Another major difference between Granger Causality and the other two methods is that Granger Causality is a statistically relevant quantity. For example, the time domain version of Granger Causality, shown in equation (1.8) is the ratio of the variance from two error time series. The DTF and PDC are ratios of spectral coefficients from the AR model, which don't have any meaningful statistical interpretation. Granger Causality is simply a more statistically rigorous measure. This does not mean that the DTF and PDC are not useful tools. In fact, these methods have produced interesting results in the analysis of neural time series including EEG (41-43), neural simulation (43, 44) and living neural networks (45-47). Fanselow et al. (46) uses PDC to reveal causal influences from the sensory cortex to the thalamus during rhythmic activity associated with whisker twitching behavior in rats. This suggests that sensory cortex driven thalamic bursting, associated with whisker twitching behavior during exploratory behavior, may

prime the thalamo-cortical loop for sensory signal detection. Schelter et al (43) calculated PDC between EEG and EMG signals and determined that the motor cortex likely participates in the generation of essential tremor. Ginter et al uses the DTF to determine if the signature of imagined movements of the index finger can be detected reliably in the cortex using EEG. This information is relevant in the creation of a brain machine interface (BMI). This research area seeks to help amputees and those suffering from various forms of paralysis (due to spinal cord injury for example) control prosthetic devices by imagining movement of the affected limb. These are just a few examples of the use PFC and the DTF. These methods were often developed to improve spectral information content but are only empirical measures that don't have a firm statistical foundation. Thus, they often are used in parallel with the Granger Causality metric.

$$F_{Y\to X} = \ln \frac{\mathrm{var}(\varepsilon_X(t))}{\mathrm{var}(\eta_X(t))} \tag{1.8}$$

Granger Causality has found similar applications within neuroscience. The original concept of Granger causality has played a significant role in the field of economics since the 1960s. Within the last 15 years, it is now increasingly used in neuroscience to understand the dynamics of brain circuitry. In addition to the time domain version of Granger Causality, shown in equation (1.8), Granger Causality also has formulations in the frequency domain and can be used to separate mediated and direct influences (31). The math behind these concepts will be explored further in Chapter 2.

There are a wide variety of systems that Granger Causality and associated methods have been applied to with success. For example, Zhu et al (48, 49) explores causal interactions between neurons during learning in the primary motor cortex of rhesus monkeys. Specifically, Zhu monitored the interactions between 8 electrode channels in the primary motor cortex. The

monkeys used in this experiment were trained in a reaching task prior to surgery implanting the electrode array into motor cortex. A string was then attached to the arm of the monkey that interfered with the completion of previously learned motor task. The monkey adapts or essentially learns to complete the same task with this perturbing string attached. Recordings from the 8 electrodes during this re-learning phase were associated with changes in the strength and direction of causal interactions over time. Coupling strength between the electrodes increased during the learning phase, but was attenuated to pre-learning levels once adaptation had been achieved. In this experiment the network appears to be essentially rewired before and after learning and may reflect plasticity associated with the re-learning process.

Functional Magnetic Resonance Imaging (fMRI) allows for three-dimensional brain activity mappings to be collected during a behavioral task over time. The dynamics observed during fMRI recordings can be used to determine functional connectivity between brain areas using Granger Causality (50, 51). An fMRI time series can be considered a filtered and sampled version of a local field potential (LFP) generated from the observed neuronal population. The fMRI time series for each area is functionally a measure of the blood oxygen levels in that area. This can be used as an indicator for brain activity based on consumption of blood oxygen. Casual analysis of a simulated fMRI time series between two brain areas shows a nearly identical relationship to that of the original LFPs generated in the simulation (50). A cognitive task where various stimuli were delivered requiring a “left” or “right” response was observed using fMRI (50) and analyzed using Granger Causality. Frontal areas were found to drive the parietal areas during these tasks. These results were interpreted as neural correlates of executive control and working memory. A similar study (51) showed that pre-motor areas could be used to predict activity in the motor cortex.

A variety of neural systems are addressed in Kaminski et al (52), including simulated local field potentials, simulated spike trains, human sleep analysis, and visuomotor integration in macaque monkeys using LFPs (local field potentials). Analysis of human EEG patterns during sleep reveals a causal influence from anterior P3 and P4 and the posterior region P3 electrode (the international 10-20 system was used for electrode placement). These patterns were found to be consistent with anatomical projections from the pre-frontal cortex. Additionally, these effects were observed to fade during the transition from sleep to wakefulness. In-vivo LFP data was analyzed from macaques that were trained to perform a visuomotor pattern discrimination task. The data was collected from 15 bipolar twist electrodes over 888 trials of a go no-go task. Using these trials to reduce the length of the data sample necessary, a 50 ms moving window of Granger Causality values was used to reveal causal interaction through the 500 ms trials. This analysis reveals that two cortical areas, a striate and prestriate area, shown to be coherent during the task, show a directional transfer from the striate to a prestriate which is followed by feedback in the opposite direction 50 ms later. Note that these directional interactions were unattainable using coherence. A more detailed analysis of this experimental paradigm can be found in Brovelli et al (53) and Chen et al (54). In Chen et al (54) a Spectral (15-30Hz) Conditional Granger Causality analysis was used to show that some cortical areas were mediating effects from other areas while other relationships were direct. Note that a conditional analysis is necessary to ascertain when mediation occurs in certain circumstances. Kaminski et al also introduces a method to address the statistical significance of results using surrogate data analysis, a method that will be used in all studies in this research. Additionally, Kaminski's methods for preprocessing point process data (A first order Butterworth set at 10% of the sampling frequency) for causal analysis between simulated spike-trains are used in this research.

Seth and Edelman (55, 56) employed granger causality to distinguish patterns of connectivity and causality within complex neural network simulations. Seth (56) defines a set of tools to analyze the output of causal analysis of a multivariate system. While calculation of pairwise granger causality in a large neural system can be straight forward, making sense of the large amount of data resulting from these data sets can be challenging. This paper defines several concepts that can help reduce the complexity of results. These include causal density, causal flow, causal reciprocity, causal disequilibrium, casual sources, and causal sinks. Causal density is defined as "the fraction of interactions among nodes that are causally significant". Causal flow is a measure of the difference between casual inflow and causal outflow from a node. Causal reciprocity is a measure of feedback between nodes. Causal disequilibrium refers to an imbalance in reciprocity and flow between nodes. Causal sinks refer to nodes where the balance of information flows into the node, while causal sources refer to nodes where the balance of information flows out of the node. These basic definitions help lead to tools that can be used to understand the effects of causal flow within a network. Seth demonstrates the use of the tools in a 32-neuron neural network model of target fixation using a head/eye system. Results from this model and analysis using these tools allow new hypothesis including being able to predict the effects of "lesions" within simulated networks. Seth's further work with Edelman (55) includes the idea of a causal core within large neural populations during behavior. A causal core is defined as neural interactions within the network present when a reference neuron, such as an output motor neuron, fires. This idea allows the linkage of neural interactions with specific outputs from the network. Seth and Edelman use the Darwin X system, an autonomous robot with a simulated neural network brain based on cortical and hippocampal anatomy. The robot performed a dry version of the water maze test for rates where the robot's goal was to find a hidden platform in a static environment with spatial clues. Over time the robot learned to find

the platform more quickly similarly to rats that have performed the water maze. The behavioral output from the Darwin X system was analyzed using the causal core idea and Granger Causality. Consistent causal cores could be identified for specific outputs of reference neurons. Changes in the causal core during learning sequences were also observed. The causal core was observed to reduce in size and become more refined as Darwin X learned to move more directly to the hidden platform.

These examples show that Granger Causality has proven to be a useful tool for uncovering effective and functional relationships in various neural systems. These tools and associated methods will be used in several experiments in simulated, in-vitro, and in-vivo neural networks. We will begin with a more comprehensive review of the autoregressive modeling and the properties of Granger Causal tools presented in the next chapter.

CHAPTER 2
MATHMATICAL BASIS FOR GRANGER CAUSALITY

Mathematical Basis for Time Domain Measures

Granger Causality

The goal of Granger Causality (GC) is to provide a strong mathematical basis to determine causal influence and direction of neural interaction. The basic idea can be traced back to Wiener (57). He proposed that, for two simultaneously measured time series, one series can be called causal to the other if we can better predict the second series by incorporating past knowledge of the first one. This concept was later adopted and formalized by Granger in 1969 (1) for linear regression models of stochastic processes. Specifically, if the variance of the prediction error for the second time series at the present time is reduced by including past measurements from the first time series in a linear regression model, then the first time series can be said to have a causal (directional or driving) influence on the second time series. The advantage over cross correlation metrics is that GC is more robust with respect to changes in overall rate of activity, provides a measure of the "causal" influence, is directional, and often requires less data for analysis. A description of this technique is provided in the following sections describing autoregressive modeling as well as time-domain, spectral, and conditional methods. A more detailed review by Ding et al in a recently published handbook on causal methods can be found here (2). The purpose of this chapter is to describe what Granger Causality does and does not do. This is accomplished by describing how GC produces a measure of effective connectivity and discussion of several of its inherent weaknesses.

Autoregressive Modeling

Autoregressive (AR) modeling of neural time series is the foundation of parametric Granger Causality methods. Time series in multivariate neural data are typically recorded from

multiple electrodes or channels. While AR models are often presented in a theoretical context, the examples reported here will be provided in the context of a multichannel recording from a neural process. Consider the multivariate random process, $\mathbf{X}(t)$, consisting of *p* independent channels of neural data.

$$\mathbf{X}(t) = \begin{bmatrix} X_1(t) \\ X_2(t) \\ \dots \\ X_p(t) \end{bmatrix} \tag{2.1}$$

A recording of time series from these channels would be considered a single realization of this neural process. Multiple realizations of the neural process are advantageous to creating a more accurate model describing this process. $\mathbf{X}(t)$ is described using an AR model of model order *m* assuming that $\mathbf{X}(t)$ is a stationary process.

$$\mathbf{X}(t) + \boldsymbol{A}(1)\mathbf{X}(t-1) + \dots + \boldsymbol{A}(m)\mathbf{X}(t-m) = \boldsymbol{E}(t) \tag{2.2}$$

$\boldsymbol{A}(i)$ are *p* by *p* coefficient matrices where $i = 1, 2, \dots, m$ and $\boldsymbol{E}(t)$ is a zero mean uncorrelated noise vector with a covariance matrix of Σ. $\boldsymbol{A}(i)$ and Σ are unknown matrices that can be estimated from the realizations of $\mathbf{X}(t)$. This is done by right multiplying Equation (2.2) by $\mathbf{X}^{\mathrm{T}}(t-k)$, where T indicates a transposed matrix. The expectation is then taken on the resulting equation yielding the Yule-Walker equations for $k = 1, 2, \dots, m$ containing a total of mp^2 model coefficients to be solved for.

$$\boldsymbol{R}(-k) + \boldsymbol{A}(1)\boldsymbol{R}(-k+1) + \dots + \boldsymbol{A}(m)\boldsymbol{R}(-k+m) = 0 \tag{2.3}$$

$R(n) =< X(t)X^T(t+n) >$ is the auto covariance function of $\mathbf{X}(t)$. Note that lag *n* is $n = |-k+1|$, ranging from 0 to *m-1*. The auto-covariance function is then calculated from each realization, $\boldsymbol{x}(t)$,of $\mathbf{X}(t)$ of length N.

$$R(n) = \frac{1}{N-n}\sum_{i=1}^{N-n} x(i)x^T(i+n) \tag{2.4}$$

If multiple realizations of the data are available the auto covariance functions are averaged across realizations. Once the auto covariance function has been calculated the mp^2 model coefficients of the $\boldsymbol{A}(i)$ coefficient matrix can be solved for because there are mp^2 equations within equation (2.3). There are several methods that can be used to solve this including simply solving for each of these coefficients or using methods such as the Levinson, Wiggins, and Robertson method or Morf's method, used for this analysis. Once $\boldsymbol{A}(i)$ is known, the noise covariance matrix Σ is obtained using the following relationship.

$$\Sigma = \boldsymbol{R}(0) + \sum_{i=1}^{m} \boldsymbol{A}(i)\boldsymbol{R}(i) \tag{2.5}$$

This preceding section describes the estimation of a MVAR for any model order *m*. However, it is necessary determine the correct model order for use with each system being studied. The correct model order can be determined using several methods including the Akaike Information Criterion (AIC) and the Bayesian Information Criterion (BIC). The BIC is more often used for neural applications as it compensates for the large N (number of data points) common to neural data sets. Thus, the BIC will be the primary method used to determine model order in these studies.

$$AIC(m) = -2\log[\det(\Sigma)] + \frac{2mp^2}{N} \tag{2.6}$$

$$BIC(m) = -2\log[\det(\Sigma)] + \frac{2mp^2 \log N}{N} \tag{2.7}$$

The BIC is plotted as a function of the model order *m*. The correct model order usually corresponds to a minimization of BIC. However, when the model order becomes too large this may result in excessive computation time. Often, a smaller model order with a similarly minimized value of BIC is used rather than the absolute minimum BIC for this reason.

The resulting time domain MVAR model is the basis for the calculation of both time and spectral domain granger causality, which will be discussed in the following section.

Time Domain Granger Causality

With the core AR modeling tools now fully described, Parametric Granger Causality can be calculated from the resulting models. GC methods make use of the variance of prediction errors from various combinations of AR models. Pairwise Granger Causality (PGC) is used to investigate the directional interactions between two time series. Two AR models are required to determine for each direction of influence. Consider two time series X(t) and Y(t) where separate AR models are created to predict current value of the X series from *m* (a previously determined model order) previous X values and:

$$\begin{aligned} X(t) &= \sum_{j=1}^{m} b_{XX}(j)X(t-j) + \varepsilon(t), \quad \Sigma_1 = \mathrm{var}(\varepsilon(t)) \\ Y(t) &= \sum_{j=1}^{m} b_{YY}(j)Y(t-j) + \gamma(t), \quad \Gamma_1 = \mathrm{var}(\gamma(t)) \end{aligned} \tag{2.8}$$

The variance of the error series $\varepsilon(t)$, Σ_1, is a gauge of the linear prediction accuracy of X(t) as Γ_1 is for Y(t). Now consider a bi-variate multivariate autoregressive (MVAR) model, $\boldsymbol{W}(t)$, where both X(t) and Y(t) are calculated from the previous values of the X and a Y time series:

$$\mathbf{W}(t) = \begin{pmatrix} X(t) = \sum_{j=1}^{m} a_{XX}(j)X(t-j) + \sum_{j=1}^{m} a_{XY}(j)Y(t-j) + \eta(t) \\ Y(t) = \sum_{j=1}^{m} a_{YX}(j)X(t-j) + \sum_{j=1}^{m} a_{YY}(j)Y(t-j) + \gamma(t) \end{pmatrix} \tag{2.9}$$

The variance of the new error series is a gauge of the prediction accuracy of the new expanded predictor.

$$\Sigma_W = \begin{pmatrix} \Sigma_2 & \Upsilon_2 \\ \Upsilon_2 & \Gamma_2 \end{pmatrix} = \begin{pmatrix} \text{var}(\eta(t)) & \text{cov}(\eta(t),\gamma(t)) \\ \text{cov}(\eta(t),\gamma(t)) & \text{var}(\gamma(t)) \end{pmatrix} \tag{2.10}$$

Based on Wiener's idea, Granger (1) formulated that if the X prediction is improved by incorporating past knowledge of the Y series, the Y time series can then be said to have a Granger-causal influence on the X time series. This is the basis for the time domain version of Granger Causality where the variance of the linear prediction error of X alone, Σ_1, is compared to the variance of linear prediction error of X including Y, Σ_2:

$$F_{Y \to X} = \ln \frac{\Sigma_1}{\Sigma_2} \tag{2.11}$$

Note that when $\Sigma_1 = \Sigma_2$ (i.e. the linear prediction error is not improved by including Y) that this relationship will yield a PGC value of zero. Driving in the opposite direction is addressed by simply reversing the roles of the two time series. It is clear from this definition that timing plays an essential role in directional causal influences.

Spectral and Conditional Granger Causality

Two additional developments of Granger's causality are important for the proposed research. First, natural time series, including ones from neurobiology, contain oscillatory aspects in specific frequency bands. A spectral representation of Granger Causality was developed by Geweke (58), allowing casual interactions to be quantified at specific frequencies. Second,

pairwise Granger Causality can often yield false direct influences due to parallel driving by or mediation through elements not included in the AR model. When data from at least 3 or more time series is available, such as from neurobiological multi-electrode arrays, conditional Granger causality (54, 59) can be used to address these limitations. These methods are described in the following section.

Spectral Granger Causality

Geweke (58) published his groundbreaking paper in 1982 where he identified a novel way to decompose the time domain causality measure into its spectral content. His method compares the intrinsic power (defined as the power of a time series generated by the stochastic processes intrinsic to that time series) of one time series and the total power of the same time series, which may contain a causal influence from a second time series, in the frequency domain. When there is no causality between the two time series (i.e. the total power is equal to the intrinsic power) the log ratio of the total to intrinsic power is equal to zero. The frequency domain function $\boldsymbol{W}(f)$ is obtained by taking the Fourier transform of the previously described MVAR $\boldsymbol{W}(t)$:

$$\mathbf{A}(f)\boldsymbol{W}(f) = \mathbf{E}(f) \tag{2.12}$$

$\boldsymbol{A}(f)$ is the spectral coefficient matrix and $\boldsymbol{E}(f)$ is the spectral noise vector resulting from the Fourier Transform performed on $\boldsymbol{W}(t)$. Rearrangement of (2.12) by setting the matrix inversion $\boldsymbol{A}(f)^{-1}$ equal to $\boldsymbol{H}(f)$ (commonly known as the transfer function) yields:

$$\mathbf{W}(f) = \mathbf{H}(f)\mathbf{E}(f) \tag{2.13}$$

The spectral matrix $\boldsymbol{S}(f)$ can now be calculated that contains the auto spectra and cross spectra of $\boldsymbol{W}(t)$.

$$\mathbf{S}(f) = \mathbf{H}(f)\mathbf{\Sigma}_3\mathbf{H}^*(f) \tag{2.14}$$

$\boldsymbol{H}^*(f)$ is the transpose and conjugate of $\boldsymbol{H}(f)$. Σ_3 is the covariance matrix of the noise terms from $\boldsymbol{W}(t)$.

This spectral matrix, containing the total power of the X time series, is retained. Spectral Granger Causality is based on decomposing the total power (variance) at a given frequency *f* for one time series into the sum of an intrinsic part and a causal part from the other series. A new spectral matrix is calculated in the same way except that both sides of equation (2.14) are left multiplied by Geweke's normalization transform:

$$P = \begin{pmatrix} 1 & 0 \\ -\dfrac{\Upsilon_2}{\Sigma_2} & 1 \end{pmatrix} = \begin{pmatrix} 1 & 0 \\ -\dfrac{\mathrm{cov}(\eta(t),\gamma(t))}{\mathrm{var}(\eta(t))} & 1 \end{pmatrix} \tag{2.15}$$

Geweke's normalization transform isolates the intrinsic power of X by allowing the intrinsic power component of the total power to be calculated separately from the causal power component of X(59). The X component of the new transfer function, shown in equation (2.16) is then used to calculate the intrinsic power of the x time series.

$$\tilde{H}_{xx}(f) = H_{xx}(f) + \frac{\Upsilon_2}{\Sigma_2} H_{xy}(f) \tag{2.16}$$

Taking the logarithm of the ratio of the total power over the intrinsic power gives the Granger causality spectrum.

$$F_{y\to x}(f) = \ln\left(\frac{S_{xx}(f)}{\tilde{H}_{xx}(f)\Sigma_2\tilde{H}^*_{xx}(f)}\right) \tag{2.17}$$

From the value of the causality spectrum, one can evaluate how much of one signal's variance at f is explained by the second signal exerting causal influence. Geweke showed that the integration of this spectral quantity over frequency is the time domain Granger causality.

Conditional Granger Causality

Highly multivariate data can be analyzed by PGC, reducing the problem to a bivariate case. This approach is straightforward and often effective for simple systems. However, this methodology can yield distorted results in more complex systems. Consider the following two situations. In one case, causal influence from Z to X is mediated through Y. For the second case, Z influences X through Y, but Z also has a direct influence on X. These two cases are indistinguishable using a bi-variate GC analysis; in fact the analysis will identify both cases as the second case. Conditional GC (CGC) is an algorithm that can be used in both in the time domain and in the frequency domain for three time series (31, 60) to overcome this shortcoming. We will only describe the time domain version of CGC, as the core idea of spectral CGC is very similar to the previously described Spectral Granger Causality.

$$\boldsymbol{U}(t)=\begin{pmatrix} X(t)=\sum_{j=1}^{p}A_{xx}(j)X(t-j)+\sum_{j=1}^{p}A_{xy}(j)Y(t-j)+\sum_{j=1}^{p}A_{xz}(j)Z(t-j)+\lambda(t) \\ Y(t)=\sum_{j=1}^{p}A_{yx}(j)X(t-j)+\sum_{j=1}^{p}A_{yy}(j)Y(t-j)+\sum_{j=1}^{p}A_{yz}(j)Z(t-j)+\mu(t) \\ Z(t)=\sum_{j=1}^{p}A_{zx}(j)X(t-j)+\sum_{j=1}^{p}A_{zy}(j)Y(t-j)+\sum_{j=1}^{p}A_{zz}(j)Z(t-j)+\nu(t) \end{pmatrix} \quad (2.18)$$

Time domain CGC compares the prediction of X including Y in a bi-variate MVAR model (from the previously described $\boldsymbol{W}(t)$), with the prediction of X including Y and Z in the tri-variate MVAR model $\boldsymbol{U}(t)$ shown in figure 2-1..

$$\boldsymbol{\Sigma}_U=\begin{pmatrix} \Sigma_{xx} & \Upsilon_{xy} & \Upsilon_{xz} \\ \Upsilon_{xy} & \Gamma_{yy} & \Upsilon_{yz} \\ \Upsilon_{xz} & \Upsilon_{yz} & \Delta_{zz} \end{pmatrix}=\begin{pmatrix} \mathrm{var}(\lambda(t)) & \mathrm{cov}(\lambda(t),\mu(t)) & \mathrm{cov}(\lambda(t),\nu(t)) \\ \mathrm{cov}(\lambda(t),\mu(t)) & \mathrm{var}(\mu(t)) & \mathrm{cov}(\mu(t),\nu(t)) \\ \mathrm{cov}(\lambda(t),\nu(t)) & \mathrm{cov}(\mu(t),\nu(t)) & \mathrm{var}(\nu(t)) \end{pmatrix} \quad (2.19)$$

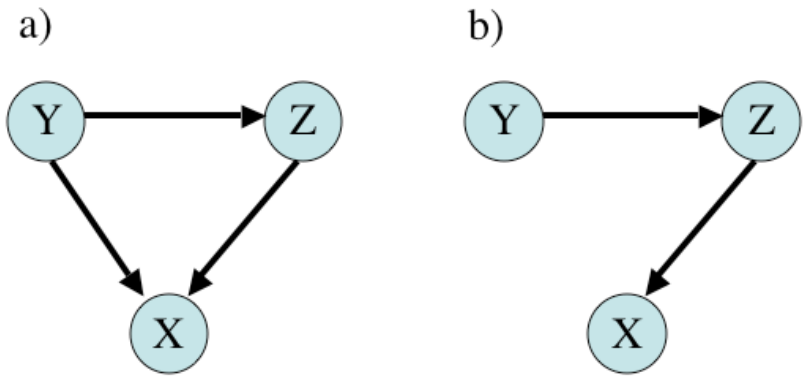

Figure 2-1 Conditional Pairwise Granger Causality Example. If Pairwise Granger Causality were applied to determine the connectivity of both of these network configurations the results for both would resemble panel a). Using Pairwise Granger Causality alone, it is not possible to differentiate between these network configurations. Conditional Granger Causality is required to determine if the connection from Y to X is real. Conditional Granger Causality does this by determining if Y affects X directly or if the effect of Y mediated through Z by determining how well X is predicted by Z with and without the influence of Y.

The influence of Z on X is entirely mediated through Y when the prediction of X is not improved in the trivariate MVAR model over the bivariate MVAR model. Specifically, CGC is calculated by taking the log of the ratio of the variance of the prediction error of X from $\boldsymbol{W}(t)$ to the variance of the prediction error of X from $\boldsymbol{U}(t)$. This is formalized in the equation for CGC:

$$F_{Z\to X|Y} = \ln\frac{\Sigma_2}{\Sigma_{xx}} \tag{2.20}$$

Conditional Granger Causality calculated using this equation is greater than zero when some of the power from Z is directly causal on X. The result would be equal to zero when the influence of Z on X is entirely mediated through Y. Thus, this method allows the two examples stated earlier to be easily differentiable. While Conditional Granger Causality addresses specific deficiencies in the original formulation of Granger Causality, there remain several further weaknesses that need to be considered when drawing conclusion from a causal analysis.

Limitations of Causal Methods

Since the time of Aristotle, philosophers have reached little consensus on a common definition for the concept of causality (61). However, causation is a concept critical to many disciplines including law, medicine, and the sciences. A functional definition of this concept is necessary to develop tests of causality that are useful in the context of these disciplines. Interestingly, the debate over the definition of causality has provided insights into several weaknesses of causal methods including Granger Causality that must be considered when designing sound experiments.

Clive Granger best describes the inherent limitations of his original method in his accounts of the origins of Granger Causality (62) (61). He describes how several of his peers noted that his method "is not real causality, it is only Granger causality". Granger also describes several axioms that must be assumed to be valid. The first among these is that "the past and present may cause the future, but the future cannot cause the past" (61). Second, everything in the universe is described and this set of information includes no redundant information. In this hypothetical universe, it would be easy to talk about the relationship between a variable X and a variable Y. However, these assumptions are difficult to satisfy in real systems. In reality, causality algorithms can be effected by many factors including sampling rate, time scale selection, seasonal influences, signal to noise ratio, variable selection, variable availability, and even chance.

Time scale and sampling rate are two variables that can have intertwined yet diametrically opposed effects on a causal analysis. Selection of time scale and sampling rate is dependent on the processes being observed. If the sampling rate is too low, it can be difficult to observe time delayed influences in the system because the system may be interacting at time scales of a higher frequency than the sampling rate. Conversely, if the sampling rate is too high it can be

computationally intractable to model far enough into the future (i.e. high model order *m*) to capture interactions. Additionally, it is possible that two time series may interact differently on two largely different time scales that may require separate analysis. These examples demonstrate that proper consideration must be given to selection of time scale and sampling rate depending on the system being analyzed. The data in these experiments are often recorded at very high (up to 25kHz) sampling rates that must be low passed filtered to provide a proper sampling rate and time scale to study causal interactions. All data is down sampled to 1kHz prior to analysis. Spike train point processes are further low pass filtered to 50Hz (10% of nyquist for 1kHz) to create a continuous time series so that AR models can be used.

It is also not possible to describe all variables in an experimental system. Consequently, unobserved time series are a factor that must always be considered when talking about causal influences. Implementation and subsequent interpretation of Granger Causality inherently depends entirely on the availability and selection of variables for analysis. Specifically, the causal relationship between two neurons may be influenced by a third and likely many other neurons that are not recorded from (e.g., a neuron too distant from an electrode to be measured). The likelihood of this situation increases with the complexity of the system being observed. Consequently, the contribution of these unobserved neurons would not be accounted for. This can have several effects on the relationships between observed time series. One possibility is that a common driving input at differing time delays could create a false causal influence where no real connectivity even exists. A priori knowledge of possible anatomical structure can help in this type of situation.

So called seasonal influences also present an interesting possibility. Two time series may be causal because of a similar common driving by an unobserved seasonal process.

Subsequently, the causality between these time series may wax and wane dependent of this seasonal influence or possibly dissapear altogether. Another possible scenario is that the influence between two time series could include mediated influences that cannon be conditioned out using previously mentioned conditional methods. This would tend to distort the magnitude of the influences reported from analysis. This is a likely possibility in complex neural systems that cannot be easily remedied. This problem impacts not only GC analysis but also every other multivariate statistic used in neuroscience today. Thus, it is clear that results from this type of analysis could potentially suffer from poor experimental designs where the important variables are unobserved or uncontrolled.

Additionally, there is another specific weakness of GC relating to the analysis of point processes. Often, the output from an observed neuron is described in terms of when that neuron fires action potentials. Point processes are not a continuous function over time. AR models can only describe continuous processes. In order to compensate for this, spike files from individual neurons must be low pass filtered prior to causal analysis. Subsequently, high frequency information above the cutoff for the low pass filter is not included in analysis. However, unpublished results from a non-parametric version of Granger Causality for point processes being developed by Mingzhou Ding and colleagues are very similar to parametric results. Specifically, the non-parametric method does not show any significant interactions over the cutoff of the low pass filter used for the parametric method.

These strengths and weaknesses of Granger Causality must be considered carefully before application to neural systems. In the following chapters, these methods will be used to describe the effective connectivity using the observable outputs of these systems to better understand the

underlying systems. These weaknesses will be carefully considered during experimental design, analysis, and subsequent interpretation.

CHAPTER 3
RECOVERY OF SYNAPTIC WEIGHTS FROM SPIKING ACTIVITY USING GRANGER CAUSALITY

Introduction

Recent advances in multichannel recording techniques enable simultaneous access to the electrophysiological activity of hundreds to thousands of neurons. These advances allow investigators to address one of the primary challenges in neuroscience, linking the structure of a network to its potential functions. For example, in cognitive neuroscience, by recording the activations of brain structures during various behavioral performances, investigators now have the technology for understanding how different brain structures interact to produce behavior. This experimental advance has been supported by a simultaneous advance in the quality of analytical tools that quantify neuronal interactions, such as the classical cross-correlation (14, 18, 21, 63-65) and coherence functions (66). At their core, however, these methods do not provide directional or "causal" relationships between different channels whether those channels are recorded from individual neurons or from different brain regions. In contrast, Granger Causality (GC) (1) has emerged in recent years as a technique of choice to provide a mathematically sound method for estimating causal relations.

Pairwise Granger causality (PGC) was initially developed in the economics community to describe and quantify the "causal relationship" between data from two different economic time series. The foundation for this technique can be traced back to Wiener (57), who proposed that for any two simultaneously recorded time series, one series could be called causal to another if incorporating past knowledge of the first time series permits more accurate prediction of the second series. Granger formalized this idea in the context of linear regression models of stochastic processes (1). Specifically, consider two simultaneously recorded time series x_1, x_2, $x_3 \ldots x_n$ and y_1, y_2, $y_3 \ldots y_n$. Suppose one would like to construct a linear predictor of the current

value of the *x* series based on *m* prior values: $x_n = a_1x_{n-1} + a_2x_{n-2} + a_mx_{n-m} + \varepsilon_n$. This is nothing more than a single variable autoregressive model in which standard procedures can be applied to yield the model order and model coefficients, where the variance of error series, ε_n, is a gauge of the prediction accuracy. Now consider a predictor of the current values of the *x* series by including both the previous values of the *x* series and the previous values of the *y* series, namely: $x_n = b_1x_{n-1} + b_2x_{n-2} \ldots + b_mx_{n-m} + c_1y_{n-1} + c_2y_{n-2} \ldots + c_my_{n-m} + \eta_n$. The variance of the error series, η_n, is then a gauge of the prediction accuracy of the new expanded predictor that includes information about the *y* series. Based on Wiener's idea, Granger formulated that if the *variance* (η_n)*/variance* (ε_n) is less than one in some suitable statistical sense (i.e. the prediction of *x* is improved by incorporating past knowledge of *y*) then we say that the *y* series has a causal influence on the *x* series.

The concept of Granger causality has played a significant role in the field of economics since 1960s. Only recently has its potential for understanding the dynamics of brain circuitry been realized in neuroscience. For example, Zhu et al (48, 49) explores causal interactions between neurons during learning in the primary motor cortex of rhesus monkeys. Fanselow et al. (46) reveals causal influences from the sensory cortex to the thalamus during rhythmic activity associated with whisker twitching behavior in rats. It is expected that Granger causality based methods will experience significant growth in applications to a wide variety of neural systems where information transfers exist among individual neurons or different brain areas, including data from neural simulations, *in vivo* electroencephalogram (EEG), and *in vivo* microwire arrays (27, 30, 37, 43-47, 49, 50, 52, 56, 67-74).

These studies have mainly focused on revealing structures of interaction in the recorded circuits. The physiological meaning underlying the statistical values of Granger causality

remains unexplored. The goal of this study is to examine whether values of Granger causality can be used to recover synaptic weights between interacting neurons in a complex network. While intracellular recording methods are able to discern the synaptic weight from postsynaptic potentials, they cannot reveal network level activity *in vitro* and are of very limited use *in vivo*. Thus, to understand the synaptic relationships that regulate network activity, a technique to reconstruct the weights from only spike train outputs must be devised.

For a simple two-neuron network in which neuron A is synaptically connected to C, our first result is to show that the aforementioned PGC can easily discriminate a direct causal relationship from A to C when the strength of that coupling is even moderately high and, more importantly, the values of PGC can be related to synaptic efficacy. For more complex networks the pairwise approach encounters significant methodological limitations when direct, mediated, and serial influences exist between neurons. For example, consider a three-neuron case in which neuron A is synaptically coupled to a mediating neuron, B, who is then connected to neuron C. First, PGC would identify an erroneous causal connection between A and C, even though this pair is not directly coupled. The reason is that the activity of A, does in fact, causally influence the activity of C, but does so only through the mediating relationship involving B.

Second, when trying to recover the synaptic efficacy from B to C, due to the serial influence from A, the values of PGC from B to C are no longer a true reflection of the synaptic weight between the two neurons. These problems can become even more acute in more complex network with many interacting neurons or brain areas. The second result of this paper is to describe a technique to recover the Direct Granger Causality (DGC) and the synaptic efficacy between neurons within networks with more realistic topologies, including direct, mediated, and serial influences.

The organization of this chapter is as follows. Existing methods such as Pairwise Granger Causality and Conditional Granger Causality are described in terms of their application to spiking neural networks. A computational shortcut that allows faster recovery of DGC is also explored. These methods are then systematically expanded to accommodate increasingly complex network conditions including direct, mediated, and serial influences. Each solution is illustrated with biologically plausible, simulated networks. Finally, we examine how DGC could be used to estimate both synaptic weights within a network and how it might provide a useful measure for describing changes in network wide plasticity.

Conditional Granger Causality and Mediated vs. Direct Relationships

In Chapter 2, the mathematical basis for both Pairwise and Conditional Granger causality was described. One of the limitations of PGC was that when it is used in a multivariate system, often these results do not reflect the true connectivity. False directed influences and cases where direct and mediated influences are confounded within the same pathway are the two primary problems. In the following section we will describe how these relationships can be untangled using Granger Methods. Chapter 2 also shows that CGC can be used to identify and remove erroneous direct connections that are actually mediated though other elements. However, at this point, we are left with a second problem. The effect of Y on X is embedded in the relationship reported between Z and X. This results in a stronger PGC value from Z to X when compared to the PGC value from Y to Z, even though the actual synaptic weights between these pairs may be identical. The direct influences need to be separated from mediated influences in order to more accurately quantify synaptic interactions within this network. Direct influences, after being recovered from an entangled pathway, will be referred to as Direct Granger Causality (DGC) to avoid confusion with values recovered using only PGC. Note that in neuron pairs that do not contain mediated influences, PGC already represents the DGC between these neurons.

One way to recover DGC from an entangled pathway would be to make the relationship between X and Z conditional on Y using CGC. This was the solution described by Geweke (59) shown in equation (3.21). However, this method is computationally expensive in small networks and possibly intractable in large networks, due to the exponential number of potential combinations that must be addressed. Interestingly, Geweke also noted that it might be possible, when the influence from Y to X is entirely mediated through Z, to directly subtract the PGC calculated from Y to X from the PGC value from Z to X. This would recover the same quantity as calculating CGC from X to Y conditional on Z, without having to perform the computationally intensive CGC analysis. This concept will be evaluated empirically later in the paper.

$$F_{Z\to X|Y} = \ln \frac{\mathrm{var}(\varepsilon_{xx(Y,X)}(t))}{\mathrm{var}(\varepsilon_{xx(X,Y,Z)}(t))} \tag{3.21}$$

Simulation and Analysis

In this section, we illustrate the analytical solutions described earlier within a simple, biologically plausible neural network model. We have chosen Izhikevitch's simple neuron model (3, 75), a stochastically driven neural network with modifiable synaptic weighting that provides biologically relevant spikes that can then be analyzed using GC(76, 77). Briefly, the model is a reduction of the Hodgkin-Huxley model (78) to a simple two-dimensional system of differential equations. One equation models membrane voltage, *v*, equation (3.22), while the other models and a recovery variable, *u*, shown in equation (3.23).

$$v' = 0.04v^2 + 5v + 140 - u + I \tag{3.22}$$

$$u' = a(bv - u) \tag{3.23}$$

The auxiliary after spike resetting of the neuron is mediated by equation (3.24).

$$if, v \geq 30mV, then \left\{ \begin{array}{c} v \leftarrow c \\ u \leftarrow u + d \end{array} \right\} \tag{3.24}$$

The variable u is a membrane recovery variable that accounts for K^+ activation and Na^+ inactivation in the neuron. The variables a, b, c, and d are dimensionless parameters that effect the temporal characteristics of the action potential, while v' and u' are the first time derivatives of v and u. These variables remain constant and are the default values used by Izhikevich for regular spiking cortical neurons (3) . Each time step of the model represents 1 ms, equivalent to a

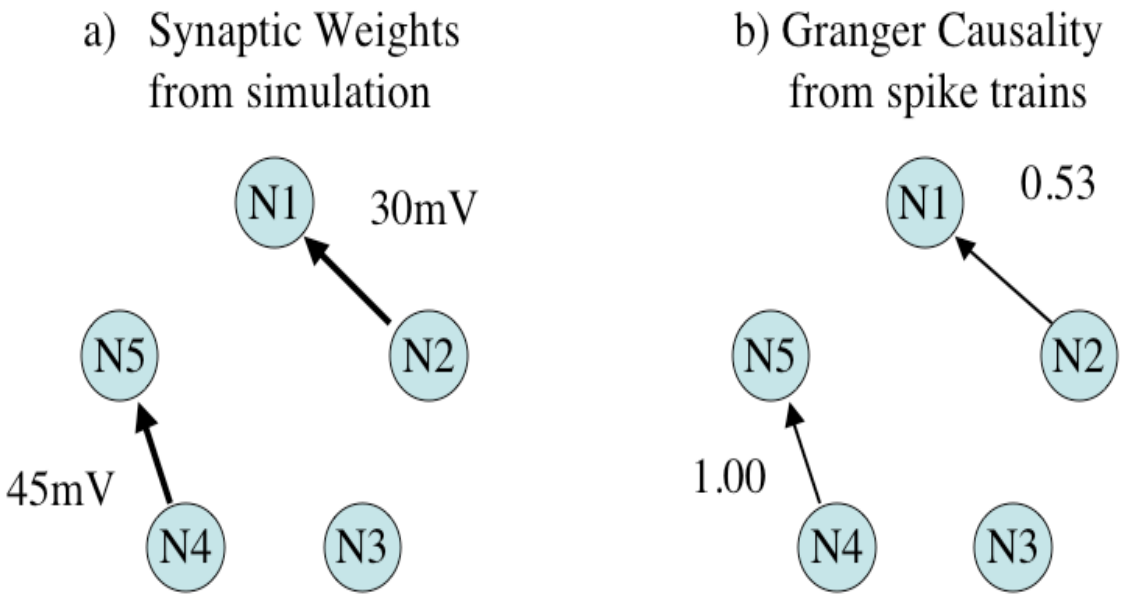

Figure 3-1 Topology diagram of a simple five neuron network. In panel a) the synaptic weights from N1 to N2 and N4 to N5 have been synaptically coupled. N3 is left uncoupled to demonstrate that PGC will indicate null connectivity. Equivalent but independent random processes drive each of the five neurons. 100 realizations of this network using Izhikevich's simple neuron model with these weights yields the results shown in panel b) using Pairwise Granger Causality. These results demonstrate that Pairwise Granger Causality can, not only resolve the difference between null and actual connectivity, but also determine the directionality of those influences.

1kHz sampling rate of a realistic neural system. During simulation, neurons can spontaneously fire based on spontaneous super-threshold fluctuations of membrane noise injected into each neuron and from synaptic inputs from other neurons in the network.

Mono-directional Simulation

The first model, illustrated in Figure 3-1, consisted of a five neuron network composed of mono-directional connectivity (i.e., one way singular direction for causal relations) from Neuron 4 (N_4) to 5 (N_5) and from Neuron 2 (N_2) to 1 (N_1), with neighboring Neuron 3 (N_3) uncoupled (zero synaptic weight). Hence, the activity of N_2 and N_4 will have a causal influence on firing of N_1 and N_5, respectively. In contrast, only the equivalent independent random process intrinsic to N_3 drives N_3. It is important to note that the intrinsic random processes that drive these neurons are equivalent, but independent. The cross-power spectra for all neurons during simulated activity are shown in Figure 3-2. During the simulation, all five neurons were active, indicated by the auto-spectra (along the diagonal) for each neuron. As expected from the configuration of the synaptic weights, the cross-power spectra for N_1 to N_2 and N_4 to N_5 is larger than that of N_3 with its neighbors. The spectra resulting from Granger causality is shown in Figure 3-3. This figure shows causality by frequency from 0 to 50 Hz between N_4 to N_5 (top panel) and the converse relation, N_5 to N_4 (bottom panel).

Peak causality between N_4 to N_5 occurred at frequencies near 20 Hz. In contrast, spectral causality within the reverse relationship, N_5 to N_4, was very low. This verifies the absence of a bi-directional relationship between the pair. Similar results using other modeling systems can be found elsewhere (48, 49, 76).

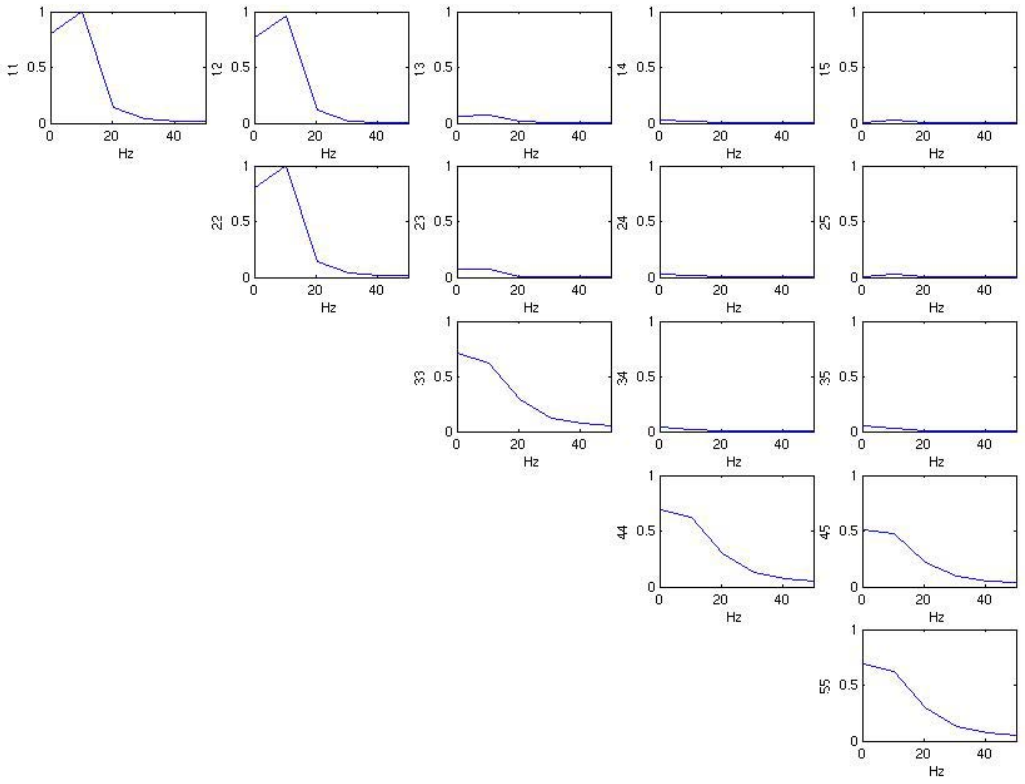

Figure 3-2 Power spectra and cross-spectra calculated from the 5 neuron model simulation. These plots are organized in matrix format mirroring that of the spectral matrix so that that row 1 column 1 represents the intrinsic power spectra for N1, while row 1 column 2 represents the cross-spectra between N1 and N2. Thus, the diagonal contains the individual neurons spectral power while the upper triangular graphs represent Cross-spectra between neurons. Notice that Neuron 3 (Row 3, Column 3) has intrinsic power but demonstrates no significant cross-spectra (Other plots in both Row 3 and other plots in Column 3) with its neighbors as it is independent and uncoupled to the other neurons. Neuron pairs 1,2 and 4,5 both demonstrate significant cross-spectra (Row 1 Column 2 and Row 4 Column 5) consistent with initial synaptic weights. However, it is not possible to determine directionality from this information.

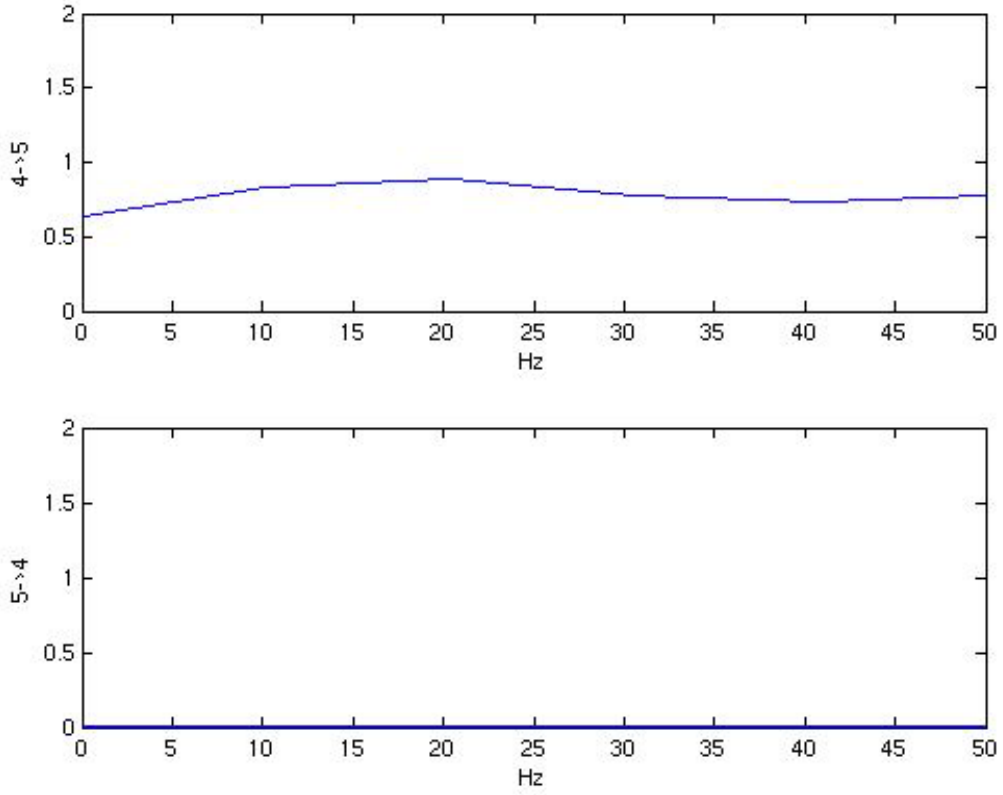

Figure 3-3 Granger Causality Spectra. The causality from N4 to N5 is apparent, with a maximum value of approximately 0.92 around 20Hz, while the reverse direction of N5 to N4 approaches zero at all frequencies and is not statistically significant. This verifies that PGC provides directional information that cannot be discerned from power spectra, shown in Figure 3-2. The Pairwise Granger Causality for this directional neuron coupling would be reported as 0.92.

Relationship between Synaptic Weight and Granger Causality

At this point, we have shown how PGC can provide an estimate of the relationships between elements. One important consideration, however, is how PGC values correspond to actual synaptic weights, especially when those weights might be in constant flux. In other words, how is an estimate of causality using PGC related to the actual underlying synaptic weight especially when those weights may be changing?

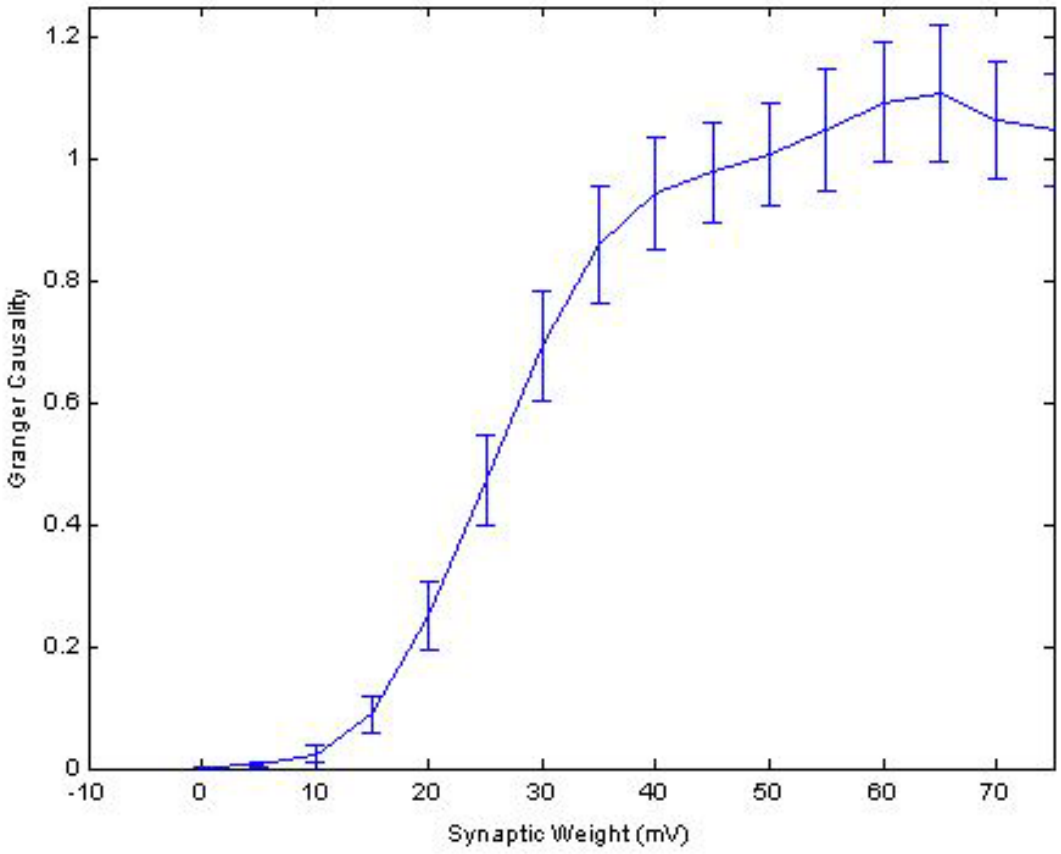

Figure 3-4 The PGC results from a mono-directional simulation with the weight from neuron 4 to 5 varied from 0-75mV in increments of 5mV. Synaptic weight is plotted on the x-axis while the resulting PGC values calculated from the spike timing is plotted on the y-axis. The relationship between synaptic weight and PGC is sigmoid described by equation 12. Notice the region approximately between 15mV and 45mV where the relationship between synaptic weight and PGC is linear. Each increment in the graph was simulated 100 times to provide the mean and variance shown in the plot.

The simulation was modified such that the connectivity between N_1 and N_2 was systematically incremented from 0 mV to 75 mV to observe the effects on our estimate of causality. Each increment was simulated 100 times to determine both the average estimate by PGC and variance of that estimate. The results of those simulations indicate a sigmoid relationship between the synaptic weight from N_1 to N_2 ($S_{1\to2}$) and resultant GC, $F_{1\to2}$ shown in Figure 3-4. There is a region between 15mV and 45mV where the relationship between $S_{1\to2}$

and $F_{1\to2}$ is linear with a slope of 0.033 causal units/mV. Synaptic weights above this range do not produce significant changes on $F_{1\to2}$, suggesting that 45mV is the maximum effective synaptic weight. Similarly, weights below 15 mV produce only slight changes in the estimate of causality. The data from this experiment were fit with a sigmoid equation, shown in Equation (3.25), to quantify the functional relationship between Granger estimates and actual synaptic weights. An example of estimated synaptic weights using this equation is presented in panel d of Figure 3-5.

$$F_{Y\to X} = \frac{1}{1+384e^{-0.2124S}} \tag{3.25}$$

Mediated vs. Direct Causal Relationships under Serial Connectivity

PGC works well for recovering synaptic weights between two neurons using Equation (3.25). However, there are situations where PGC values will not adhere to this relationship due to added complexity within the network. Often PGC values include not only the direct information between nodes but also include mediate influences that could distort the relationship between PGC and synaptic weights. This becomes more common as the number of elements and connectivity increase within a network. This issue is addressed in the second simulation, where a serial topology was created to demonstrate discrimination between direct and mediated connectivity as well as separation and recovery of individual synaptic weights within a "chain" of serially connected neurons. The five-neuron topology, shown in Figure 3-5 a), consisted of causal

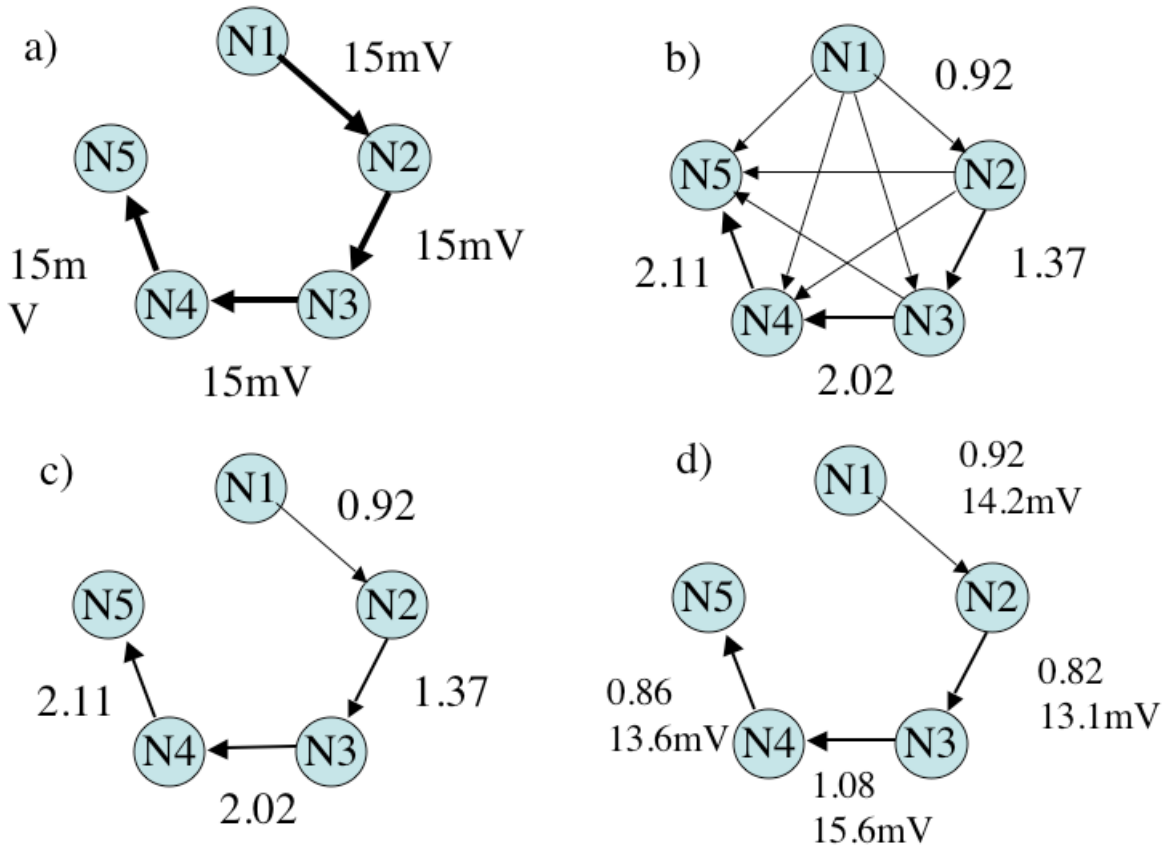

Figure 3-5 Five neuron simulation. This was carried out where a) shows the synaptic weights before simulation. Calculation of PGC for all possible connections for the 5 neurons yields the plot shown in b). Notice that using PGC alone many new false connections are shown. When CGC is used to eliminate the false connection the plot is reduced to what is shown in c). After CGC plot c) begins to resemble the connectivity pattern as shown in a), however, the values associated with c) do not scale with the synaptic weights shown in a). A further step using CGC a second time or using Geweke's subtraction method is required to detangle direct and mediated influences. The results after the use of Geweke's subtraction method to calculate DGC are shown in d) along with corresponding approximations of synaptic weight.

synaptic weights of 45 mV from N_1 through N_5 similar to a synfire chain (79, 80). The original PGC estimate of causality, shown in panel (b), indicates erroneous connections among the entire pool of neurons reflecting the complex causal relationships between each element. Table 3-1 shows the PGC results for each relationship. Note also that the PGC values, shown along the elements of the serial chain, steadily increase from N_1 to N_5 (diagonal in Table 3-1), reflecting the embedded mediated causal influences cascading throughout the chain.

Table 3-1 A table of the Pairwise Granger Causal influences calculated between the 5 neurons in the simulation displayed in Figure 3-5. The right column indicates what the from neuron is and the top row indicates what the to neuron. For example, to locate the influence of neuron 4 on neuron 1 a value of 0.01 is reported in From N4, To N1.

	To N1	To N2	To N3	To N4	To N5
From N1	-	0.92	0.55	0.38	0.48
From N2	0.01	-	1.38	0.94	0.78
From N3	0.01	0.01	-	2.02	1.25
From N4	0.01	0.01	0.02	-	2.11
From N5	0.00	0.01	0.02	0.01	-

CGC was applied to discriminate between false direct from mediated connections in order to determine the network's true connectivity. Panel c of Figure 3-5 shows the results of CGC, where the topology has been correctly estimated but includes the systematic errors in estimating the strength of coupling inherent within this method due to the causal cascade inherent in serial chains. The problem arises because values remaining after calculating CGC represent a combination of direct and mediated values that correspond to an increase in total information flow down the chain. This is due to the accumulation of mediated influences towards the end of the chain. Thus, the direct components between any two neurons must be separated from mediated influences to relate the direct component to a meaningful synaptic weight.

Recovery of direct synaptic weights could be achieved using CGC for a second time on the mediated pathway. However, a simpler solution may exist. If PGC simply sums the effects

Table 3-2 Pairwise Granger Causal influences calculated between the 5 neurons in the simulation displayed in Figure 3-5 after the use of significance thresholds, conditional granger causality analysis, and removal of mediated influences. This table contains only direct causal influences. All other values reported in Table 3-1 were found to be false or insignificant. The right column indicates what the from neuron is and the top row indicates what the to neuron. For example, to locate the influence of neuron 4 on neuron 1 a value of 0.01 is reporten in From N4, To N1.

	To N1	To N2	To N3	To N4	To N5
From N1	-	0.92	-	-	-
From N2	-	-	0.82	-	-
From N3	-	-	-	1.08	-
From N4	-	-	-	-	0.86
From N5	-	-	-	-	-

of previous elements along a serially connected chain, then it may be possible to simply subtract the previously conditioned out PGC values that represent the mediated component of the distorted PGC value. For example, by subtracting $N_{1\to3}$ (0.55) from $N_{2\to3}$ (1.37), a value of 0.82 is obtained, which better estimates the actual synaptic weights incorporated into the model. This process was repeated for each pair and the resulting estimates are shown in panel (d) of Figure 3-5 and Table 3-2. The relationship between CGC and the simple subtraction of $N_{1\to3}$ to $N_{2\to3}$ is derived from the properties of both PGC and CGC, as stated by Geweke (77), and shown in Equation (3.26).

$$F_{Y\to X|Z} = F_{YZ\to X} - F_{Y\to X} \tag{3.26}$$

In the special case where the bivariate PGC influence of Y on X, $F_{Y\to X}$, has been previously conditioned out (i.e. equal to zero) using CGC, equation (3.27) is valid.

$$F_{YZ\to X} = F_{Z\to X} \tag{3.27}$$

This allows for the derivation of equation (3.28), which explains the empirical relationship that allows subtraction of PGC values to retrieve the DGC value between .

$$F_{Y\to X|Z} = F_{Z\to X} - F_{Y\to X} \tag{3.28}$$

A direct comparison of the efficacy of these methods for calculating DGC was achieved using a Monte Carlo simulation of a 3 neuron chain. 100 realizations of this simulation were run and both methods were used to recover DGC from the PGC output of the synapse at the end of the chain. The synaptic weights were randomly generated between 15mV and 45mV for each realization of the simulation. The results of this simulation are shown in Figure 3-6. These results suggest that the subtraction method presented in equation (3.21)[12] can produce DGC values similar to that of CGC as shown in equation [5].

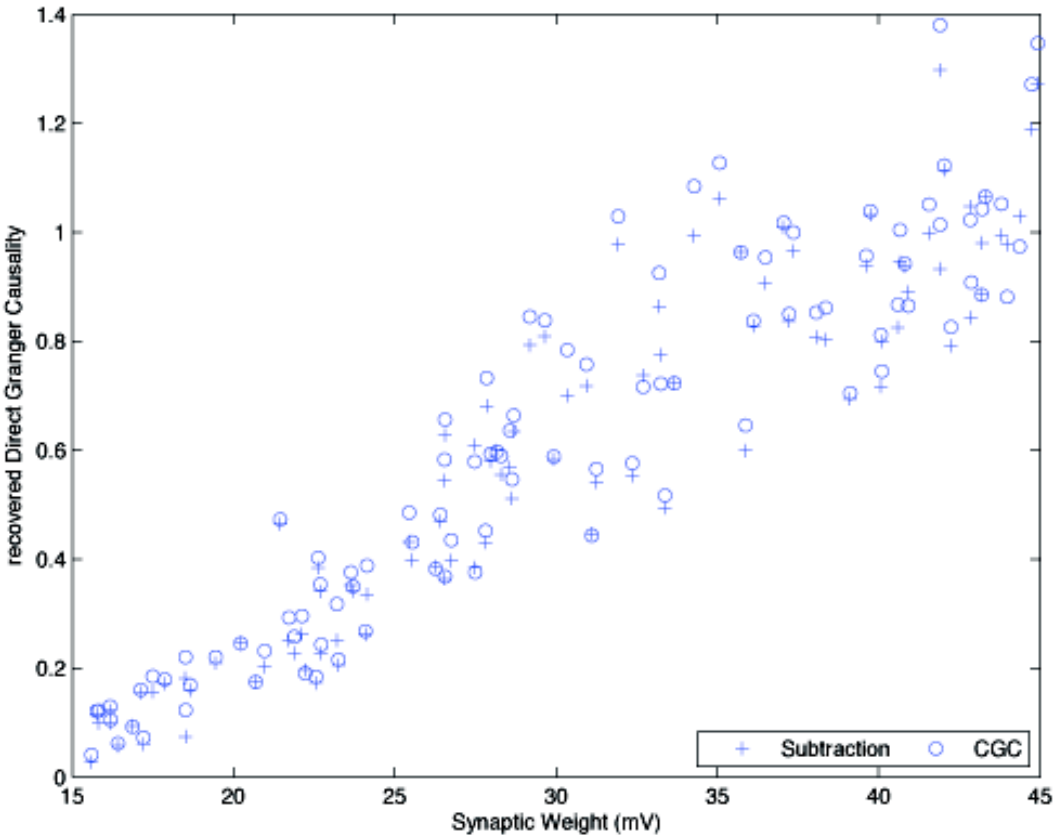

Figure 3-6 Direct influences between N2 and N3 were recovered by both methods to allow a comparison of Geweke's subtraction method to CGC. Each point was generated from a Monte Carlo simulation of the serial simulation using randomly generated synaptic weights between 15mV and 45mV. This plot suggests that both methods provide results consistent with the linear region expected from the sigmoid plot shown in Figure 3-4. However, Geweke's subtraction method is computationally simple providing the researcher with a clear advantage in large networks that may require repetitive calculation of DGC.

Monte Carlo Simulations with Random Serial Topologies

A Monte Carlo simulation was conducted to further test DGC in a 5 neuron serial chain with random synaptic weights. This experiment was designed to describe the relationship between synaptic weights and the recovered DGC for each synapse in the serial chain. The synaptic weights $S_{1\to2}$, $S_{2\to3}$, $S_{3\to4}$, and $S_{4\to5}$ were randomly generated for each simulation using a uniform distribution from within 15 mV to 45 mV linear range of the sigmoid relationship derived from the first experiment. The DGC for pathways with mediated influences ($F_{2\to3}$, $F_{3\to4}$,

& $F_{4\rightarrow5}$) was calculated for each synapse by subtracting the conditioned $F_{(N-1)M}$ pathway from $F_{N\rightarrow M}$ and

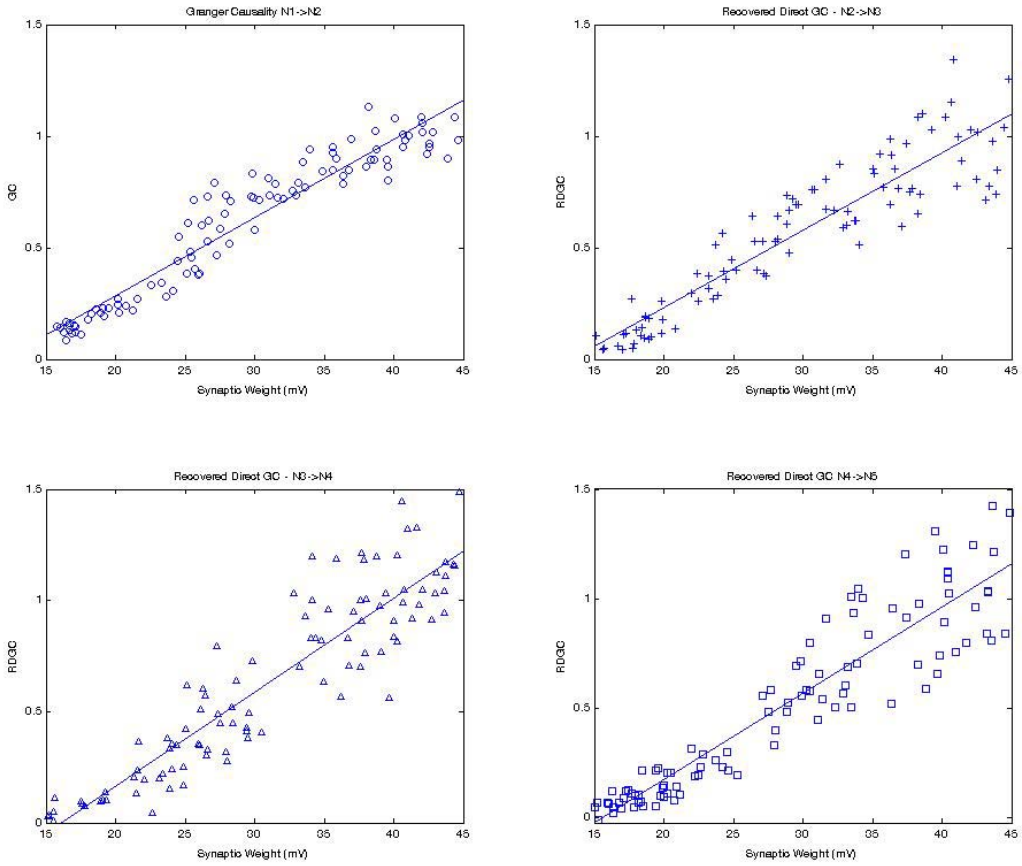

Figure 3-7 DGC values can be recovered at each of the synapses in the serial chain. This was done with randomly generated synaptic weights between 15mV and 45mV at all synapses. The weights for each synapse were generated independently within each simulation and the simulation was replicated 100 times. These plots demonstrate that DGC values recovered from entangled pathways (top right, bottom right, and bottom left) along the serial chain mirror those calculated using PGC on the first pathway (top left). This suggests that DGC values represent the direct influence between two neurons similar to the PGC relationship that can be calculated between neurons that are not entangled by mediated influences.

retained. The synaptic weights $S_{1\rightarrow2}$ and $F_{1\rightarrow2}$ were also retained to serve as a baseline for comparison. According to the hypothesis, Monte Carlo distributions for the DGC pathways

should mirror the relationship between $S_{1\to2}$ and $F_{1\to2}$, a purely direct pathway. This simulation was repeated 100 times.

Figure 3-7 a) shows that the distributions for the DGC at each synapse mirror the linear distribution from the purely direct $S_{1\to2}$ to $F_{1\to2}$. The higher variance for the DGC farther down the chain is due to additive error because of the way DGC is calculated. This empirical relationship shows that the conditioned pathway, $F_{(N-1)M}$, is a representation of the mediated component of the remaining pathway, $F_{N\to M}$. The empirical relationship also suggests that DGC is an accurate representation of the DGC component between two neurons and can be used to calculate a meaningful synaptic weight for the synapse using the relationship described in Equation (3.25).

100 Neuron Neural Network

A larger more complex neural network simulation was used to further test the ability of Granger Causality to recover synaptic weights from spiking activity. This simulation consists of 80 excitatory and 20 inhibitory neurons connected with 20,000 synapses. Excitatory neurons are connected to all other neurons using randomly generated weights from a exponential distribution where most connections are weak (1-4mV) while strong connections (up to 70mV) are sparse. Inhibitory neurons are connected to the network using a flat distribution of weights ranging from -1 to -10mV. Five excitatory neurons in this network were chosen and linked in a serial chain, resembling the earlier 5 neuron chain, with synaptic weights of 40mV as shown in Figure 3-8 panel A). This network produces spontaneous spiking and bursting shown in panel B). Pairwise Granger Causality is then used to determine the relationship between these 5 neurons shown in panel C). Pairwise Granger Causality alone reveals that information flows directionally down the chain with no information flow in the opposite direction. However, the structure and

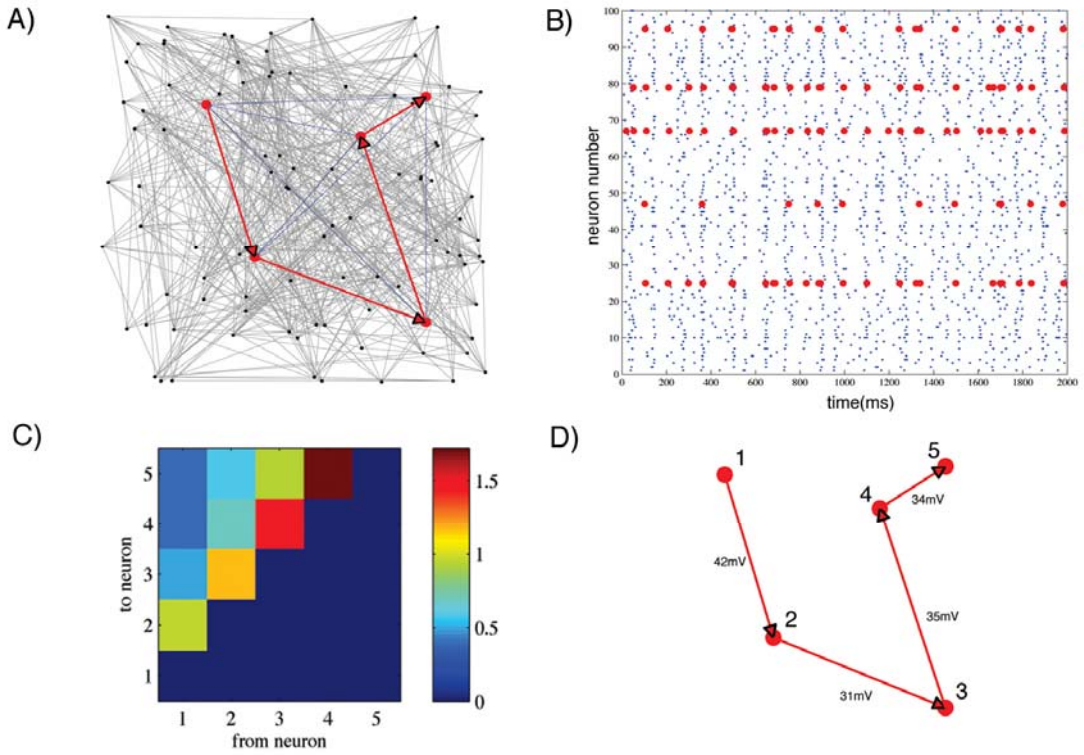

Figure 3-8 100 Neuron Simulation. A chain of 5 neurons is imbedded within a 100 neuron neural network. The goal of this simulation is to extract the causal core shown in panel A using Granger Methods. Each synaptic weight in the chain is is set at 40mV. Panel B shows the activity of these five neurons within the full network. Panel C shows the results from only PGC analysis. Panel D shows the remaining significant connectivity after CGC analysis and their corresponding synaptic weights. Note that the weights down the chain are significantly underestimated, this is likely due to the influence of the rest of the network on recovered weights.

connectivity of the chain are not clear enough to disseminate the structure underlying this network. Conditional Granger Causality is then used identify and remove spurious connection revealing the structure shown in panel D). Thus, Granger Causality effectively identifies the serial chain embedded within this 100-neuron simulation. Conditional Granger Causality and the previously demonstrated sigmoid relationship are then used to recovery of synaptic weights also shown in panel D). Interestingly, results from a larger neural network are not as accurate as results shown previously from a simpler network. Further testing has shown that interaction with

the rest of the network subtly distorts the magnitude of the recovered synaptic weights. Future work will focus on the use Conditional Granger Causality to condition out the influences of the other 98 neurons on each paring to improve the accuracy of recovered synaptic weights.

Application to Spike Timing Dependent Plasticity

The brain is an ever-changing, non-stationary system that belies the fact that many measures of activity require stationarity to derive meaningful conclusions. Take for example studies that attempt to demonstrate plasticity (4, 21, 81). One of the most common paradigms measures activity (e.g., spike rate) during a "baseline" phase that is followed by some treatment (e.g., learning phase, such as delivery of a tetanic pulse train). Activity is then measured again to determine if any changes (e.g., spike rate) have occurred. The core notion is that changes in connectivity will result in a change in the number of spikes. Unfortunately, measures like spike rate are highly susceptible to spontaneous (random) fluctuations in brain activity. In contrast, changes in the rate of spiking alone do not substantially influence causality estimates until the spike rate becomes so low that either method begins to suffer. Hence, GC may provide a novel and more reliable method to measure activity changes, while also outlining the structural information of the network as these changes occur.

A simple neural model sensitive to spike timing dependent plasticity (STDP), a proposed mechanism for changes in synaptic plasticity, was created using CSIM (82, 83) to investigate this notion. This model was constructed to determine if changes in synaptic weight due to STDP could be reliably detected with Granger Causality. The simulation was designed so that an STDP synapse, with parameters adopted from Markram et al., between two neurons would be exposed to a paired pulse stimulation similar to that of Bi et al. (84). This paired pulse was designed to elicit long-term potentiation (LTP).

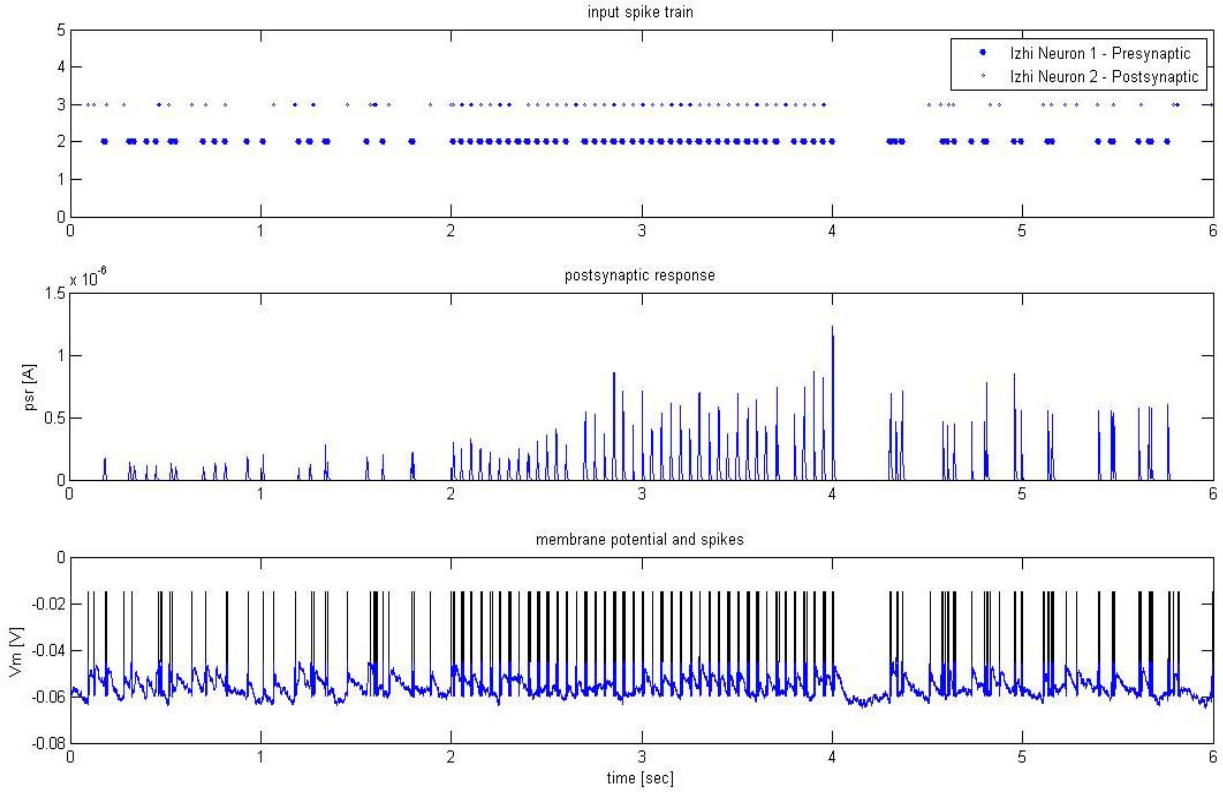

Figure 3-9 A simulation to determine if changes in synaptic weight consistent with stimulation timing dependent plasticity (STDP) at a synapse between two biologically relevant neurons could be detected after a paired pulse stimulation was applied to the neurons. The paired pulses were designed to produce potentiation at the synapse. The top plot shows the action potentials generated from the pre and post synaptic neurons. The paired pulse stimulation was delivered between seconds 2 and 4. The middle plot shows the amplitude of the post-synaptic response in amps, note that the post synaptic response was amplified due to the paired pulse stimulation, consistent with the effects STDP. The bottom plot shoes the membrane voltage and action potentials fired for the post synaptic neuron.

PGC should detect and quantify the change after the paired pulse stimulation in the post stimulation spontaneous activity. However, changes in activity from the paired pulse stimulation may not be great enough to detect using granger causality. The simulated neurons used were also based on Izhikevitch's simple model of spiking neurons (3). Each simulation was six seconds long, sampled at 1000 kHz, and repeated 10 times. The first two seconds of spontaneous activity are the baseline, the middle two seconds are during the application of the

paired pulse stimulation to the synapse, and the final two seconds of spontaneous activity are used as the post treatment recording.

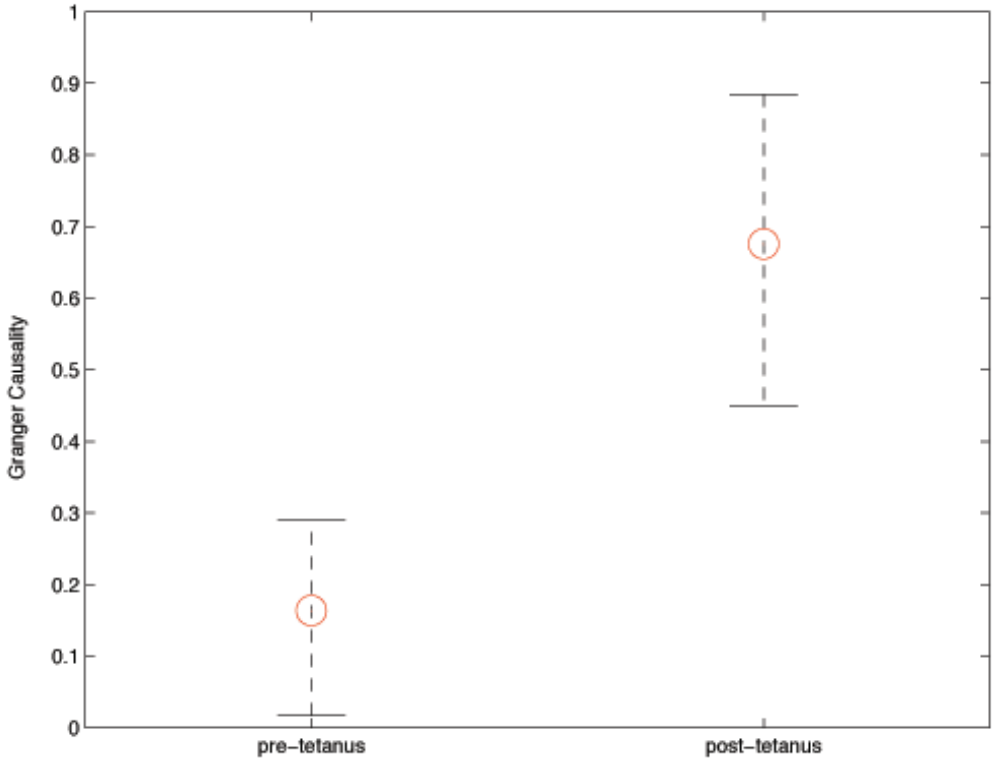

Figure 3-10 Statistical Analysis of Plasticity Simulation. The simulation ran in Figure 3-9 was repeated 10 times and the resulting pre and post spike trains were used to calculate the causal interaction between the neurons using PGC. The pre and post-tetanus values of PGC were compared using an analysis of variance. Plotting the analysis of variance demonstrates that the PGC values pre and post-tetanus are statistically independent suggesting that the change in causality due to the paired pulse stimulation can be detected and quantified using PGC.

One realization of the simulation is shown in Figure 3-9. Note that the post-synaptic response increased after the paired pulse stimulation was applied. The spike trains for the baseline and treatment were low-pass filtered and PGC was calculated from the pre-synaptic neuron to the post-synaptic neuron. Ten replicates of this experiment produced 10 PGC values for both baseline and treatment that are then pooled and compared using an analysis of variance, shown in Figure 3-10. This analysis shows that the values are statistically different post treatment suggesting that changes resulting from STDP can be detected using PGC.

Conclusions

Granger Causality is a powerful statistical technique that can quantify causal relationships, ranging from interactions between different brain areas to recordings from single neurons. However, there are a number of potential issues in interpreting synaptic efficacy that results from PGC, including false directed influence and separation of direct and mediated influences. In this paper, we explored several additional techniques specifically to address those issues. Specifically, CGC is used to untangle direct and mediated influences and provide estimates of DGC. Additionally, a less computationally intensive subtractive process can provide DGC under special conditions. When these special conditions are not met, CGC would be required to recover DGC values. Through network simulations, we then described how these techniques could potentially be used to provide additional information about the underlying network structure and to estimate the relationship between synaptic strength and DGC estimates. These methods are useful when that strength is static or changing due to changes in plasticity.

There still remains several important weaknesses and limitations of Granger Causality that must be considered. For example, synaptic weight estimates using DGC are dependent not only on the variability of the system being measured and the measuring instruments, but also on the quantity of data recorded. Thus, short recording times with little activity can substantially affect estimates using either method. Multiple realizations of the process being examined are recommended to produce an accurate representation of causality within a system. Perhaps one of the most challenging problems remaining with this technique in living systems is detecting the presence of unobserved units, where apparent causal relationships are due to unobserved elements. This possibility must be considered when drawing conclusions about complex systems that may contain multiple unobserved processes.

DGC was also investigated for its potential to estimate synaptic weights. The model intentionally represents a simplified case of neural connectivity where the independent stochastic processes that drive the neurons, along with the spike firing rates, are based on the behavior of one type of cortical neuron. Changing these stochastic processes and neuron types in the model may alter the sigmoid relationship between synaptic weight and GC. Different model parameters or data from neural culture, where neuron type and synaptic weights may be unknown, will require calibration in order to recover valid synaptic weights. However, in this study we demonstrate that there is a linear region within the sigmoid relationship between synaptic weight and GC, where changes in synaptic efficacy can be observed.

The 100-neuron simulation demonstrates that as the complexity of the network grows the PGC results underestimate the synaptic weights. This may be due to the contributions of the other 95 neurons on activity within the causal chain. While the sigmoid relationship may not always apply, the existence of a region where synaptic weight changes linearly with PGC suggests that DGC values from that system are comparable (i.e. a larger Granger Causality value translates to a larger synaptic weight). This gives an investigator confidence that changes observed during an experimental manipulation are also comparable in magnitude. This linear relationship allows for pre-experimental and post-experimental values of DGC to be subtracted in order to quantify plasticity. It is possible that these observations can be quantified with proper calibration between synaptic weight and DGC values.

Conversely, we have also demonstrated that there are regions in the relationship where changes in synaptic weight will not be reflected as changes in causality. Specifically, when the post synaptic potential is significantly sub threshold or when it is already so large that the post synaptic potential will almost always cause a post synaptic action potential. Changes in synaptic

weight within these regions may not be reflected in changes PGC values calculated between the observed neurons. However, it should be noted that changes in synaptic weight in these regions will not produce and observable changes in the spiking output of the neuron either.

Perhaps a more fundamental problem with any Granger based method is the ability to detect the presence of inhibitory, rather than excitatory, contributions. Inhibitory synapses, unlike excitatory synapses, do not produce a post-synaptic action potential. Thus, an inhibitory synapse will produce GC values near zero, similar to that of null connectivity. Additionally, inhibitory influences decrease activity in their targets and may distort serial causal influences, even though they may be strong. Including steps to untangle inhibitory influences, perhaps through conditional logic, may help address this problem. However, GC remains one of the most powerful techniques to estimate causal relations or untangle complex structural topologies in networks where that information is unknown.

CHAPTER 4
ASSESMENT OF PLASTICITY IN-VITRO USING GRANGER CAUSALITY

Introduction

Microelectrode array (MEA) technology has been used to quantify and record multichannel neural activity from in-vitro dissociated neural cultures for nearly three decades (85-87). However, the underlying structure and connectivity that is responsible for producing the neural activity observed from these cultures has remained largely unknown. Subsequently, difficulties arise when trying to accurately relate changes in observed neural activity to physiological changes within the network such as plasticity. Detection of plasticity across a network is now a common theme in recent neuroscience research (20, 67, 81, 88-92). Spike timing dependent plasticity (STDP), a process where the efficacy of a synapse is governed by the timing of pre- and postsynaptic action potentials, is thought to be a potential mechanism by which in-vitro plasticity occurs (83, 84, 88, 93). However, neural activity recorded using MEAs is extracellular, whereas STDP experiments often use intercellular voltage clamp methods on isolated neuron pairs. Ad hoc algorithms and measures are often developed to quantify possible plasticity related changes in-vitro with varying levels of success (4, 18, 20, 81, 89). However, these algorithms often do not provide a statistically sound measure of effective connectivity that can be related to the actual connectivity underlying the dissociated neural network.

Jimbo et al has demonstrated that changes in the synaptic strength of pathways within living neural networks could be identified by describing changes in elicited spike rates after induction by high frequency stimulation or tetanization (4). Specifically, Jimbo's data suggested that tetanization resulted in pathway specific potentiation and depression. The metric used to identify those changes is based on changes in the spike rates recorded on each electrode before and after a tetanic pulse train is delivered, a simple and elegant way to observe output related

changes in neural connectivity. However, observations that can be made using spike rate are limited providing only a course quantification of neural connectivity. First, spike rate observations are non-directional and they are also non-causal. Second, this method relies on using a difference between pre and post treatment measurements of spike rate to detect underlying pathways, limiting the ability to observe connectivity prior to a treatment which modifies the underlying strength. Several methods (17) including correlation (4, 21, 94, 95), likelihood methods (36-38), partial directed coherence (30, 50, 96), and Granger Causality (48, 49, 76) can address some of these deficiencies and have been used to identify connectivity patterns between spiking neurons in neural simulation, in-vitro and in-vivo.

Pairwise Granger Causality (PGC) (1), a robust statistical forecasting tool borrowed from economics, is unique among these measures because it can address all of these issues and it can quantify the degree of causal connectivity between neurons (76). PGC makes use of autoregressive modeling (66) to determine if the temporal activity of a pre-synaptic neuron can be used to predict the activity of a possible post-synaptic neuron. Additionally, neural network simulations from Chapter 3 suggest that PGC can be used to quantify synaptic connectivity from simulated spontaneous neural activity. This chapter will explore the use of PGC as a method for detecting pathway specific changes in plasticity in-vitro. PGC will be validated against the pathway information derived using Jimbo's method of spike rate changes pre and post tetanus. PGC should allow for a deeper analysis of plasticity related effects from Jimbo's protocol and new insights will be presented after PGC has been compared against this method.

What do PGC values mean in neural networks?

Connectivity in terms of neural networks is usually expressed as a synaptic weight or synaptic efficacy that can be related directly to the amount of voltage or current that is induced from the pre-synaptic to the post-synaptic neuron. However, it is not intuitively clear what the

values generated by PGC mean in terms of synaptic coupling. A computer simulation, using Izhikevitch's simple neuron model (3), was used in Chapter 3 to determine the effect of known synaptic weights on causality estimates using PGC. These values were calculated from pre and post-synaptic spike trains in order to better demonstrate the relationship between PGC values and synaptic efficacy. Within this simulation the synaptic weight between two regular spiking cortical neurons were systematically increased and the resulting spike trains from the simulation were analyzed using PGC. The results indicated a sigmoid relationship between PGC and the actual synaptic weight in which PGC is insensitive to variations with very low and very high synaptic strengths. The was, however, a linear region (cf. Figure 3-4) in the middle of this sigmoid indicating a region where PGC values are linearly related to synaptic efficacy (and also can be subject to linear arithmetical operators such as subtraction). Based on this relationship, the PGC values recovered from the cortical cultures on the MEA will likely represent the synaptic coupling between these two channels but may be distorted if those weights are excessively low or high. Of course this value may not represent a specific synaptic weight as the connections between neurons in culture may consist of thousands of synapses (97) and may be mediated through several pathways (21). It should provide an overall estimate of the synaptic weights coupling two neurons. Hence, this method could be used to detect changes in synaptic weights among the pathways coupling neurons indicative of plasticity.

Methods

Dissociated Cortical Cultures

Dissociated cortical neural cultures consisted of cortical hemispheres (Brain Bits Inc.) from E18 Wistar rat embryos that were digested using the Papain Dissociation System (Worthington Biochemical Corporation) and mechanically triturated separating the neurons soma from the surrounding connective tissue. After dissociation, approximately 50,000 cells were placed in the

center of a MEA that has been first coated with polyethyleneimine (96) (98) and then also treated with laminin (Sigma) (99). The neurons were cultured in medium consisting of 90 % Dulbecco's modified Eagle's medium (DMEM) (Gibco cat# 10569-010) and 10% Equine Serum (HyClone cat# SH30074.03). The medium was equilibrated in an incubator to 5% carbon dioxide and 35.5C temperature before use. The medium in each culture was exchanged once per week. Freshly dissociated neurons rapidly begin to reestablish a network when placed on the MEA, forming synapses to neighboring cells and producing spontaneous action potentials within the first few days (100). During the first two weeks the neurons mature and begin to express the full complement of receptors, a process completed after one month in vitro (101-104). In this experiment, data from six cultures were analyzed. All cultures were older than 30 days in vitro in this experiment.

Microelectrode Arrays

The MEAs that were used for this experiment were obtained from Multichannel Systems GmBH. The 60 electrodes of each array are arranged in an 8 x 8 grid, spaced 200 μm apart, to measure neural activity over a 1.6 mm^2 area. These arrays consist of a glass wafer over which a gold surface is deposited and the electrode traces are etched using photolithography. An insulating layer of silicon nitride (SiN) is then deposited via vapor deposition over the surface providing an electrical barrier between the gold and culture media. 30 μm diameter holes are then plasma etched over the circular pads and Titanium nitride (TiN) is plated onto the gold forming a low impedance interface between the recording amplifiers and culture media. Each electrode measures the voltage changes produced by neural soma, dendrite, and axons within an approximate radius of 60 μm as they fire action potentials (105). Conversely, application of bi-phasic current or voltage pulses (e.g., 100 to 800 mV or 50 to 200 μA) will elicit action

potentials from neurons near the stimulated channel. Neural activity was sampled and digitized at 25 kHz using Multichannel Systems MEA1060 amplifier and A/D hardware. Action potentials were distinguished from noise using a voltage threshold 5 standard deviations above or below estimated noise levels. Spike events were recorded into a file containing the time, channel, height, width, and context information surrounding each event. This spike file was later processed offline to extract information about any bursts that may have occurred. Bursts were detected using a modification of the leaky integrator algorithm described by Gross (91) which is applied to the spike times for each electrode. The environment both within and surrounding the MEA during recordings was temperature and gas compositionally controlled at 35.5C and 5% CO2 duplicating the environment within the incubator in which these cells were maintained. Media temperature within the array was controlled using Multichannel Systems TC02 temperature controller.

Stimulation Induced Plasticity Protocol

The study of plasticity is a field where much remains unexplored. However, it is one of the most actively investigated areas of brain research. Two distinct and closely related phenomena, long term potentiation (LTP) (106) and long term depression (LTD), have come to be accepted as possible mechanisms by which synaptic efficacy is increased and decreased respectively. While the timing rules thought to underlie LTD and LTP between individual neurons are easily investigated by monitoring the magnitude of post synaptic potentials (PSP) delivered to post-synaptic neurons using patch clamp, single neuron electrophysiological methods are problematic when trying to determine how these mechanisms function at the network level. Neural cultures maintained on MEAs present an opportunity to observe these phenomena on 60 electrodes however MEAs only provide extra-cellular voltage information from these cultures. Thus, while

action potentials can be detected from the neurons grown on MEAs, subtle fluctuations like PSPs are indistinguishable from background noise.

Jimbo et al devised a clever experiment (4) to overcome this limitation to determine the efficacy of a tetanus to induce plasticity changes after its delivery to a single electrode in a dissociated cortical network grown on a micro-electrode array. The protocol consists of a baseline probe sequence, treatment induction tetanus, and a post-treatment probe sequence. Jimbo identifies neural pathways by indicating where LTP and LTD may have occurred by determining the change in spike rate between the probe sequences. The induction tetanus consists of trains of 11 biphasic 600mV pulses delivered at 20 Hz repeated 20 times at 5s intervals. The probe sequences deliver biphasic sequential probes of 600mV to each of the 60 channels (including the ground channel) in a randomized order that is repeated 10 times for a total of 600 probes. Each of these probes evokes a burst of activity resulting from activation of the cortical neural network across all 60 channels. The number of spikes generated from the probe within a 200 ms time window on each electrode quantifies this activity. The baseline and post-treatment spike rate over this 200 ms window for 60 channels for each probe are then compared by difference plot (as shown in the left panel of Figure 4-1) to determine the change in spike rate between baseline and post-treatment probes. The red horizontal lines show instances where the protocol enhanced the spike rate resulting from probing on that channel and the blue lines show instances where the effect of the protocol resulted in depression of the spike rate for probes delivered to that channel.

The use of PGC on these same spike trains should allow for more detailed description of changes in the effective connectivity induced by the tetanus. The protocol yields spike trains for all 60 electrodes following each of the 1200 total probes (60 channels probed x 10 probes per

channel x 2 probe series pre and post tetanus) that are delivered to the neural culture. The ten probes per channel can be considered to be realizations of the same process, thus when calculating PGC between the two channels the 10 source spike (pre-synaptic) trains and 10 response (post-synaptic) spike trains are pooled.

PGC can also be directionally calculated from each channel to every other channel for each probe yielding a 60x60 matrix of directional influences for each probe, 60 times more information than that provided by spike rate. Incidentally, directionality can be eliminated by combining the two directional PGCs between a pair of channels to yield a measure called total causality, similar to coherence, that is more appropriate for validation of PGC against established non-directional spike rate methods. When PGC is calculated for each of the probed channels, this yields a 60x60x60 matrix of PGC results for each probe sequence before and after tetanus. For simplification these PGC matrices generated from elicited data sets will be referred to as elicited Granger Causality (EGC) matrices. When the post-tetanus EGC matrix is subtracted from the pre-tetanus EGC matrix, this will be referred to as the EGC difference matrix. The axes of this EGC difference matrix are stimulus (probed) channel, source channel, and response channel and each entry in the matrix contains the change in PGC from the first set of probes to the second set of probes.

Results

Spike Rate versus PGC

Jimbo's experimental procedure was replicated in our lab[1] on six cortical MEA cultures. Data from neural culture 6686 is used to present results that were consistent across all of the subjects. The timing of spikes was collected from the raw waveforms and then cleaned of noise

[1] The data for this experiment was collected by Ping He as a part of a larger experiment to determine long-term changes in plasticity in the DeMarse laboratory.

spikes by template matching. These remaining spikes were then used to create the rate based stimulus-response plot shown in the left panel of Figure 4-1. This figure plots the changes in the number of spikes post-tetanization by color (blue = decrease, green = no change, red = increase) for each response channel (x-axis) for every probed channel (y-axis). The plot suggests

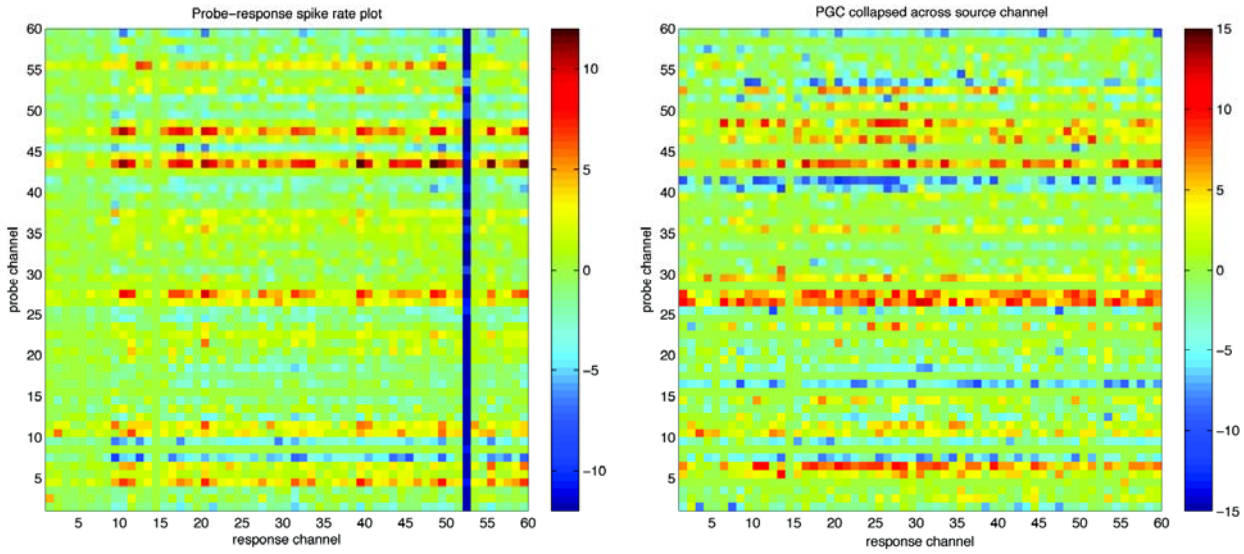

Figure 4-1 Comparison of spike rate to Pairwise Granger Causality. The left plot shows the change in elicited spike rate post tetanus at each channel (x-axis) for each probed channel (y-axis). Each pixel on the plot represents the change, post-tetanization, in elicited spike rate at the response channel from a stimulation delivered to the probed channel. The pathways stimulated by the single channel probes on a particular channel tend to uniformly increase (red horizontal lines) or uniformly decrease (blue horizontal lines). The blue vertical line at response channel 52 is a result of drift during the experiment a noisy channel. This channel would normally be removed from analysis. The right plot is an analysis of the same data using PGC. This plot shows the change in PGC post-tetanization for each response channel (x-axis) for each stimulated probe channel (y-axis). The change in PGC for each pixel can be interpreted as the change in the effective connectivity of the response channel to all other channels. PGC similarly detects pathway specific plasticity, but does so by looking at changes in effective connectivity between channels rather than changes in spike rate. Notice that the analysis of channel 52 yields no effect (green represents no change in PGC) as the noisy spikes from channel 52 have no effective relationship with other channels. Additionally, PGC offers greater contrast of post-tetanus effects. The enhanced contrast can especially be seen when comparing response channels 1-9 between both plots.

simultaneous enhancement and depression of spike rates similar to the data previously reported by Jimbo et al. (4). PGC was then calculated for each of the probe sequences and reported as a stimulus-response difference-plot shown in the right panel of Figure 4-1. This is essentially interpreted the same as the left panel except that the colors represent a change in PGC instead of spike rate. Note that the 3-dimensional EGC matrix is separately collapsed across the source and response axes and the results are summed to create the 60x60 plot shown in Figure 4-1. This is done to reduce the complexity of the EGC matrix to allow direct comparison to the spike rate results. A simple visual comparison between the left and right panels in Figure 4-1 shows that, in general, any changes in rate are also reflected in changes in causality. Of the 60 probe channels, the results of more than 95% of probe channels match direction of change when comparing spike rate and PGC stimulus-response plots.

However, there are some noticeable differences between the two plots . PGC is influenced by changes in rate but only when the rate increase on the pre-synaptic channel is complemented by an increase on the postsynaptic activity. The data from dish 6686 was specifically chosen to help reinforce this notion due to a unique event that occurred. Most noticeable, the spike train data from channel 53 (the dark blue vertical stripe) in the left panel of Figure 4-1 was contaminated with background noise and generated false spikes that were similar enough to real spikes that they could not be filtered out. During the recording following tetanization the source of the noise was removed resulting in a large decrease in spike rate for this channel. When PGC is calculated for the noisy uncorrelated random spikes from this channel PGC yields values near zero, as one would predict for temporally unrelated time series. Thus, PGC reports the changes in the temporal relationship between channels rather than a simple change in rate. This is further reinforced by the data from channels 1-9 that show little change in spike rate across all probe

channels in the left panel of Figure 4-1 but show changes in PGC (right panel of Figure 4-1). Additionally, some channels show stronger changes in PGC than those shown by spike rate as shown in examples depicted in Figure 4-2a for LTP and Figure 4-2b for LTD. This is not surprising considering that changes in synaptic efficacy can be reflected by changes in the pre and postsynaptic spike timings that may appear in changes in spike rate.

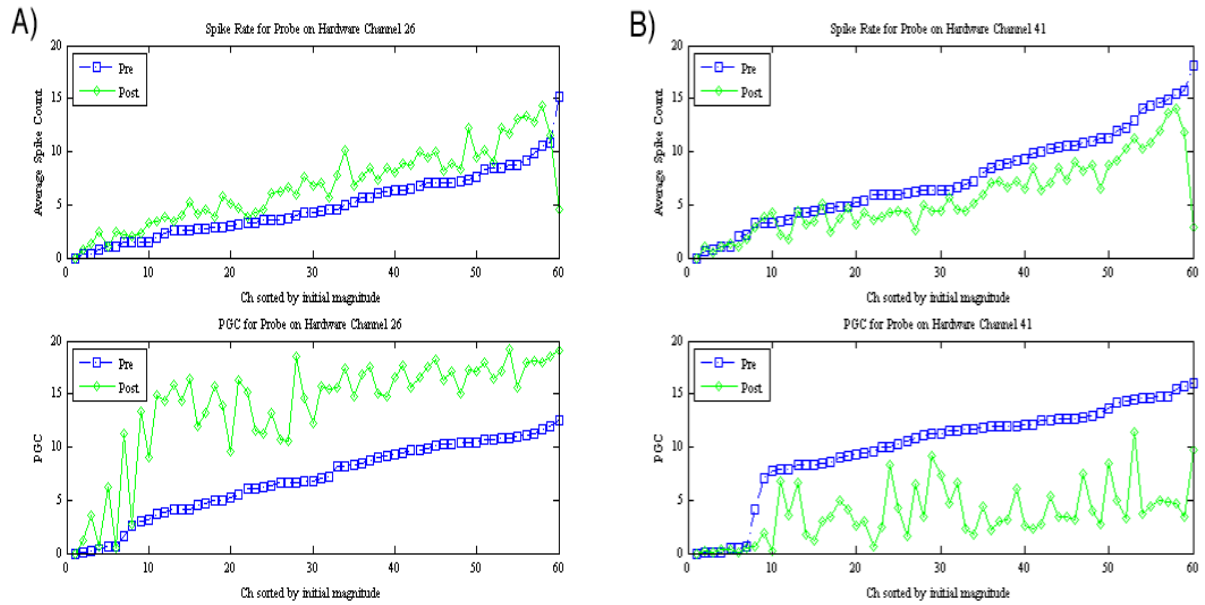

Figure 4-2 A comparison of spike rate and PGC analysis for enhanced channel 26 and depressed channel 41. This figure highlights the increased contrast provided by PGC over spike rate by comparing spike rate (top panels) or PGC analysis (bottom panels), sorted by initial strength (x-axis), before and after tetanization (blue square vs. green circles, respectively). Panel A shows potentiation in terms of spike rate (top) and PGC (bottom) for channel 26 from Figure 4-1. Panel B shows the same relationship for the depressed channel 41. In both cases PGC provides greater contrast between baseline and post treatment measurements for both potentiation and depression. The increased contrast provided by PGC makes it easier to establish the statistical significance of pathway specific changes.

Surrogate Analysis

A subtle but important difference between the two methods is that the right panel of Figure 4-1 has considerably higher contrast between effected channels and surrounding unaffected channels i.e. less regions that are light yellow or light blue. This suggests that the signal to noise

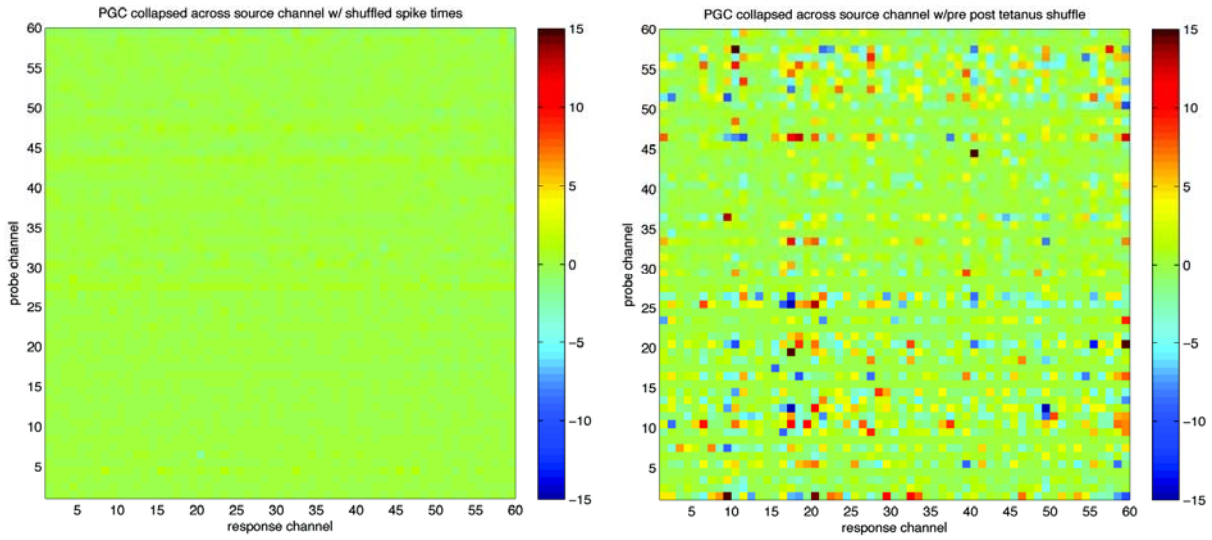

Figure 4-3 Surrogate analysis of the PGC analysis. Two surrogate analyses were performed on the data from the Jimbo protocol. The first, shown in the left plot, is a result of randomly shuffling the spike timings within the 200ms post stimulation window for both the pre and post-tetanus prior to PGC analysis. This effectively destroys the spike timing relationships while maintaining the spike rate over this window. The resulting PGC analysis yields near zero PGC results for both pre and post-tetanus probe sets. The resulting change in PGC post-tetanus shown in the left figure is near zero (hence a uniform green field) for all pathways. This spike-shuffled surrogate analysis also establishes a significance threshold that can be used to distinguish actually changes shown in Figure 4-1 from noise. Note that if the spike shuffled data were used to generate a spike rate plot, it would be identical to the left panel in Figure 4-1. The second surrogate analysis, shown in the right panel, shuffles the pre and post-tetanus spike trains. The pathway specific patterns observed in Figure 4-1 are obliterated. This suggests that the plasticity induction protocol is responsible for producing these pathway specific patterns and that these patterns are not randomly generated.

ratio for PGC is higher, allowing for a greater contrast between effected channels and background noise. Additionally, the use of PGC also has the added benefit of having a statistical significance level. A surrogate data set can be created from the original spike trains that maintains the spike rate information in the spike train but scrambles the interspike intervals by randomizing the spike timings for a given spike train. The null hypothesis for this first surrogate is that changes in spike rate are responsible for the corresponding changes in PGC. A well established principle of PGC is that when the two time series being regressed are made up of

independent white noise PGC=0. In practice with real spike trains a surrogate data set with randomized spike timings will produce a value that approaches zero establishing a threshold by which the significance of the unscrambled can be determined from. GC values falling above this threshold can be considered significant and non-random. Once the spike timings were scrambled the same causality analysis was performed on the surrogate spike trains. The resulting analysis, shown in the left panel of Figure 4-3, confirms that the patterns demonstrated by the original data set are significant considering that the significance levels generated from the surrogate data set are all in the green (i.e. close to zero change) region of the color scale. This also invalidates the null hypothesis suggesting that the PGC analysis is not simply dependent on rate and is likely dependent on changes in interspike timing between channels.

A second surrogate analysis was created by randomly swapping out pre-tetanus spike trains with post tetanus spike trains from the same stimulus and source/response channels. This surrogate, while not restricted to use with only PGC analysis, serves the purpose of determining whether the pathway specific patterns resulting from the Jimbo protocol are randomly produced. The null hypothesis for this surrogate is that failed probes are responsible for the patterns seen in rate and PGC analysis. Thus, swapping probes between post and pre-tetanus analysis would test this hypothesis. PGC analysis is then performed on this surrogate data set with results shown in the right panel of Figure 4-3. Notice that the pathway specific patterns inherent to the non-surrogate data set have been obliterated. This surrogate analysis randomized the pre/post-tetanization temporal order of the spike train realizations. If the pathway specific plasticity effects were randomly generated from failed probes, the effects should have persisted in the surrogate analysis. Subsequently, these results suggest that the second surrogate null hypothesis is invalid.

Discussion

The original hypothesis for this experiment was that PGC could be used to describe pathway specific plasticity effects in dissociated cortical culture. Comparison of PGC results against spike rate validated this hypothesis. Over 95% of the pathways described by spike rate were found to agree with the PGC analysis. Often, those channels that differed from the spike rate analysis were channels that showed no spike rate change but showed a change in PGC. This was likely due to fact that PGC specifically models changes in the fine temporal dependencies between spike trains rather than relying on course changes in rate. While spike rate has the advantage of being simple and easy to obtain, use of PGC compliments spike rate as a more statistically rigorous and perhaps more sensitive metric. PGC was also shown to be more resilient to the introduction of noise spikes into the analyzed spike trains as demonstrated by the noisy channel 52 in Figure 4-1. PGC was also shown to provide a higher contrast between pre and post-tetanus analysis as shown in Figure 4-2. Statistical significance was more easily established using a spike-shuffled surrogate analysis. This surrogate analysis also suggests that pathway specific PGC plasticity results are not simply spike rate dependent but reflect true changes in causal strength between the channels.

However, these are not the only benefits to using PGC. For comparative purposes the SGC matrix was intentionally collapsed and the benefit of directionality was removed in order to better validate and compare the results of PGC against the non-directional spike rate method. The following discussion explores these directional effects providing a deeper analysis including amplitude dependent plasticity, comparisons of spontaneous and elicited PGC analysis, and directional plasticity that can be described by PGC.

Amplitude Dependent Plasticity

Directionality is a fundamental property of PGC that distinguishes it from other methods such as correlation and coherence. Directionality has been intentionally removed from the analysis so far to enable better comparison to non-directional spike rate based methodology. However, directionality is a key component of STDP timing rules for plasticity. Directional information about plasticity changes should allow a more complete understanding of how induced plasticity affects the underlying structure of the network. When the EGC difference matrix is calculated without using total causality several new options emerge for visualizing plasticity. One use of the EGC difference matrix is that it can be used to determine how the initial magnitude of a pathway affects magnitude and direction of change of that pathway after tetanization. The EGC difference matrix contains 60x60x60 entries whose values can be compared to the same number of pre-tetanus EGC matrix values.

According to amplitude dependent plasticity (ADP) shown by Bi & Poo, changes in synaptic weight due to correlated time dependant spiking are a function of initial synaptic strength. While potentiation of excitatory postsynaptic potentials (EPSPs) is larger for weak synapses, those experiencing depression are reduced by a constant percentage (84). EPSPs are commonly measured postsynaptically using single electrode voltage clamp techniques. In this analysis, we investigate ADP among the pathways observed during Jimbo's protocol. However, unlike in Bi & Poo's experiments, MEA electrodes are extracellular and cannot measure EPSPs. Thus, the starting effective connectivity is compared to the change in effective connectivity using pairwise Granger Causality (PGC) calculated from prior analysis. If the observed changes in plasticity by PGC are accurate then one would expect that the magnitude and direction of changes within the network would agree with previously reported ADP results (84).

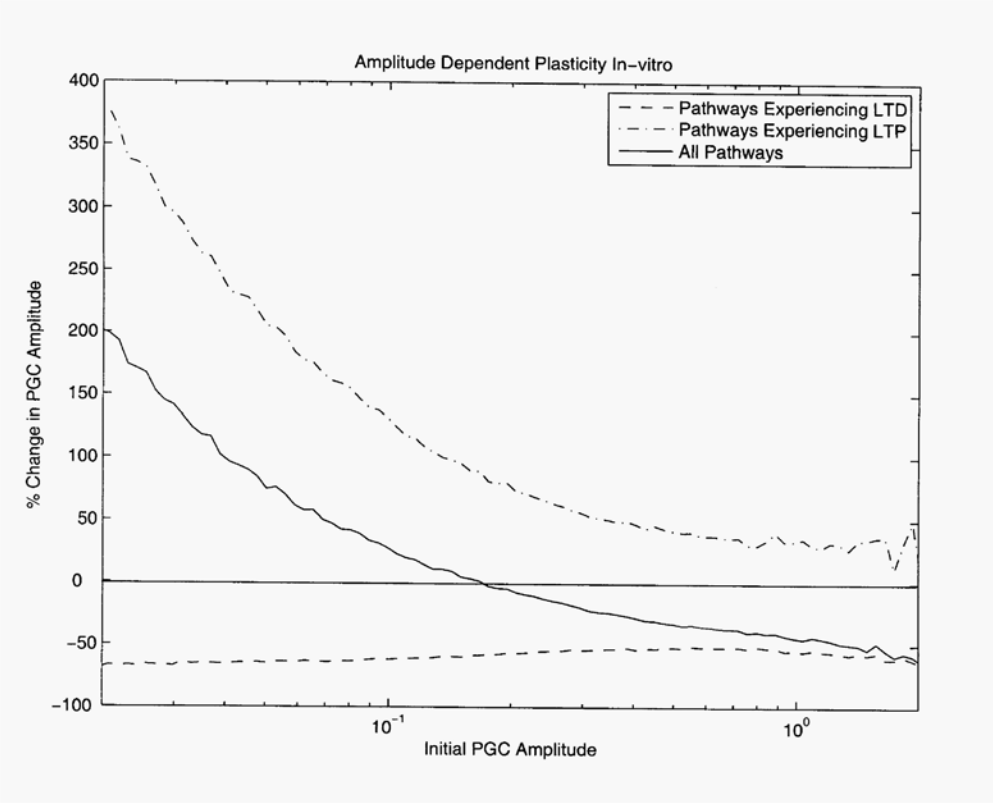

Figure 4-4 Amplitude dependent plasticity (ADP) can be explored in-vitro using PGC. According to amplitude dependent plasticity (ADP), changes in synaptic weight due to correlated time dependant spiking are a function of initial synaptic strength. This plot shows initial magnitude of PGC prior to induction (x-axis) and the corresponding directional change magnitude after induction (y-axis). This demonstrates that the tetanic induction generally increases weak connections and decreases strong connection. This plot resembles results reported by Bi & Poo 1998 where postsynaptic potentials were observed using intercellular recordings. Data shown is a compilation from six cortical cultures exposed to tetanization.

The entire pre-tetanization EGC matrix was used as starting weights and the EGC difference matrix was used to report changes in those weights. These results were plotted Figure 4-4 where the initial PGC amplitude for all pathways was plotted on the x-axis and the % change in the PGC amplitude was plotted on the y-axis. This plot contains data from 6 MEA cortical cultures where Jimbo's protocol was used to induce plasticity. Overall Figure 4-4 suggests that weak pathways are most often enhanced while strong pathways are weakened. At around initial PGC values of 0.25 depression begins to be favored over potentiation as the initial strength of the

pathway increases. These results suggest that changes in connectivity post tetanus may be amplitude dependent which is consistent with the results from Bi & Poo.

Directional Causal Influences

The EGC difference matrix is large which can make detection of network changes difficult to visualize. Thus, when trying to understand what is happening in the EGC difference matrix it is preferable to collapse the matrix along one of its axes for simplification. However, when

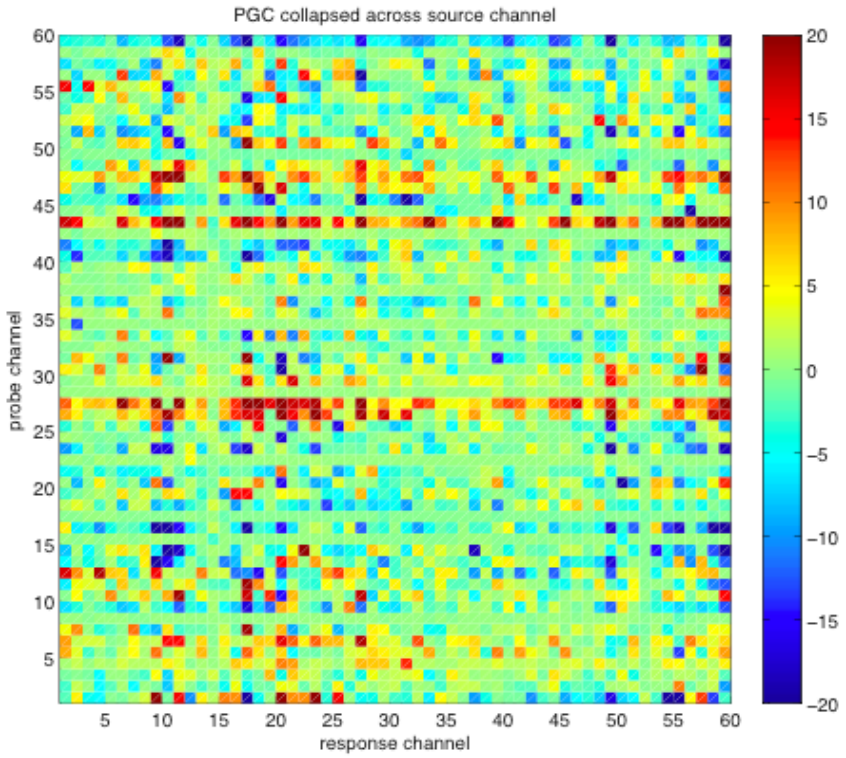

Figure 4-5 Stimulus-Response difference plot of PGC where the EGC difference matrix is collapsed by source. While similar to the left panel of Figure 4-1, this plot makes use of the directional properties of PGC. Essentially each pixel represents the change in causal information coming *in* to each response channel. This plot shows the directional change in PGC post-tetanization for each response channel (x-axis) for it corresponding stimulated probe channel (y-axis). Red pixels indicate a potentiation of inward causal flow while blue pixels indicate depressed inward causal flow. The change in PGC for each pixel can be interpreted as the change in the effective connectivity of the response channel to all other channels.

directionality is involved, which axis is collapsed has a profound impact on what information that figure will present. The available axes to collapse upon are source, response, and by probe channel. When collapsing the EGC difference matrix by source (as was done earlier to match spike rate plots), each pixel is a summation of all of the causal influences from all source channels into each individual response channel for a given probe. This is shown in the resulting stimulus-response PGC plot shown in Figure 4-5. Thus, collapsing the EGC difference Matrix by source reveals the information flow coming into every channel for each probe and produces a

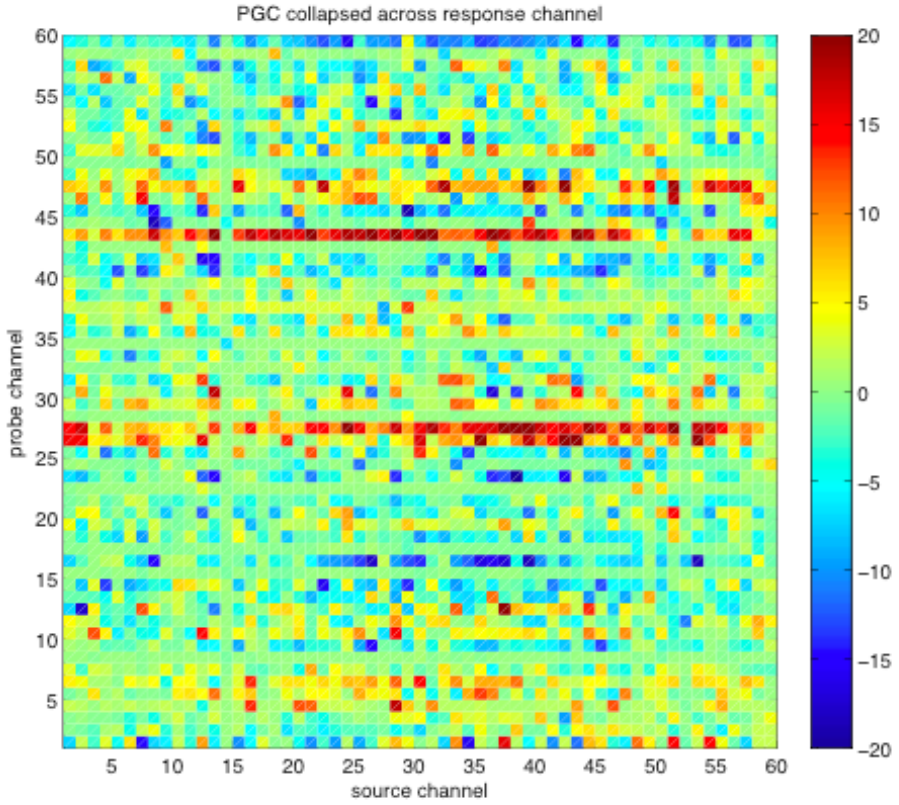

Figure 4-6 Stimulus- Source difference plot of PGC where the EGC difference matrix is collapsed by response. This plot makes use of the directional properties of PGC, essentially each pixel represents the change in causal information coming *out* of each source channel. This plot shows the directional change in PGC post-tetanization for each source channel (x-axis) for it corresponding stimulated probe channel (y-axis). Red pixels indicate a potentiation of outward causal flow while blue pixels indicate depressed outward causal flow. The change in PGC for each pixel can be interpreted as the change in the effective connectivity of the source channel to all other channels.

stimulus-response plot. When collapsing across the response axis, as shown in Figure 4-6, the stimulus-source plot's pixels represent the summation of information flow from each individual source channel to all response channels. Thus, collapsing the GC Matrix by response channel reveals the information flow coming from every channel for each probe resulting in a stimulus-source plot. Comparison of Figures 4-5 and 4-6 suggests that while after tetanization a pathway may experience an increase consistent with LTP, a subset of the response channels experience an increase in total information outflow while others experience an increase in total information inflow. The same complementary observation can be seen with depressed probe channels that are thought to experience LTD. Logically, this is consistent with the idea that an increase/decrease in information outflow pre-synaptically should be matched by a corresponding increase/decrease in information inflow post-synaptically. This reinforces the notion that the tetanus elicited changes in the neural network consistent with STDP mechanisms.

When collapsing across the remaining probe channel axis, as shown in Figure 4-7 the source-response plot's pixels represent the summation of information flows from a source channel to a response channel for every stimulating probe. Thus, collapsing the EGC difference matrix by stimulus channel reveals the directional information flow for each source-response pair for all probes. Collapsing on this axis produces a source-response plot that is more consistent with what could be observed in a recording of spontaneous activity from a MEA culture. The 60 source-response slices of the EGC difference matrix of size 60x60 are also shown in Figure 4-8 at their respective probe locations in a spatial arrangement meant to replicate the placement of the electrodes in the MEA culture dish. These plots specifically speak to the larger amount of information available when using PGC methods instead of spike rate. Using the spike rate method an investigator can observe the change in spike rate at 60 channels following a probe.

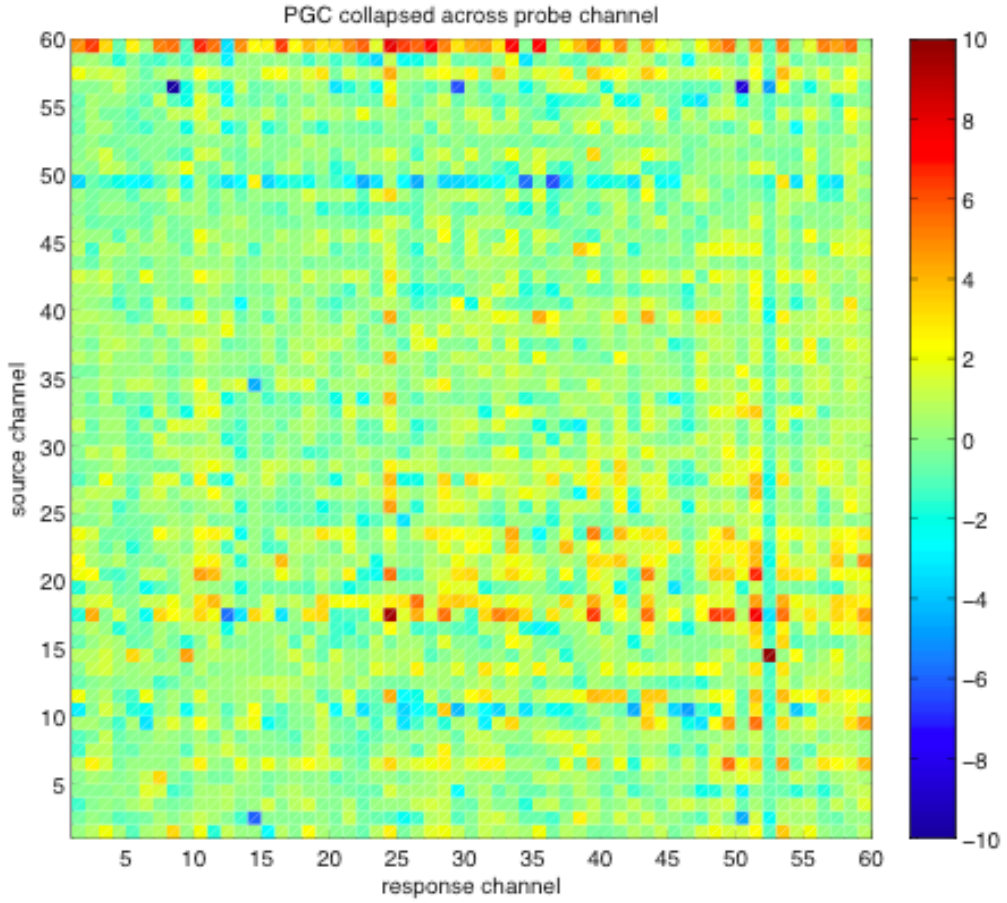

Figure 4-7 Source-Response difference plot of PGC collapsed by probe before and after application of tetanus. This plot shows the directional change in PGC post-tetanization for each source channel (x-axis) for it corresponding stimulated probe channel (y-axis). Each pixel shows the total information flow from each source to each response channel over all probes. This plot is a sum of all of the source response plots that are plotted later in Figure 4-8. This represents the total change in causality from elicited activity over all probes for every pathway.

However, when using PGC, 3600 possible directional pathways can be observed for each probe. This is largely due to the fact that rate based changes are non-directional and non-causal. So when a probe is delivered only the changes in spike rate at distant channels can be observed. When using PGC spike trains from any channel can be compared to any other channel. One of Jimbo's observations was that the spike rates at distant electrodes for a specific probe channel tend to change uniformly in one direction either depression or potentiation.

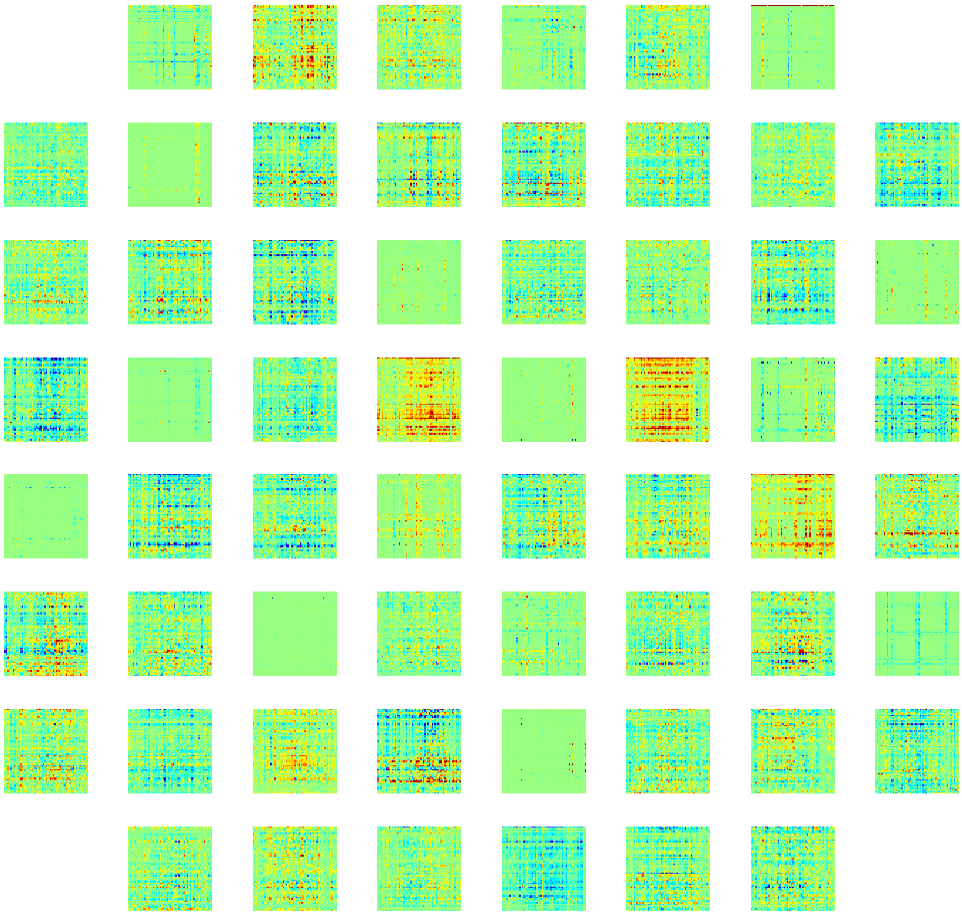

Figure 4-8 Source-response plots by spatial probe location. These source-response plots (each interpreted the same as the source response plot in Figure 4-7 but for single probes rather than all probes) are arranged topographically by the location at which the probes were delivered to create the respective source response plots. This plot is a difference plot showing the entirety of the 60 x 60 x 60 PGC difference matrix for one MEA culture treated with Jimbo's protocol. Notice that while some channel were dominated by potentiation (red) and others dominated by depression (blue), most channels simultaneously demonstrate both potentiation and depression.

Interestingly, the plots in Figure 4-8 tell a slightly more complex story. While there are some probes that produce changes in activity that fit this profile, in fact most probes show both depression and potentiation within the network, information that is lost when averaging across source or response channel axes. While potentiation or depression may win out after collapsing to create a source-response plot, both mechanisms are most often present before collapsing. However, PGC produces results that agree with some of Jimbo's major points. While probing at

a channel activates the entire network, the pathways and synapses activated depend on where the probe was delivered. This explains how a pathway can produce potentiation for one probe channel and in turn show depression when a different probe channel activates those same neurons. Thus, a similar conclusion as Jimbo's can be drawn from these source-response plots that the observed changes are pathway-specific and not neuron specific.

Spontaneous/Elicited Connection

PGC can also be applied to spike trains from spontaneous rather than evoked activity. This presents an interesting opportunity to compare source-response plots from the EGC difference matrix to source-response plots from spontaneous activity. Recordings of spontaneous activity were taken before and after tetanization during this experiment. Spike trains were collected from population bursting events inherent to spontaneous activity in MEA cortical cultures, as opposed to collection from a time window after stimulation as with elicited bursts. The spontaneous burst events were detected using a burst detection algorithm based on several found in literature. A window of 200ms is used to capture the activity from the burst. Unlike data collection from an elicited time series the number of events is based on the spontaneous bursting activity of the culture rather than based on a predetermined number of probes. The spike trains are low pass filtered and used to calculate PGC values for every source and response pair for both pre and post tetanus spontaneous recordings. The resulting difference matrix, or spontaneous Granger Causality (SGC) difference matrix, is 60x60 and includes PGC values for every source to every response channel. The resulting plot, shown in Figure 4-9, is most similar to the source-response plot generated from the GC matrix collapsed across probe shown in Figure 4-7. Theoretically these two plots should resemble each other as they are both source-response plots.

The connectivity in the spontaneous source-response plot is a result of the expression of spontaneously activated pathways during population burst events. The pathways activated are

dependent on the patterns of the bursts expressed by the culture, which is dependent on many factors possibly including spatial origin, connectivity, and environmental factors. While the patterns are similar between elicited and spontaneous activity and are likely linked there are many reasons why they should not completely agree. Spontaneous activity is a direct result of the probabilistic processes that drive single unit activity in the network. Which bursts patterns occur and those that do not are dependent on this process. In contrast, elicited bursting is not dominated by this process. Each electrode is systematically probed and responses are observed. It is likely

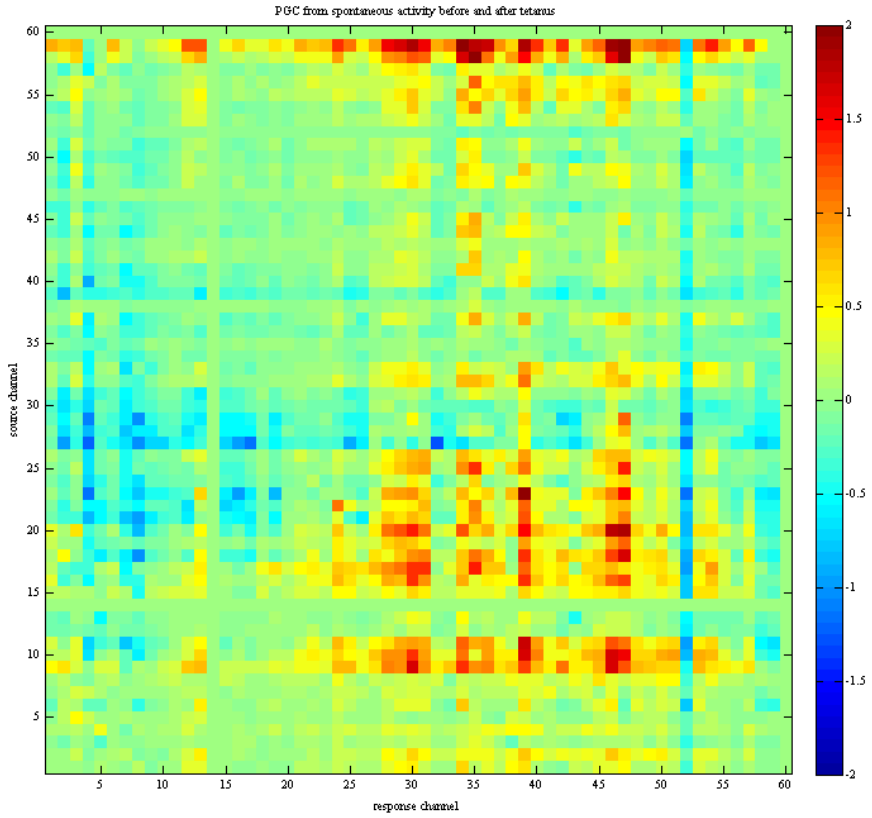

Figure 4-9 Spontaneous Source-Response plot calculated from windowed bursting events during spontaneous (no stimulation probes) activity. This source (y-axis) response (x-axis) plot represents the difference in PGC calculated from spontaneous bursts before and after the delivery of the tetanus. Again the colors represent the change in causality (blue = decrease, green = no change, and red = increase). This source response plot should resemble the source response plot after collapsing by probe shown in figure 4-7 if PGC analysis of spontaneous and elicited data is similar. Some similarities are seen between these plots suggesting a connection between stimulated and spontaneous neural activity.

that many of the pathways activated by probes are part of forced burst patterns that may be rarely if ever generated from spontaneous activity and are thus missing from spontaneous connectivity plots. Additionally, the elicited patterns are generated from 600 elicited burst events while the spontaneous activity produces perhaps 20-30 burst events. Despite these differences, there is similarities between the patterns from spontaneous and elicited source-response plots reinforcing the linkage between spontaneous and elicited activity patterns.

Conclusions

The inverse source problem has proven a formidable obstacle for neuroscientists when exploring network level plasticity mechanisms in vitro. While synaptic efficacy can be monitored using glass pipette electrodes to detect and measure post-synaptic potentials, large-scale use of these electrodes to monitor network activity is problematic. MEAs are a well-established means of obtaining multichannel recordings from living neural networks but do so extra-cellularly. To estimate plasticity using these arrays Jimbo et. al. devised a protocol that reveals some pathway information for dissociated culture grown on an MEA by observing changes in spike rate after the simultaneous induction of LTP and LTD. While spike rate is an elegantly simple means of detecting pathways using this protocol, it is that same simplicity that limits the amount of information that can be garnered. We have proposed the use of PGC as a means of extracting synaptic efficacy from the spatiotemporal activity generated from elicited and spontaneous activity. The linear relationship between PGC values and synaptic weight was demonstrated in a simple biologically relevant neural model. The model demonstrates a linear relationship in the region beginning where the synaptic efficacy is large enough to cause some post-synaptic action potentials and ending where the synaptic weight is so large as to cause post-synaptic action potentials every time the pre-synaptic neuron fires. It is only within this region that PGC values change significantly in relation to synaptic weight suggesting that experimental

changes in PGC likely scale linearly to synaptic efficacy. Thus, there are circumstances, when changes in synaptic efficacy are not reflected in neural spiking activity changes, and will not be reflected in changes in PGC. However, based on this modeling it is reasonable to assume that changes in PGC values are likely reflective of changes in synaptic efficacy.

The applicability of PGC to plasticity studies in-vitro was verified against established experimental plasticity protocols with an established analysis method, spike rate change. Comparison of PGC results to spike rate results shows that PGC is not only sensitive enough to be used to detect plasticity but also provides information on the structural connectivity underlying recorded neural activity prior to treatment.

While the two methods did not agree on all pathways, this can be easily explained by the fact that PGC is sensitive to changes in inter-spike timing associated with LTP and LTD that changes in spike rate may not detect. Conversely, some changes in spike rate may not be reflected in a change in causality for similar reasons. Additionally, the creation of surrogate data sets by shuffling the spike timings within individual realizations demonstrate that PGC possesses a sound statistical foundation that allows discrimination between signal and noise events. Directionality was intentionally removed to make the comparison to spike rate, however when included it enables several new analysis methods to be used in conjunction with plasticity experiments. With baseline connectivity available, it is possible to track changes in connectivity after treatment in the context of these beginning values. This analysis yields results similar to previously reported empirical observations of STDP in-vitro where whole cell patch-clamp methods were used to monitor synaptic efficacy directly (84). Additionally, this plot suggests that synaptic efficacies may be being driven towards equilibrium, illustrated by the transition from potentiation to depression around values of 0.25 for PGC. Not only does this show that the

connectivity changes within the network are unlikely to be random, it also shows that there may be some sort of homeostatic mechanism (107) at work within the network.

Changes in information outflow from a channel can be visualized when the EGC difference matrix is collapsed across the source axes, making use of the directional property of PGC. Conversely, changes in information inflow can be visualized when the EGC difference matrix is collapsed along the response axis. Comparison of these two plots for individual probe channels that experience LTP (or LTD) certain groups of neurons experience and increase (decrease for LTD) in information outflow while other distinct groups specifically experience a complimentary increase (decrease for LTD) of information inflow. This result suggests that the observed changes in connectivity are specific and directional rather than uniform across the dish. A uniform increase in connectivity could be indicative of fluctuations in environmental conditions such as temperature rather than a result of STDP. Directionality also allows collapsing the probe axis to create source-response plots for each channel probed, rather than just being able to observe distant changes in spike rate in relation to the probe channel. These plots show that, while one STDP mechanism may dominate for a probed channel, often LTP and LTD both occur among the various pathways activated. Also, these plots reaffirm the concept that changes in plasticity are pathway specific rather than neuron specific. This can be seen when a pathway demonstrates potentiation in one source-response plot but shows depression when the location probed changes. This suggests that, even though the same neurons are involved, the pathway is different. Collapsing across these source-response plots by probe also has a logical connection to PGC source-response plots generated from spontaneous activity. This connection may prove useful in the design of future experiments in that it may not be necessary to perform a probe sequence in order to observe changes in neural network structure. It is clear that PGC can

describe changes in network connectivity and not only compliments the use of spike rate but also exceeds it in terms of the amount of information provided about the pathways underlying neural activity. However, there are limitations of PGC that must be considered.

A causal relationship between two channels may be due to a common unobserved driving influence. Additionally, it is possible that PGC values for a pathway will contain mediated influences in addition to direct causal influences. These mediated influences would distort the relationship between PGC values and synaptic weight. However, even with mediated influences included, the changes observed are indicative of changes in the underlying structure of the network for that pathway, not necessarily directly between two individual neurons. The complexity of the synaptic connectivity within any given pathway prohibits a complete description of all the synaptic weights within that pathway, given the finite fixed electrode placement of MEAs. However, PGC makes the most of the data available by enabling a deeper analysis of these pathways, than previously implemented methods. Results from simulated pathways suggest that PGC can relate changes in "synaptic weights" within a pathway to changes in the spiking output of postsynaptic targets. This suggests that changes in PGC observed in pathways in-vitro represent changes in synaptic weights somewhere within these pathways. This conclusion is further reinforced by in-vitro PGC results that suggest that amplitude dependent plasticity occurs within pathways. This phenomenon has been well described at the cellular level but never at the network level. These results suggest that PGC can describe changes within in-vitro pathways that are known to occur at synapses between individual neurons. Additionally, directional analysis of the EGC difference matrix suggests that some areas experience specific changes in output while others experience corresponding specific changes in input. This further suggests that pathway specific changes are real and

directional rather than random and undirected byproducts of natural variation. While much work needs to be done to fully capture individual changes between neurons, these results suggest that PGC is a useful tool for uncovering effective relationships in dissociated in-vitro cortical neural networks grown on microelectrode arrays.

CHAPTER 5
DIFFERENTIAL TETANAZATION OF SINKS AND SOURCES IN DISSOCIATED CORTICAL CULTURE

Introduction

Granger Causality was used in the previous chapter to identify changes network within in-vitro cortical networks grown on microelectrode arrays. Granger Causality was also shown to provide a better representation of the effective connectivity between channels before and after the application of a tetanus. Moreover, unlike spike rate based methods, Granger Causality could measure connectivity without the necessity of tetanization (i.e., it does not require a difference between pre and post measurements). In this chapter, information about effective connectivity will be used to predict *a priori* changes in plasticity prior to experimental manipulation. The central hypothesis of this chapter is that if information about connectivity can be known before hand and it is accurate, then this information can be used to predict the direction in which plasticity will change when tetanizing a specific channel on the array.

Granger Causality provides information about which channels are causality related to other channels and the direction of that relationship. In essence, the experimenter knows who is connected to whom and how they are connected (i.e., direction). Between single neurons where a presynaptic neuron is synaptically connected to a post synaptic neuron, it has been shown that stimulating the presynaptic neuron followed ~1 to 100 ms later by a stimulation of the postsynaptic neuron will increase the efficacy of that synapse. Conversely, stimulating the post synaptic neuron before the presynaptic neuron results in the depression of that synapse (a decrease in efficacy) (84, 108). This is known as spike timing dependant plasticity (STDP) (83, 109) where the timing of activity or stimulation determines the strength of the synapses in a network. If information about the structural connectivity between neurons recorded with our MEAS were known then it should be possible to select a causally connected pair of neurons and

stimulate that pair to either potentiate or depress the synapses between them dependant on the timing of the stimulation (pre vs post or post vs pre).

However, each channel on the MEA records from several neurons simultaneously. In addition, a single stimulation pulse (e.g., a single biphasic 600 mV 200 us pulse) may activate neural activity in *a wide area* surrounding the stimulation electrode, but this is of course dependant on the voltage that is applied. Instead of attempting to identify a particular pair of neurons perhaps identifying channels whose primary relationship to others was to drive activity in those channels could be a solution (i.e., an analog of a pre-post synaptic relationship). Stimulating that driving channel would essentially be similar to a presynaptic-stimulation /postsynaptic-activation. In other words, spike timing dependant potentiation of that synapse and perhaps result in an increase in causal strength between that channel and others. Conversely, stimulating a channel, whose primary relationship with others is as a target (i.e., a sink where other channels converge to drive activity on this channel), should result in the depression of that pathway. In other words, a postsynaptic neuron stimulated before its presynaptic counterparts.

Of course, identification of causal sinks and sources within the cortical culture would be critical for the execution of this stimulation paradigm. For this study, a sink is defined as a node (channel) within the culture where the balance of causal information flow is inward to the node. In contrast, a source is defined as a node where the balance of causal information flow is outward from the node. When PGC is calculated between two channels A and B, PGC analysis yields results from A to B as well as from B to A. Sinks and sources could then be identified when PGC analysis is carried out amongst all channel parings. Summing PGC values for all pathways leading out of a channel, ΣF_{out}, represents total information flow coming out of that channel. Summing PGC values for all pathways coming into the same channel, ΣF_{in}, represents total

information flow coming in to that channel. Positive values of the difference, $\Sigma F_{out} - \Sigma F_{in}$, would indicate a source within the neural network (i.e. dominated by information outflow) while negative values would indicate a sink (i.e. dominated by information inflow). See Seth et al for a similar identification technique that has been tested in artificial networks (55).

In this chapter, an experiment is described that tests whether differential tetanization of sink channels versus source channels produces differing outcomes. Activity from in-vitro cortical networks will be measured to identify the location of potential sinks and sources among the channels on the array. A source channel will then be tetanized and changes in plasticity will be measured. The prediction is that the causal flow out of this source channel should increase. A sink channel will then be tetanized and the prediction is that causal flow into this sink channel should decrease.

Background

Identification of Neural Sinks and Sources

Identification of sources and sinks of neural activity in multichannel data has proven useful in many theoretical and experimental neuroscience paradigms. For example, identification of sinks, sources, and the corresponding current flow within hippocampal slice is useful for mapping neural circuits within the hippocampus (110, 111). Causality in the form of the Directed Transfer Function has been used in epilepsy to detect the source of seizure generation also known as the seizure focus (112) from EEG. This is done so that the seizure focus can be surgically removed, effectively ending seizures in a patient. Essentially, the seizure focus is located by finding a source of causation within the epileptic brain. This method has also been used with ECoG signals to determine the ictal source (113, 114). Ding et al. refined the use of

the Directed Transfer Function so as to be used with EEG rather than ECoG because the use of ECoG electrodes is invasive requiring placement under the dura.

Plasticity by Tetanization

Plasticity has been studied in-vitro using MEAs in several published experimental protocols (4, 18, 21, 115). Most often plasticity is induced at an active channel (where activity has been recorded) using a tetanic stimulation. The frequency, amplitude, and duration of these tetanic stimulations have varied between investigators. For example, Jimbo (4) applied a tetanization sequence of 100ms (20 trains of 10 bipolar 100μs 0.6V pulses at 20Hz every 5 seconds) while Shahaf (18) employed a constant train at 1, 0.5, or 0.3Hz (each pulse is biphasic 50μA 500μs) until the desired plasticity was achieved. Tateno et al (21) applied tetanic pulse trains (similar to those used by Jimbo) to two channels simultaneously in the same culture.

Where the tetanus is delivered in the culture varies between investigators as well. Often the tetanus is simply delivered at a highly active channel that elicits a network burst response when stimulated. Interestingly, it has been shown that channels whose activity is strongly correlated with the channel during tetanus are most often potentiated while those that are weakly correlated are most often depressed (4). This sort of reasoning is merely an observation however and requires the experiment to be conducted first before the direction can be determined. In contrast, we are able to determine what the effective connectivity is for a channel *prior* to tetanization based merely on spontaneous neural activity recorded before any stimuli are delivered. The correlated changes described by Jimbo et al are however consistent with our notion that when these channels are tetanized (they would appear as sources in our analysis) the activity produced by that channel should be enhanced (i.e., increase).

Experimental Design

The experiment used 10 mature (all subjects were more than 35 days old) cortical neural networks grown on MEAs. Each subject was exposed to 2 tetanic pulse trains (20 0.2Hz trains

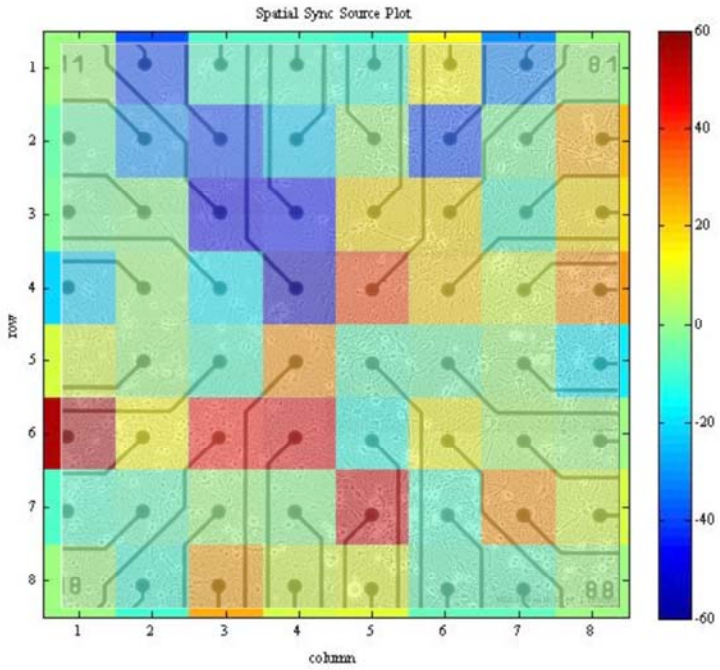

Figure 5-1 Topographical map of sinks and sources spatially laid out and superimposed on a picture of the microelectrode array. Sinks are blue while sources are red (green indicates neutral) all calculated from spontaneous bursting activity using Pairwise Granger Causality. Row 4, Column 4 represents a strong sink and Row 7, Column 5 represents a strong source. Each of these would be candidates for tetanization to differentially induce depression or potentiation, respectively..

of 10 bipolar 100μs 0.5V pulses at 20Hz) 1 per day delivered to either a sink or source. Sinks and sources will be identified immediately prior to tetanization from baseline recordings of spontaneous activity for 10 minutes. We will then identify burst events in these spike trains using an algorithm that uses a thresholded global spike rate to detect the onset of each burst. The end of the burst is detected using the quiescent time after the burst where no spiking occurs (116). A 200ms window of spiking activity is then extracted following the onset of each burst.

These spike trains windows were then low pass filtered at 50 Hz so that Pairwise Granger Causality can be used to determine causal relationships between all combinations of channels. Since each burst is treated as a realization of the same process over 100 realizations can typically be used to calculate PGC from the 10-minute recordings.

The total inflow of causation into an electrode is calculated by summing the PGC values that include the specified electrode as the destination of causation. Similarly the total outflow of causality is calculated by summing the PGC values that include the specified electrodes as the source of causation. The difference between total outflow and total inflow will be used to determine whether a particular electrode is a sink (negative values of this difference) or a source (positive values of this difference). This value will be calculated for every electrode in the MEA and displayed spatially to allow selection of the electrode for tetanization. An example of a map of sinks and sources within a cortical culture is shown in Figure 5-1. This plot shows the difference of total inflow and total outflow represented by color (red = source, green = neutral, and blue = sink) for each electrode overlaid over an image of a microelectrode array. This type of arrangement allows for easy spatial identification of where sinks and sources are in the cortical culture. The electrode selected for tetanization will be limited to electrodes that are not on the edge of the culture to better allow observation of effects from tetanization. Each dish will be tetanized once per day on either a sink or a source depending on the requirements of the experimental design lattice. The first day of this protocol will consist of 5 randomly selected cultures tetanized on sinks and 5 cultures tetanized on sources. The second day will reverse the tetanization of sinks and sources for each culture. Thus, over the course of this two day experiment each dish will be tetanized on a sink and a source.

Spontaneous vs. Elicited Activity as a Measure of Plasticity

Spontaneous and elicited bursting are both based on the structure of the same underlying network and logically reflect similar patterns of connectivity. However, spontaneous bursting activity is initiated with firing probabilities and patterns that are generated dynamically within the neural network. Elicited bursting patterns, while dependent on the same underlying structure, is evoked artificially and can generate patterns that spontaneous activity may not (also a possible reason the test probe sequences can induce plasticity). Changes in spontaneous bursting activity revealed using correlation matrix based methods have been used to identify plasticity related changes post tetanus (20). In this experiment, the difference between pre-tetanization connectivity estimated by PGC from spontaneous baseline activity prior to tetanization will be subtracted from PGC estimates post-tetanization to determine the changes in connectivity that result from tetanization protocol.

This experiment will use two primary means of detecting plasticity after tetanus. Both of these methods were developed in chapter 4. First, PGC will be used on spontaneous activity (pre and post tetanization) to create a source response difference-plot to determine whether pathway specific potentiation and depression occurs as a result of the tetanization. Essentially this will mean looking for potentiated and depressed source and response pathways. Blue (depressed pathway) or red (potentiated pathway) horizontal and vertical lines in source response plots would be an indicator that plasticity may have occurred. Additionally, an amplitude dependent plasticity effect (ADP) (84) was also found from the data analysis in chapter 4. Bi and Poo found that the post synaptic potentials (PSPs) (the magnitude of the voltage will be referred to as "weight") in the post-synaptic neuron in a simple neuron pair exposed to negative spike timing (post-synaptic neuron fires before pre-synaptic neuron) would elicit depression. These depressed pathways would decrease by a constant percentage independent of starting "weight". However,

when exposed to a positive spike timing (pre before post) potentiation would occur that was dependent on the starting "weight". Specifically, smaller PSP were increased by a larger percentage than larger ones. In chapter 4, this relationship was found in pathways analyzed using PGC from elicited spiking activity, rather than measing PSPs directly. This analysis is made possible by PGC providing a measure of effective connectivity in the pre and post

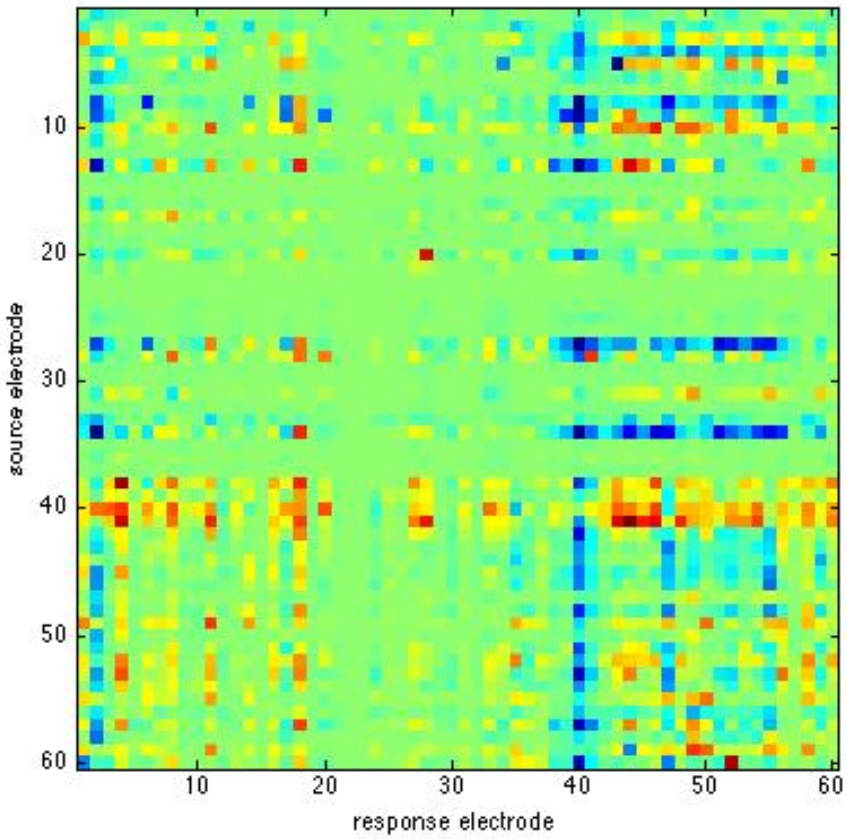

Figure 5-2 Source response plot for culture 9059 tetanized on a sink. This plot shows the change in PGC post-tetanization. The y-axis is the source electrode while the x-axis is the response electrode. Changes range from depression shown in blue to potentiation shown in red. Green indicated no change. Notice that channel 40 experienced a increase in causal output (red horizontal stripe at source electrode 40) and simultaneously experienced a decrease in causal input (blue vertical stripe at response electrode 40).

tetanization results. Thus, it is possible to use the pre-tetanization PGC analysis as starting "weights" for the observed pathways and use the resulting post-tetanization PGC analysis to

calculate a change in these “weights”. This ADP analysis will also be used to determine whether plasticity occurs during this experiment. ADP results will also be statistically analyzed to determine the direction of any change in plasticity is consistent with out predictions.

Results and Discussion

Results

The experiment was run over the course of two days as described earlier. During the experiment it was easy to notice that cultures grown on certain MEAs showed a larger amount of causality between electrodes than those that were likely experiencing failures in the insulation of the electrode tracing. Cracks in the insulation cause leakage of current from the electrode tracing (117). These cracks can decrease the signal to noise ratio of the electrodes making it increasingly difficult to distinguish actual spiking events from noise events. Based on this observation, 2 of the cultures were removed from the statistical analysis (dish 9299 and 9058). The are included in the tables, however. Several of the MEAs, where insulation damage was likely, were not removed because the effect was not as severe. PGC was calculated for before and after the tetanization for all subjects in the experiment. The measures mentioned earlier we used to first determine whether plasticity occurred during the course of this experiment.

First, a source-response difference plot was constructed for each trial to qualitatively determine what type of plasticity effects were seen post-tetanization. An example of these plots are seen in Figure 5-2 for a culture tetanized on a sink and Figure 5-3 for a culture tetanized on a source, demonstrating that both potentiation (indicated by red) and depression (indicated by blue) occurred when tetanizing on sinks and sources. Notice that there are horizontal lines representing changes in the output of a channel and vertical lines representing changes in the input to a channel. These results are consistent with plasticity shown by Jimbo, showing

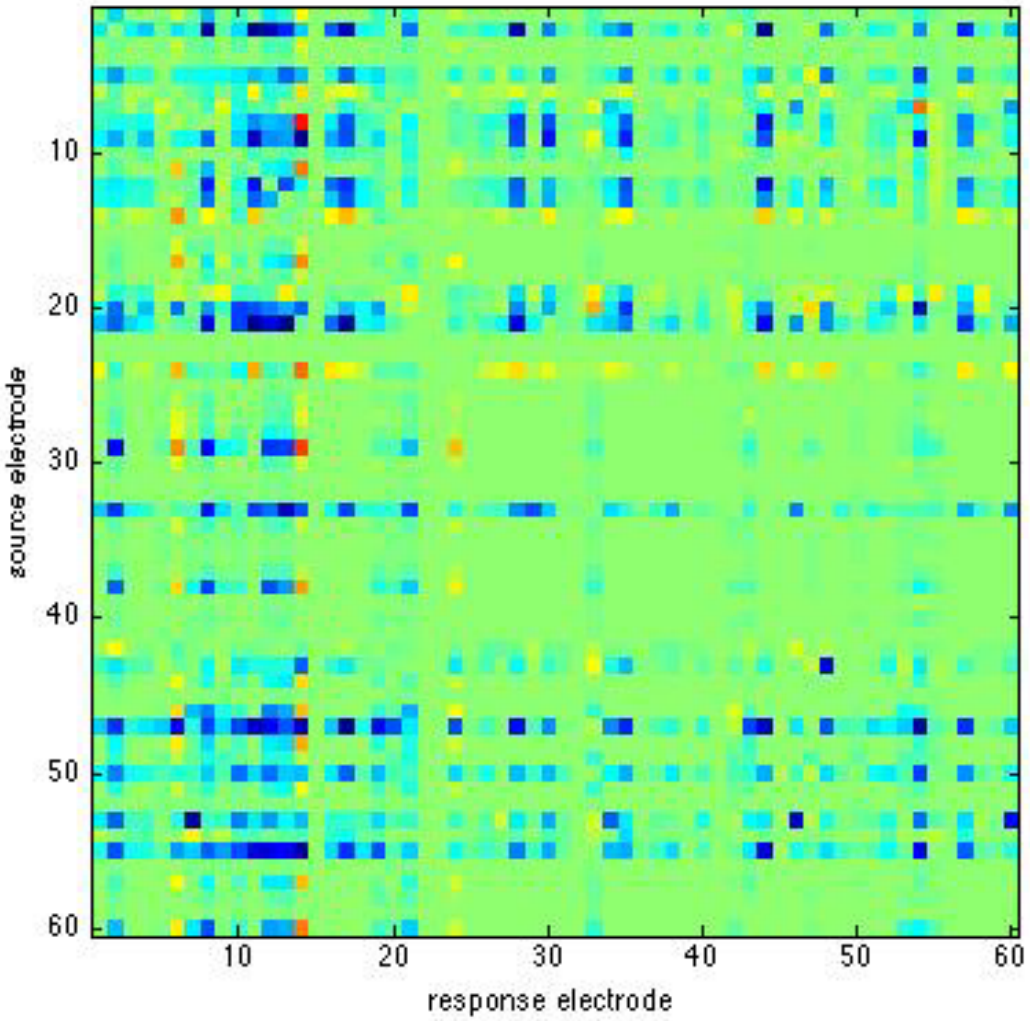

Figure 5-3 Source-response plot for culture 9449, which was tetanized on a source. This plot shows the change in PGC post-tetanization. The y-axis is the source electrode while the x-axis is the response electrode. Changes range from depression shown in blue to potentiation shown in red. Green indicated no change. Some channels were depressed while others were potentiated.

simultaneous potentiation and depression for pathways in the culture. Second, the PGC analysis was examined to look for any ADP trends. Plasticity effects similar to those reported in Chapter 4 were found. This analysis will be elaborated on in the ADP analysis section. However, both of these key indicators suggest that plasticity consistent with the experiment in Chapter 4 occurred. The remaining analysis will determine if these effects were consistent with the predictions made earlier.

Table 5-1 Global culture causality changes post-tetnanization. The change in causality was assessed for sinks and sources by summing total causality for all of the pathways in the culture pre and post tetanus and taking the difference between these values. No consistent differential is seen between sinks and sources. Greyed out values were not used in statistical analysis.

Culture	Change in total causality after Tetanization at a Sink	Change in total causality after Tetanization at a source
9447	42.22	118.86
9449	-229.07	-97.04
9448	-89.39	-90.88
9450	-22.82	-155.91
9299	12.16	14.77
9291	51.9	-17.26
9272	16.2	62.67
9059	9.34	11.25
9058	21.95	3.06
9053	-13.85	-39.65
Mean	-29.43	-25.99

Qualitative inspection of the stimulus response plots for each subject shows no observable difference between tetanization of a sink versus a source. A variant of this metric used was quantitatively comparing the difference in a sum of all causality for all pathways pre and post-tetanization. This was done for the entire array as a global measure and also for the tetanized channels alone. A statistical analysis of the resulting difference in causality finds that there is no difference between tetanization on a sink versus a source ($F(7,7)=0.001$, the raw results are shown in Table 5-1). Cultures experience both global increases and global decreases for tetanization both on sinks and sources. This result is not unexpected since changes described by Jimbo involve correlations with the tetanized channel. When looking at the tetanized channels alone there is a noticeable change in the magnitude of the causality for the pathways leading out of sources and into sinks. Statistical analysis shows that while the direction of change (potentiation versus depression) is not consistent across all subjects sinks or sources, the magnitude of the changes are statistically significant ($F(7,7)=6.40$ for sinks and $F(7,7) = 3.23$

Table 5-2 Tetanized channel total causality changes post-tetanization. The change in causality was assessed for sinks and sources by summing total causality for only the tetanized pathway pre and post tetanus and taking the difference between these values. No consistent differential is seen between sinks and sources. Grayed out values were not included in statistical analysis.

Culture	Tetanized Sink Change in Outward Pathways	Tetanized Sink Change in Inward Pathways	Tetanized Source Change in Outward Pathways	Tetanized Source Change in Inward Pathways
9447	1.84	10.44	-0.78	-1.24
9449	-1.78	-10.12	-15.44	0.42
9448	-0.44	-8.18	-3.87	-0.09
9450	-0.04	-11.01	-1.38	-0.92
9299	0.12	-1.68	0.10	0.60
9291	-0.07	-1.56	1.04	-0.59
9272	-0.29	-.012	0.58	-0.01
9059	-0.78	0.80	1.72	0.22
9058	1.88	0.12	1.63	-0.06
9053	-3.16	-4.12	-3.91	0.38
Mean	-0.59	-2.97	-2.75	-0.22

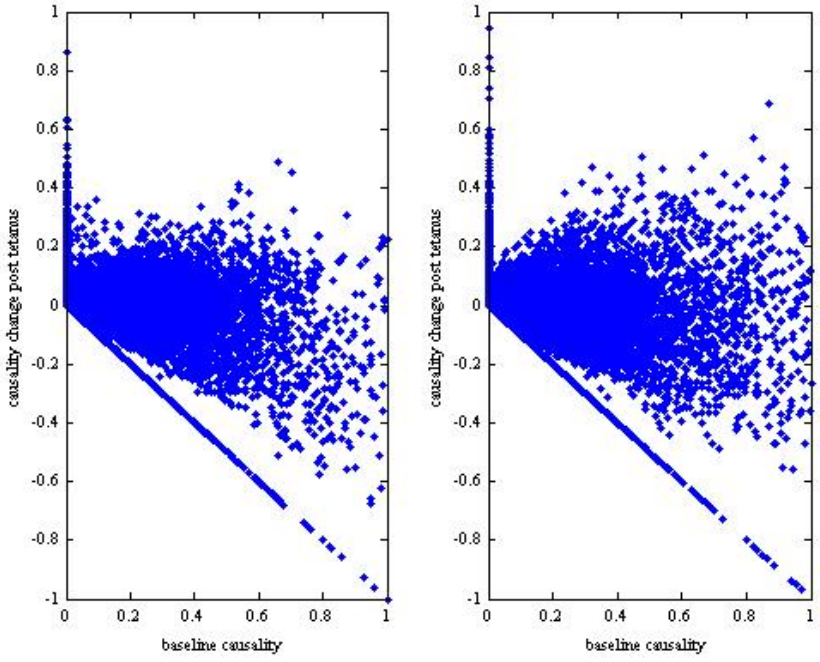

Figure 5-4 Culture wide Amplitude Dependent plasticity. Each pathway's initial causality is plotted on the x-axis while it's corresponding change after tetanization is the y-axis. This is a compilation of the effects seen for all 10 cultures. The effect for sinks is seen in panel A while the effect for sources is seen in panel B. There is no observable or statistical difference between these two plots and no differential effect between sinks and sources.

sources) for pathways leading out of sources and into sinks when compared to the magnitude of changes for pathways in the opposite direction.

ADP is the final method used to determine if plasticity related effects followed the primary hypothesis. This was not only used to compare sinks versus sources, but to also get an idea of whether a pathways magnitude could be used to predict changes post tetanization. Again, the results are compared globally across the entire dish and on the tetanized channels alone. Global ADP is plotted for all pathways in Figure 5-4 panel A) for all sinks and panel B) for all

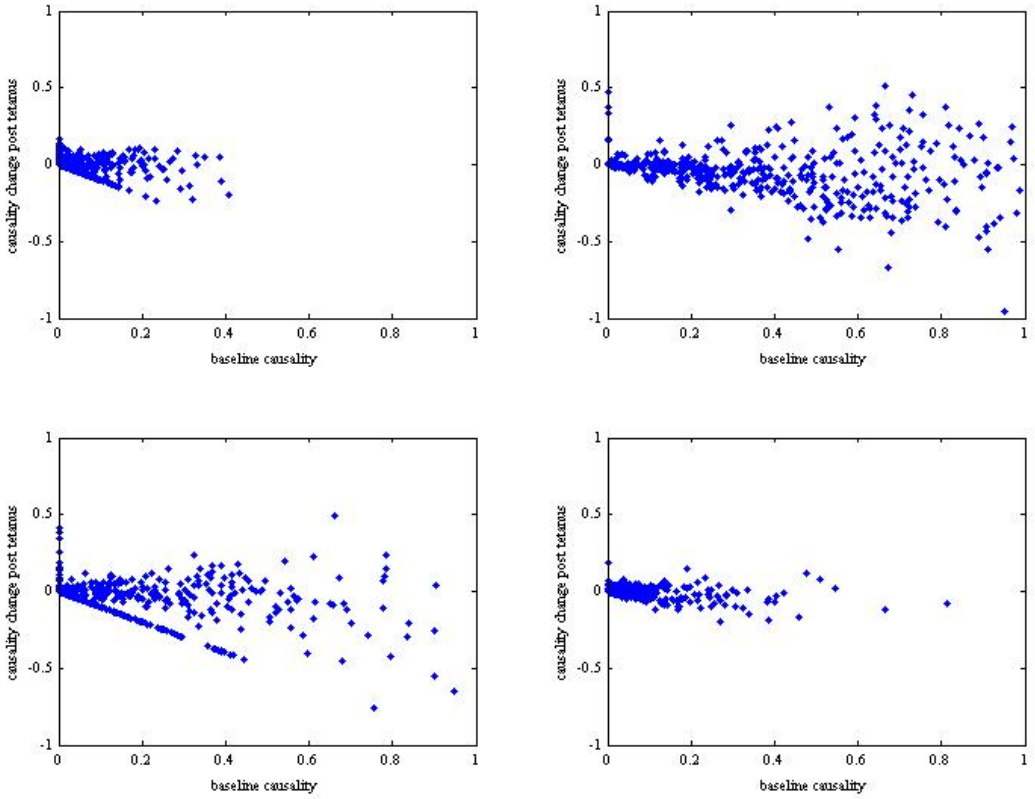

Figure 5-5 Tetanized channel amplitude dependent plasticity. The initial causality of pathways involving the tetanized channel's is plotted on the x-axis while it's corresponding change after tetanization is the y-axis. Panel A are the pathways coming out of the tetanized sinks. Panel B are the pathways coming into tetanized sinks. Panel C are the pathways coming out of the tetanized sources. Panel D are the pathways coming into tetanized sources. There is no observable or statistical difference between these two plots showing no differential effect between sinks and sources.

sources. Visual inspection of these graphs shows them to be very similar. A linear model for ADP (initial causality versus change in causality) was calculated for each of these graphs to allow for a quantitative comparison. Both models are standard linear models of the form y=mx+b. The slope, m for the sink plot is -0.20 while the slope for the source plot is -0.14. These slopes suggest that larger weights in both cases typically are depressed. This is true for all models in this study. It is worth noting that the intercepts of all models in this study are small and positive, suggesting a small region where small weights are typically potentiated. It is of immediate interest that the norm of the residuals is high for both models at 13.0 and 13.8 respectively. The variability in higher magnitude starting causalities is likely the source of the poor fit. Essentially, these models cannot be considered different, thus there was no global differential effect. This finding is in line with previous global observations. The same metric and methods are then applied to only the tetanized channels segregated by sink and source as well as by pathways coming into and pathways coming out of that channel, shown in Figure 5-5. The parameters for the models fit to the plots are shown in Table 5-2. These plots and models fit to them may explain why large significant deviations were found on channels coming out of sinks and into sources from earlier sink source analysis. On first inspection the slope of tetanized sink pathways average -0.23 while tetanized source pathways average -0.11, suggesting that sink pathways may be depressed more. However, the norm or the residuals for pathways coming into sinks and pathways out of sources remain large at 3.22 and 3.94 respectively, suggesting high variability especially in the higher starting causality region. The norms of the residuals pathways coming out of sinks and into sources is much better at 1.06 and 0.70 respectively. However, it's easy to notice that the goodness of fit for these pathways is likely improved because of the virtual lack of strong initial causalities for these pathways. This

suggests that the statistical effect shown in the earlier sink source analysis may be a result of the way sinks and sources were chosen rather than any differential effects due to tetanization. Overall, this suggests that no significant differential effects were detected.

Conclusions

This experiment did produce plasticity similar to the results reported earlier in Chapter 4. This can be seen in the comparison of the ADP trends from this experiment and the replicate of the Jimbo experiment. These results suggest that the tetanic stimulations in this experiment produced similar ADP related changes seen in Chapter 4. The cultures also showed simultaneous potentiation and depression another hallmark of the Jimbo protocol. This result suggests that changes that occurred post tetanization are not simply dependent on global shifts in spike rate. These effects were seen in Figure 5-2 and 5-3 for both sinks and sources. This suggests that it does not matter whether spontaneous or elicited activity is used to reveal the effects of tetanization using PGC.

The predicted direction of that changes based on stimulating a sink versus a source were not supported. The prediction made in this experiment was that a differential effect would be seen when sink and sources, identified using connectivity derived from spontaneous activity, were tetanized. It is possible that the effective connectivity revealed from spontaneous activity is not a good predictor of what pathways will correlate with a pathway when it is tetanized. However, this only explains why an ADP effect may not be seen. This does not account for the predictions made based on STDP rules. The likely reason why these predictions did not work is because STDP rules are based on changes between a single pre synaptic neuron and a single postsynaptic neuron. Predictions in such a simple network would be easy to predict. The cortical culture used in these experiments is created from 50,000 dissociated embryonic neurons that randomly connect to form a neural network. The actual connectivity in these cultures is

much more complex than the controlled conditions in the experiments by Bi and Poo (118). The MEA can simultaneously observe the activity of nearly 100 neurons. These neurons may have thousands of synapses with other neurons in the culture (97) and many of these connections may be bidirectional. Additionally, it is difficult in this complex network to control what pathways experience positive and negative spike timings. Reverberating connections and feedback loops may present many spike timings to the same synapse. Additionally, the effects of the spike timings from spontaneous bursting during and after the tetanus may have an effect. Perhaps the STDP based predictions, which were based on results from two isolated mono-directionally coupled neurons, are too simplistic given the complexity of the connectivity in these dissociated cultures.

This experiment was devised to be a proof of concept for being able to measure the effective connectivity in the dish and then be able to manipulate that connectivity based on this knowledge. While the predictions for this experiment may have been too simplistic for this system, future studies could benefit from the use of PGC to reveal connectivity before experimental manipulation. Future studies may also benefit from a reduction of the complexity of the cortical culture by reducing the density of the culture. Another possible strategy may be to use a paired pulse paradigm to better control the spike timings in the targeted pathways.

CHAPTER 6
ANALYSIS OF TEMPORAL LOBE SEIZURES USING GRANGER CAUSALITY

Introduction

Prior research in this body of work have focused on using Granger Causality metrics to reveal effective connectivity relationships in neural simulations and in in-vitro dissociated cortical culture. These experiments provided new insights into the connectivity underlying these networks and new metrics of plasticity. However, one ultimate goal for this research is to provide an analytical technique to better understand on how the intact brain functions. Data from the Evolution into Epilepsy Project at the University of Florida presents a unique opportunity to explore the in-vivo dynamics and effective connectivity relationships of seizures from an animal model of temporal lobe epilepsy (TLE). High quality 32 channel data from microwires was continuously recorded in vivo from rats at a high sampling rate (25 KHz per channel). The data from these animals include multiple seizure events from several animals. The 32 electrodes were bilaterally located in the hippocampus and afforded the opportunity to look at 992 $\left(\frac{n!}{(n-k)!}; \text{n=32 channels, k=2 for bivariate model} \right)$ different directional hippocampal interactions on multiple time scales using Granger Causality.

In this chapter, the first goal is to first determine if Granger analysis can provide anatomically relevant descriptions of effective connectivity in that anatomical structure. In contrast to the dissociated cortical cultures used in the previous two experiments, the anatomy and the physiology of the hippocampus is well established (119). However, descriptions of the effective connectivity of the hippocampus from implanted microwire arrays are rare in general and nonexistent for seizure behavior. The second goal is to provide a better description of the dynamics and causal relationships with and between hemispheres underlying seizure activity and

how they differ from those observed during baseline activity. This chapter will also provide a brief description of TLE, animal models of TLE, and the Evolution into Epilepsy Project.

Temporal Lobe Epilepsy

Epilepsy is a disorder that effects roughly 2% of the population. The most common type of epilepsy among adult patients is Temporal Lobe Epilepsy (TLE) (120). The symptoms of TLE are well defined and classified by the International League Against Epilepsy (ILAE). Simple Partial Seizures involve small areas of the temporal lobe and typically do not affect consciousness. They are often characterized by auras or periods where sensations such as sounds or smells are felt that are not actually present. Complex partial seizures can affect consciousness and the ability to interact with others. Often, the symptoms include staring, automatic movements of the hands and mouth, and other abnormal behaviors. Seizures associated with TLE can also spread to the rest of the brain causing Secondarily Generalized Tonic-Clonic seizures. The tonic phase of this type of seizure is characterized by stiffening of the limbs and body in either a flexed or extended position. The following clonic phase is characterized by uncontrolled jerking of the limbs and body. Electrophysiologically, TLE is characterized by seizure activity that can be recorded from the hippocampus. Physiologically, TLE is also characterized by hippocampal sclerosis consisting of pyramidal cell loss, granule cell dispersion, and gliosis within the hippocampus. Also, patients with TLE can often be cured of seizure activity (80-90% success) by the removal of the hippocampus, suggesting that the hippocampus implicating it as a potential source of TLE seizures.

There are several animal models used to study TLE. These include models where TLE is induced pharmacologically and also those that use electrical stimulation. Of those that use stimulation some require stimulation to elicit a seizure while others involve spontaneous seizure generation. For example, kindling is produced by repeated subthreshold focal electrical

stimulation of the brain. After these stimulations have been delivered for sufficient time the targeted area reaches a “kindled state” where a single stimulation will produce a secondary generalized seizure. However, these seizures remain stimulus locked requiring a stimulus pulse to generate seizure events. In contrast, Lothman (121) has developed an animal model with spontaneous seizures in which the rat is stimulated once with a high frequency superthreshold stimulation designed to immediately induce status epilepticus. The resulting limbic seizures damage the hippocampus and result in recurrent spontaneous seizures that develop and increase in severity over time. This model is used by researchers at the University of Florida in the Evolution into Epilepsy (EIE) Project (40) to study the electrophysiological and physiological changes that occur between the time of stimulation and the expression of spontaneous seizures.

Animal Model of Chronic Limb Epilepsy

The TLE animal model used in the Evolution into Epilepsy Project has been in use for the last two decades (121). In the weeks that follow this stimulation, the rat progressively demonstrates recurrent spontaneous hippocampal seizures. The temporal and electrographic progression of rats treated with this model closely resembles that of human patients that have chronic mesial temporal seizures. The surgical and electrophysiological techniques used by the Evolution Into Epilepsy (EIE) project team at the University of Florida are described below.

The rats were prepared according to procedures approved by the University of Florida IACUC. The rats are adult male Sprague-Daly rats that are 50 days old. The surgical procedure consists of a craniotomy from 1.7 mm lateral to 3.5mm lateral of the bregma so that electrodes could be implanted into areas due to their prominent role in epileptic discharges (122). A 2x8 rectangular array of electrodes was implanted bilaterally in both hemispheres so that they cover the CA1/CA2 area to the DG. The electrode placement is shown in Figure 6-1 with the surgery shown in the left panel of Figure 6-2. The spacing between electrodes is 400 μm on the short

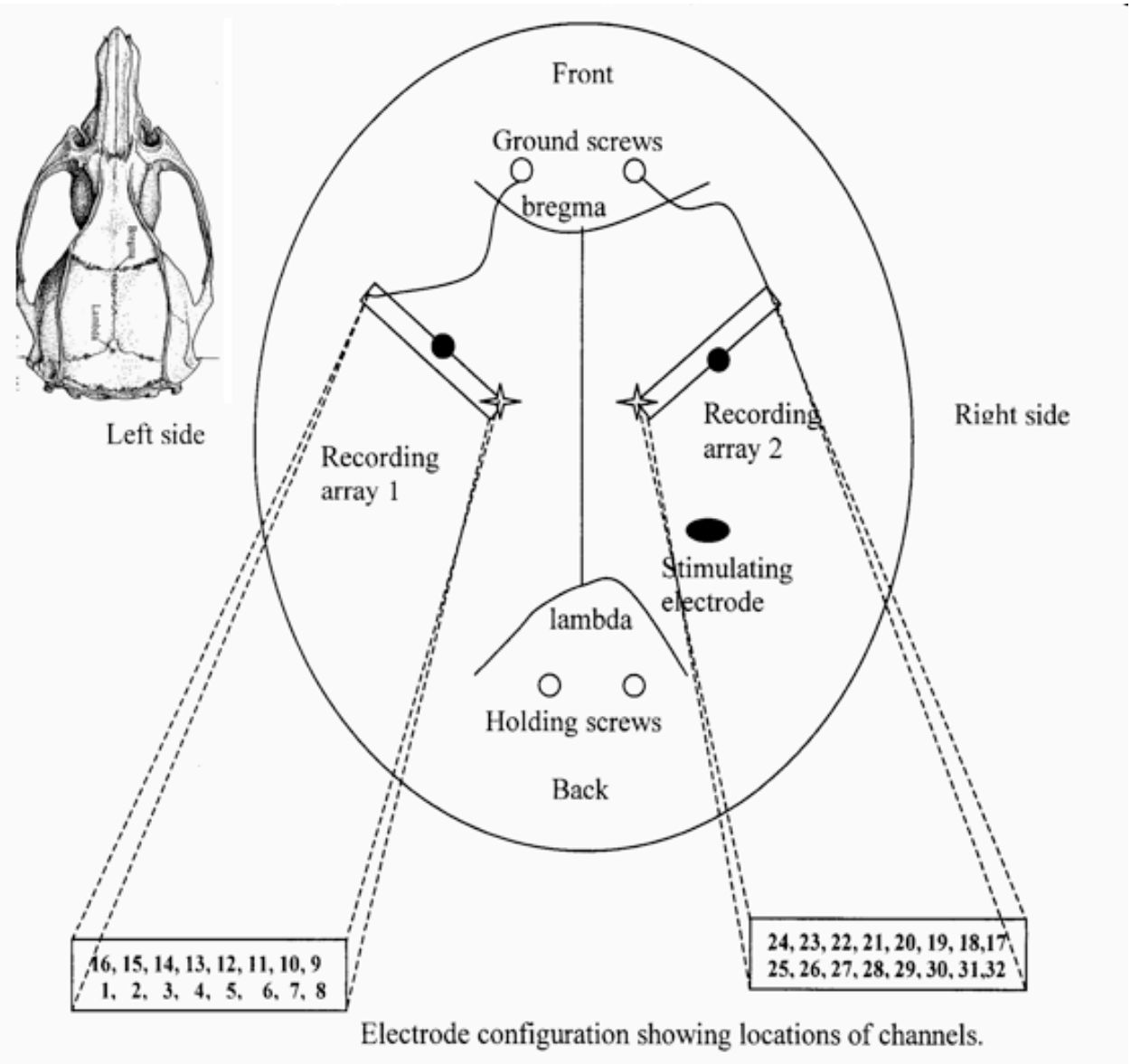

Figure 6-1 Diagram of microelectrode placement in the rats brain. The upper left is a representation of the skull of a rat showing the bregma and lamda locations. The cartoon in the main caption shows the orientation of the electrode strips and the corresponding location of individual electrodes. (Used with permission from Dr. Paul Carney).

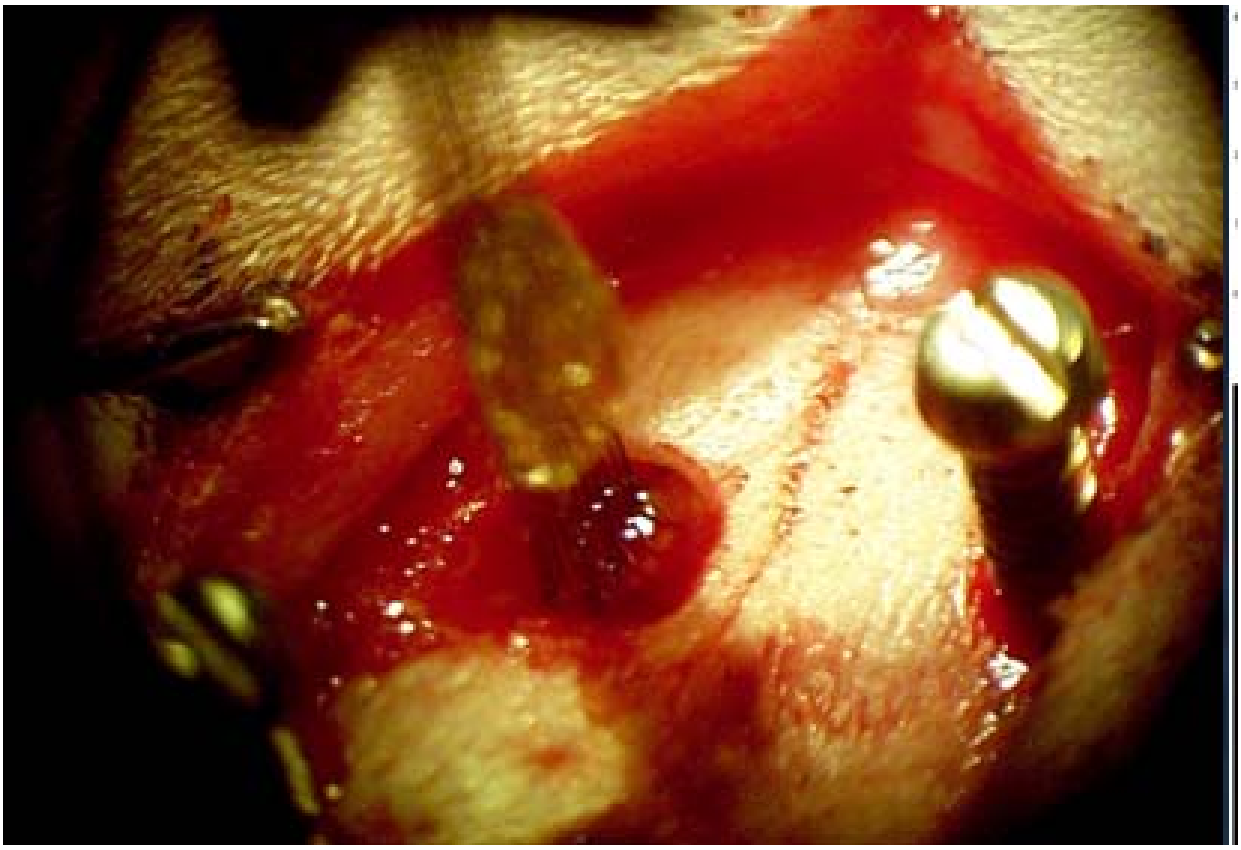

Figure 6-2 Placement of the electrodes during surgery. This image shows a single 16 electrode array being lowered into position into the rat's hippocampus. The electrodes vary in depth so that they are lowered to a depth where targeted structures lie in the hippocampus. The location of the electrode tips was later confirmed using MRI after the rat has been sacrificed.(Used with permission of Dr. Paul Carney).

axis and 200 μm on the long axis at a depth of 4 mm from the surface of the brain. The length for each electrode is designed such that the tip of each electrode is within the brain region of interest. The location of the end of each array closest to the centerline of the brain is 4 mm caudal to the bregma and 1.7 mm lateral. A single Teflon coated bipolar twist electrode was placed in the posterior ventral hippocampus in the right hemisphere of the animal, posterior to the electrode array for stimulation into status epilepticus. After the experiment was completed the rats were sacrificed and high-resolution magnetic resonance imaging (33) was used to verify the position of the electrodes, as shown in the lower right panel of Figure 6-2.

Figure 6-3 Example of the rat environment and recording chamber. These cages are designed so that the electrode cables can be constantly attached to the rat's head while also allowing the rat to freely explore its environment.

The rats were kept in an 30 cm enclosure designed to permit the electrodes to be connected to the data acquisition system while the rats engaged in exploratory activity. This enclosure is shown in Figure 6-3. The rats were allowed to heal for one-week post surgery before stimulation. A 10 second train of 50Hz 1 ms bipolar 240μA pulses was delivered every 12 seconds for 60 minutes to induce status epilepticus in the rats. 32 channels of simultaneous recordings were taken from the rats 24 hours a day for 76 days while the rat was engaged in sleep and normal exploratory behavior. Data was acquired using a Tucker-Davis (Alachua, FL) Pentusa at a sampling frequency of 24.4141 kHz, band pass filtered from 0.5 Hz to 12kHz, and stored to disk.

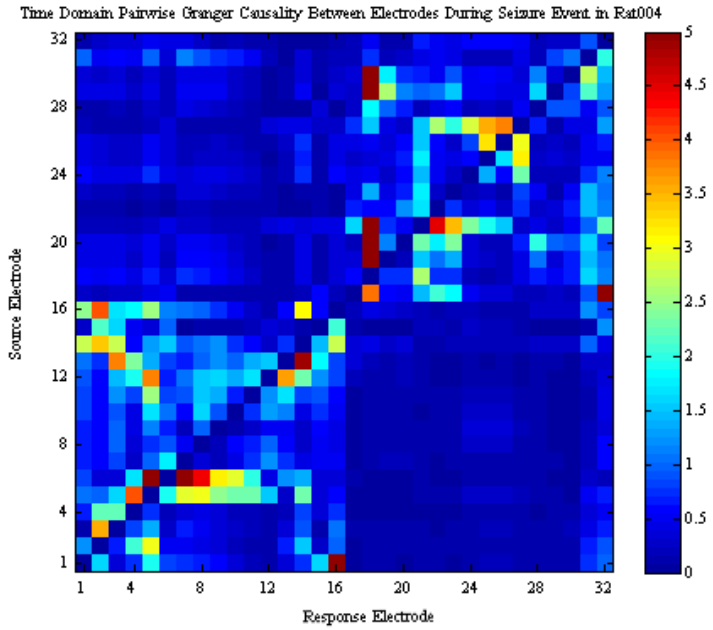

Figure 6-4 Initial Pairwise Granger Causality analysis of four 60-second seizures for a single animal. These plots are used to display the causal interactions between all electrode combinations. The plots are organized in terms of the source electrode (y-axis) and the response electrode (x-axis) for the Granger analysis. The magnitude of the causal interaction between source and response electrodes is represented by the color scale in the left of the figure, with blue being zero and red being strong interaction. This plot clearly shows two regions, once consisting of the first sixteen electrodes (bottom left quadrant) and the other consisting of the last sixteen electrodes (top right quadrant). These areas correspond to the electrode arrays in each hemisphere. The average within-hemisphere interactions are strong while the hemisphere to hemisphere (top left and bottom right quadrants) interactions appear weak across the four seizures.

Seizure Analysis with Pairwise Granger Causality

Seizures detection was conducted manually by visual detection of the raw traces and verification against video records. The seizures were catalogued and the start time of the seizure was noted. A 10-minute window surrounding each seizure was then extracted for all 32 channels from the raw recording and low pass filtered to 1kHz. This frequency was chosen because it maintains most of the features in the data while allowing for a reasonable model order for autoregressive modeling required for parametric PGC. A 60 second window was then chosen within the 10-minute period of filtered data that encompassed the seizure.

Spectral Pairwise Granger Causality was then calculated for all possible electrode pairings (992 directional combinations) for the entire 60-second window for 4 seizures to see if PGC was able to describe causal interactions for epileptic seizures. The stationarity of the time series was addressed by normalizing the mean and variance. The Bayesian information criterion (BIC) was used to determine the correct model order, which was found to be m=25. The resulting spectral analysis was then integrated across the spectral domain to produce a single time domain value for each electrode pairing for each window resulting in a 32x32 matrix. Granger analysis was then plotted as 32x32 image, shown in Figure 6-4. These plots are organized so that each pixel represents the causal influence of a driving channel (y-axis) and a driven channel (x-axis). The magnitude of this causal relationship is represented by color with blue being zero ranging through light blue, green, yellow, and red with red being the strongest interactions. This plot clearly distinguishes two distinct regions, a lower left and a top right quadrant, that have strong within region causality but weak cross-hemisphere interactions.

Based on promising results from this initial analysis, a higher resolution analysis was conducted where PGC was calculated over a series of 1 second moving windows for each seizure independently. The overlap between these 1 second moving windows could be modified to create a real time movie of the interactions. A 50% overlap was used for each seizure resulting in 129 data windows for PGC. This data for each window was then plotted as 32x32 image and combined into a movie at 2 frames per second. This allows the dynamics of 32 interacting channels for each seizure to be better visualized for qualitative analysis.

Calculation of average PGC values by the eight electrodes in each area (L-DG, R-DG, L-CA1, R-CA1) allowed creation of an additional PGC index to condense the spatial and temporal interactions quantitatively. Each seizure was visually analyzed to identify and window specific

stages. A single value for the interaction between each indexed area was calculated that represents the average for that stage and was independent of the length of the stage. This provides 4x4 matrix for each stage for each seizure. Analysis of variance was calculated between different directional interactions over the pool of 15 seizures from the three animals used in this analysis. Additionally, baseline interictal activity was analyzed using this method for comparison.

Finally, a higher time resolution movie was made for one of the seizures. This movie is 30 frames per second and includes behavioral video, a trace of the recorded waveforms, and the corresponding PGC analysis. The same one-second data window was used to calculate PGC interaction, however this analysis window was moved by $1/30^{th}$ of a second for each corresponding video frame. Frames from this movie are displayed in the following figures to better describe the seizure stages that will be identified and described in the results.

Results

Qualitative visual analysis of the raw waveform, behavioral videos, and PGC movies reveal a common progression of events during all 15 seizures into five major stages. Figures 6-4 through 6-9 highlight examples of interictal activity 60 seconds prior to seizure and also from each of these stages. These plots are frames from the high-resolution movie compiled for one animal. Each figure includes a snapshot of surveillance footage of the rat in the bottom left corner, four of 32 electrode voltage traces (one from each major region L-DG, R-DG, L-CA1, R-CA1) on the right, and a 32 x 32 Granger Causality analysis in the upper left quadrant. The electrode traces are normalized against each other and are time locked to the surveillance video. A one second window highlighted between the red bars in on each voltage trace represents the current analysis window whose results are depicted at the top left.

Each Granger analysis plot represents the interactions by electrodes in the source area (y-axis) versus electrodes in the destination area (x-axis) for each electrode combination. The magnitude of the Granger Causality analysis for each pairing is represented by color with blue being near zero ranging to red representing the strongest interactions. For example, in Figure 6-5 the bright red area in the lower left are interactions from electrodes in the L-CA1 (y-axis) to electrodes in the L-CA1 (x-axis). This example would be interpreted as interactions within the L-CA1 area during the pre-ictal period roughly 30 seconds before seizure.

The seizures begin in stage 1, shown in Figure 6-6, in which a mixture of intrahemisphere activity was dominated by causal activity within the CA1 region and from the CA1 region to the DG. This activity gradually builds up over time. Behaviorally, Stage 1 often includes the beginning of the tonic phase of the seizure, where the animal remains motionless and blinks its eyes. As this causal activity becomes stronger, it begins to spread across hemispheres at the beginning of stage 2.

Stage 2 is the most striking, marked by high-magnitude mono-directional causal reverberations across hemispheres as well as substantially increased intra-hemisphere causal interactions. These transfers often reverberate sequentially from one hemisphere to the other. An example of a directional transfer between hemispheres is shown in Figure 6-7 from the left to the right hemisphere. After several directional transfers the seizure moves into stage 3, shown in Figure 6-8, marked by mainly intra-hemisphere activity. However, unlike the intra-hemisphere waveforms of stage 1, the intra-hemisphere Granger causality interaction patterns are both more dynamic, of larger magnitude, and less confined to a single area or pathway. Only week occasional cross hemisphere directed transfers occur in stage 3.

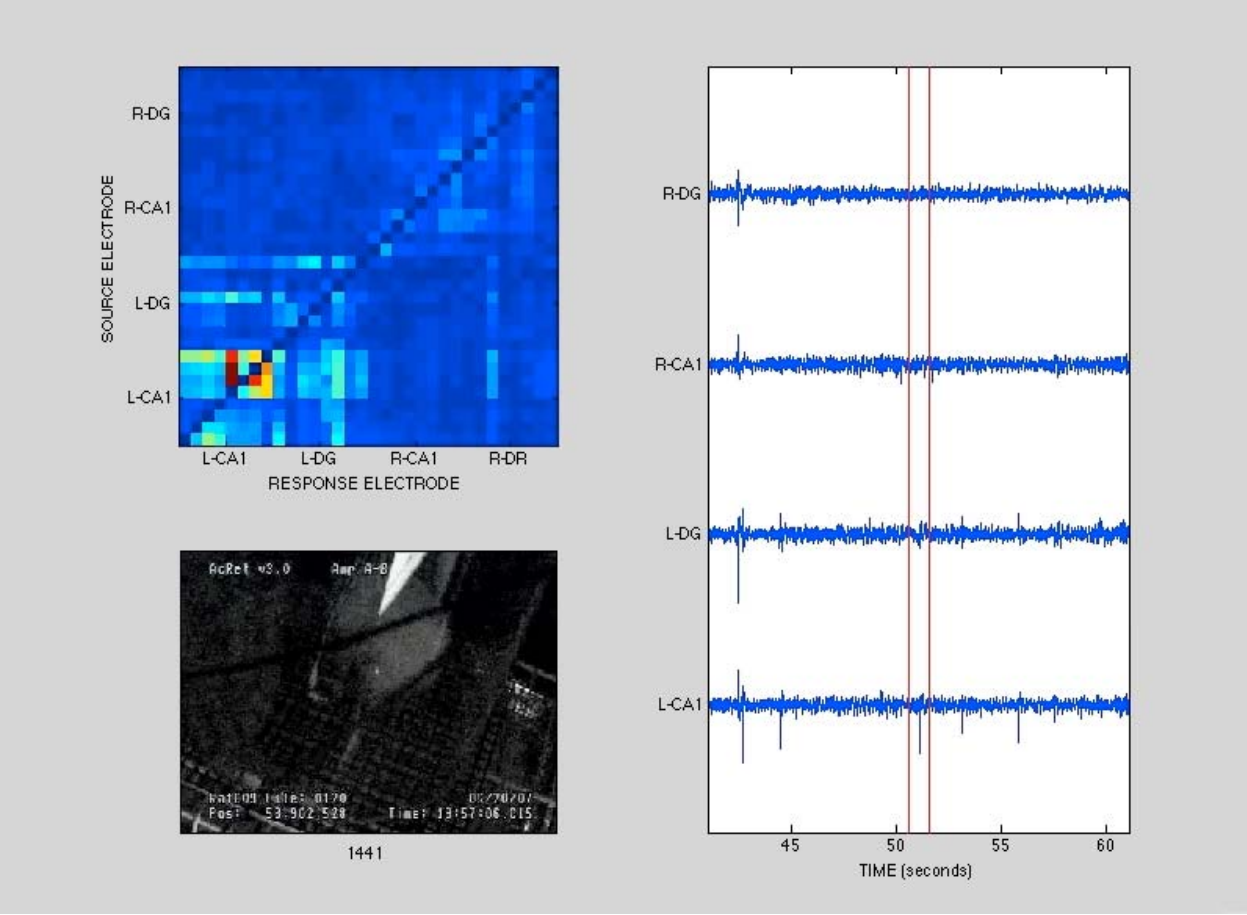

Figure 6-5 Example of data and Granger analysis during the interictal (pre-ictal) stage. This plot is of one frame approximately 30 seconds prior to seizure. The right panel includes sample raw data traces from each of the four main areas recorded from including the right and left DG and the left and right CA1. The segment of data analyzed is between the vertical red lines in the sample electrode traces. The top left panel is a source (y-axis) response (x-axis) representation of the PGC analysis with the electrodes organized by area. An interictal spike is included in the analysis for this frame. Most of this activity is within CA1 and is also directed from the CA1 to the DG. The bottom left panel is a frame from surveillance footage of the rat's behavior. In this frame the rat is either resting or sleeping.

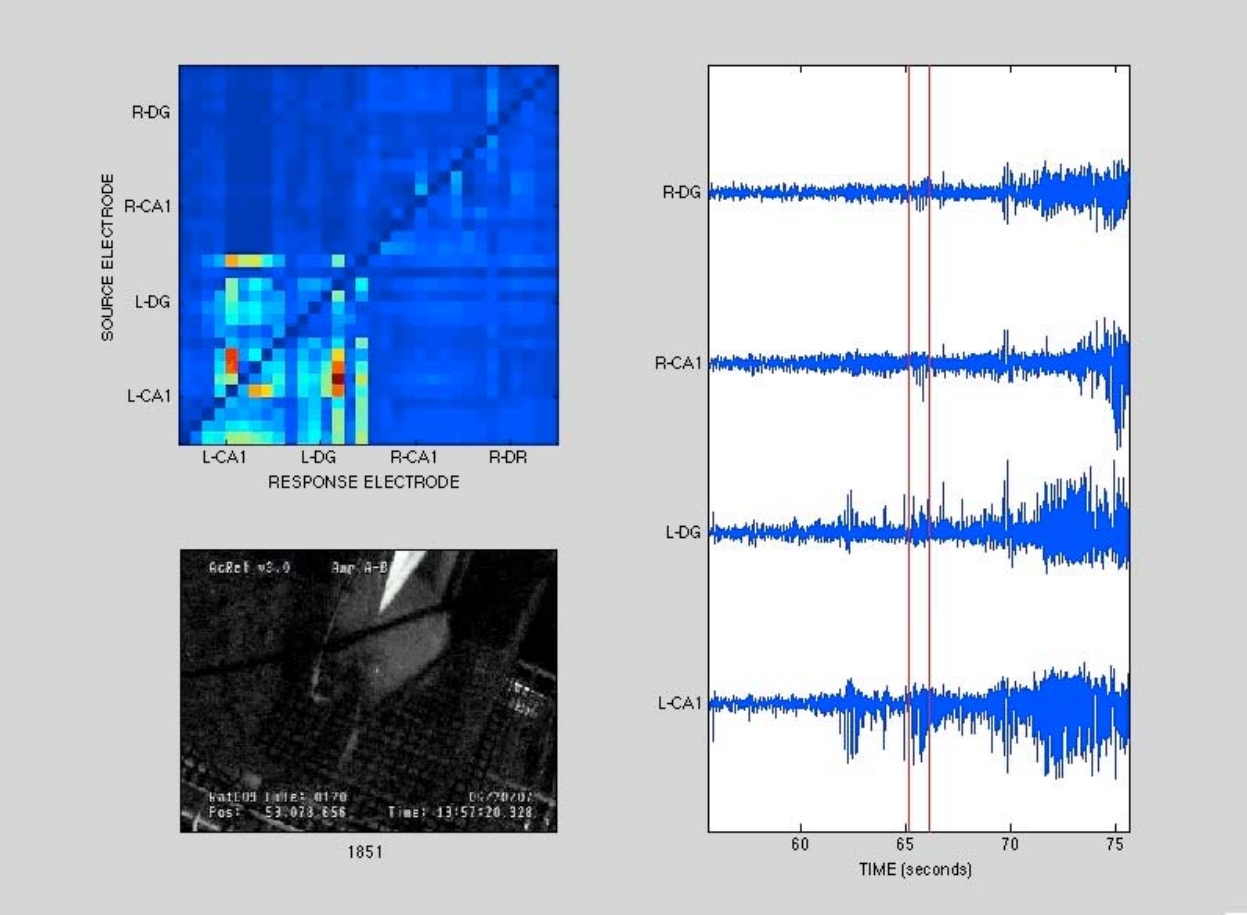

Figure 6-6 Beginning of the seizure in the high resolution movie classified as Stage 1. Intra-hemisphere activity is the primary interaction unique to this seizure stage. The right panel includes a sample raw data trace from each of the main areas recorded from including the right and left DG and the left and right CA1. The segment of data analyzed is between the vertical red lines in the sample electrode traces. The top left is a source (y-axis) response (x-axis) representation of the PGC analysis with the electrodes organized by area. The PGC analysis shows directional activity within the left CA1 as well as a directional influence of the left CA1 on the left DG. The bottom left panel is surveillance footage of the rat's behavior. In this frame the rat has just woken up and may be exhibiting tonic behavior.

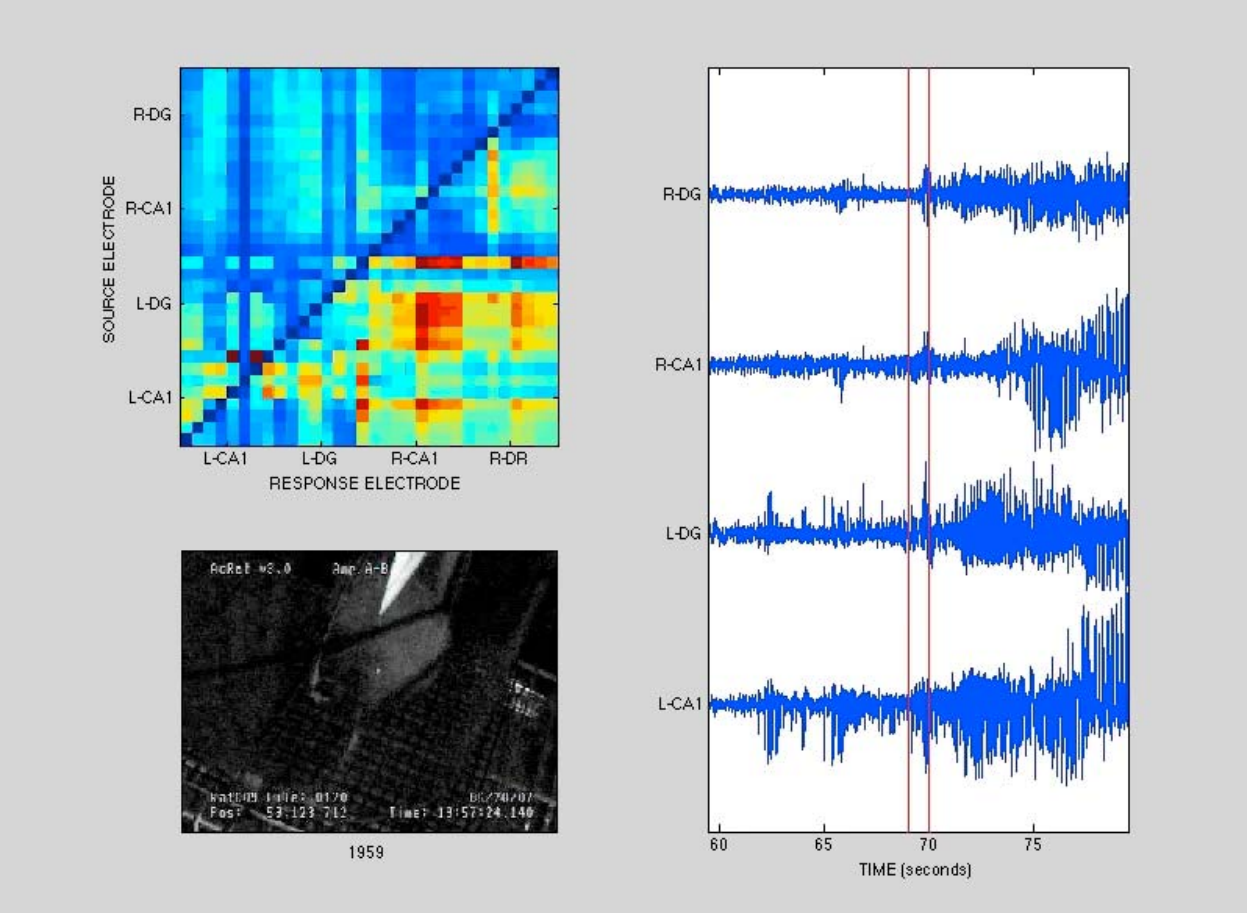

Figure 6-7 Example of a directional transfer during Stage 2. The right figure includes a sample raw data trace from each of the main areas recorded from including the right and left DG and the left and right CA1. The segment of data analyzed is between the vertical red lines in the sample electrode traces. The top left is a source (y-axis) response (x-axis) representation of the PGC analysis with the electrodes organized by area. This frame shows an example of a directional transfer from the left hemisphere to the right hemisphere. In following frames this transfer is reciprocated from right to left. The bottom left panel is surveillance footage of the rat's behavior. In this frame the rat is exhibiting tonic behavior where the rat is awake and blinking its eyes but not moving.

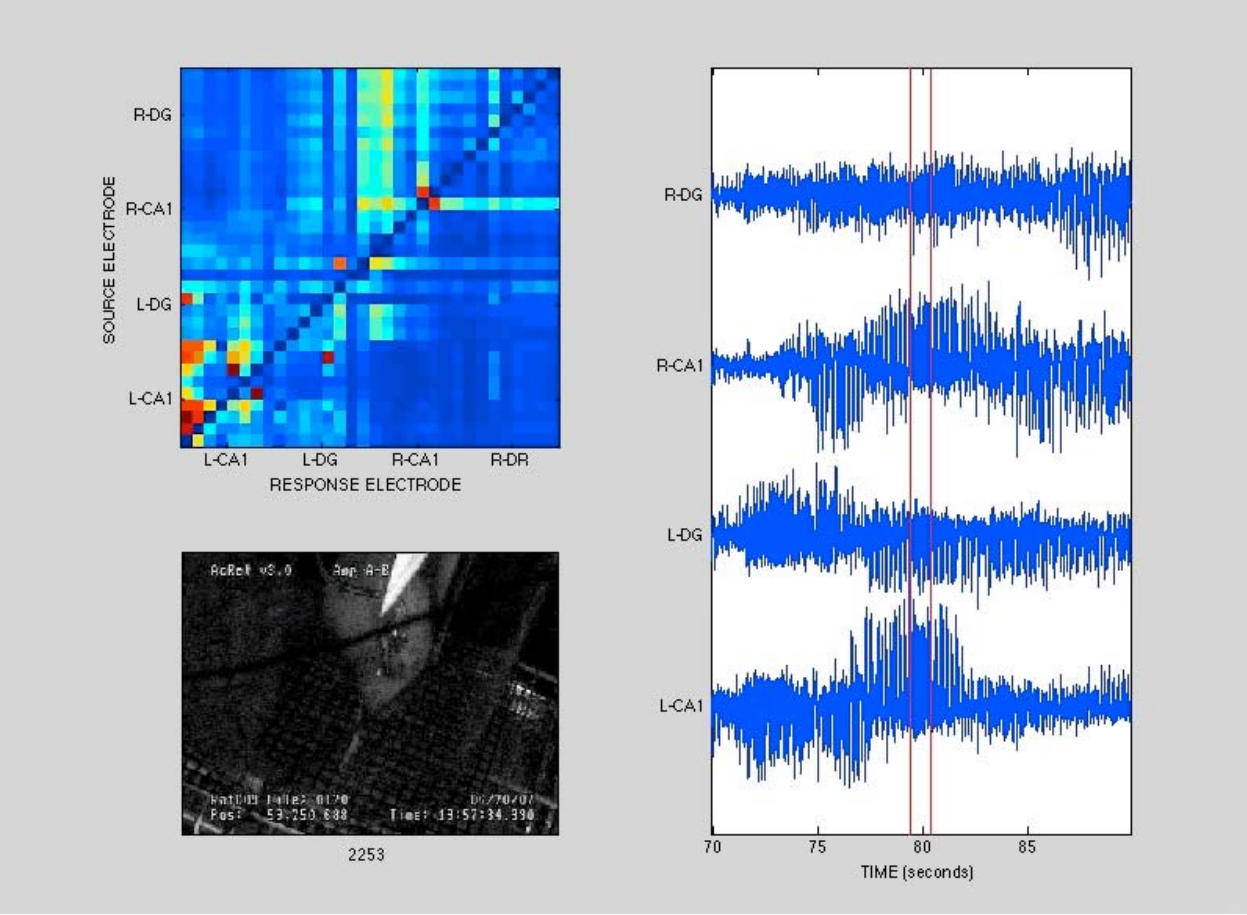

Figure 6-8 Example from Stage 3 – Late intra-hemisphere. The right figure includes a sample raw data trace from each of the main areas recorded from including the right and left DG and the left and right CA1. The segment of data analyzed is between the vertical red lines in the sample electrode traces. The top left is a source (y-axis) versus response (x-axis) representation of the PGC analysis with the electrodes organized by area. Most of the causality is isolated within hemisphere with occasional weak cross hemisphere interactions. The bottom left panel is surveillance footage of the rat's behavior. In this frame, the rat is still exhibiting tonic behavior.

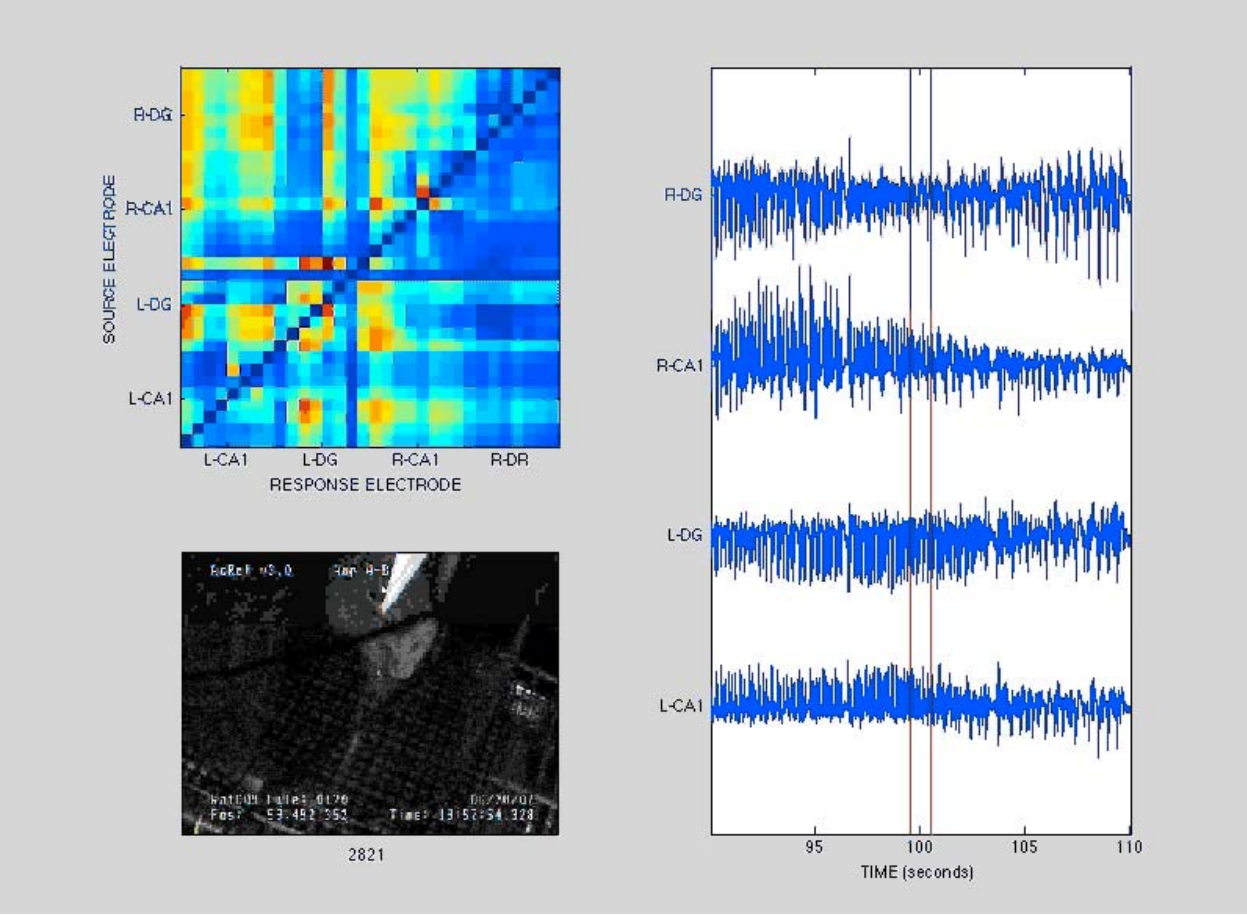

Figure 6-9 Stage 4 - Transition. The right figure includes a sample raw data trace from each of the main areas recorded from including the right and left DG and the left and right CA1. The segment of data analyzed is between the vertical red lines in the sample electrode traces. The top left is a source (y-axis) response (x-axis) representation of the PGC analysis with the electrodes organized by area. The causality here seems to be bidirectional for nearly all electrodes. The bottom left panel is surveillance footage of the rat's behavior. In this frame, the rat is beginning to transition from tonic to clonic behavior.

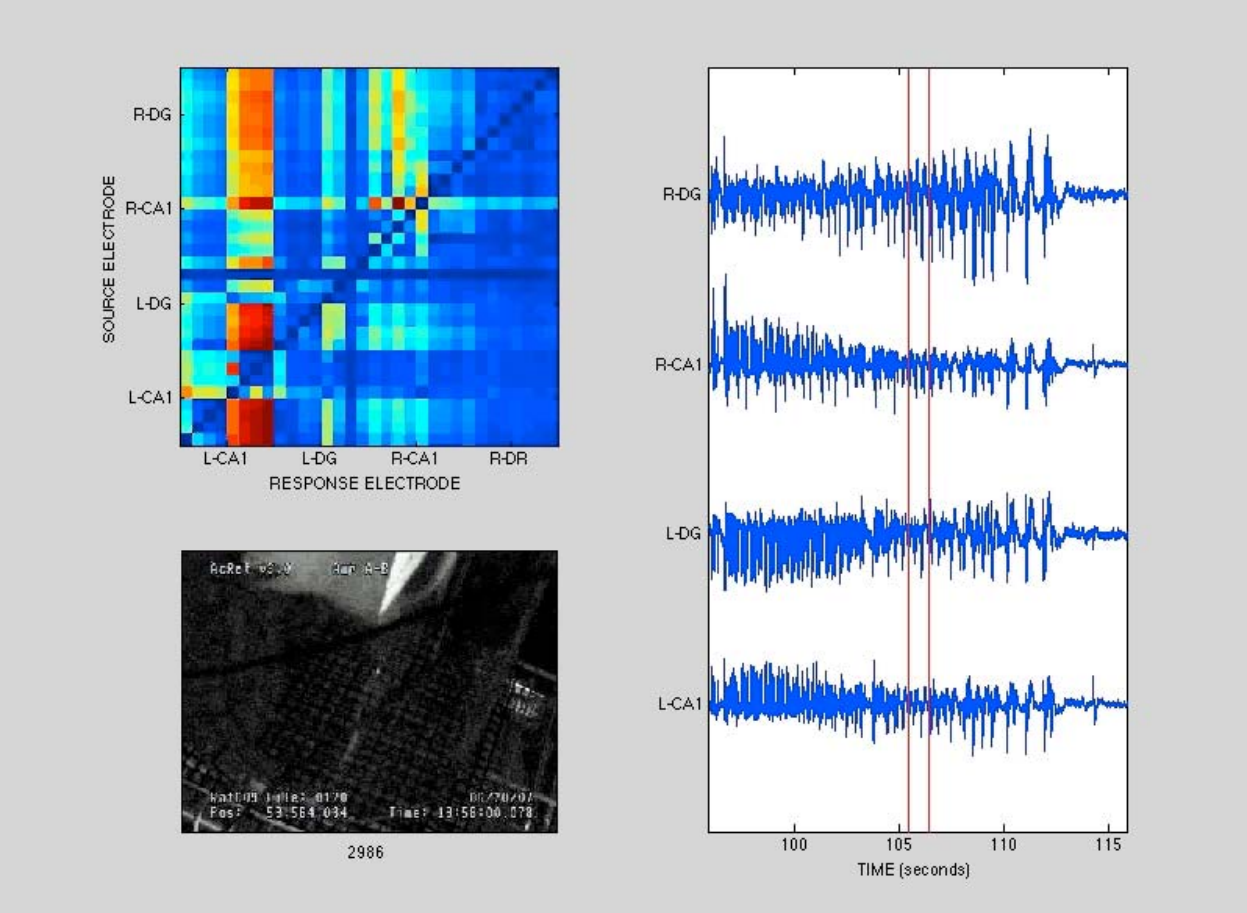

Figure 6-10 Stage 5 – Post transition. The right figure includes a sample raw data trace from each of the main areas recorded from including the right and left DG and the left and right CA1. The segment of data analyzed is between the vertical red lines in the sample electrode traces. The top left is a source (y-axis) response (x-axis) representation of the PGC analysis with the electrodes organized by area. The dominant driving pattern is from the DG to the CA1 in this stage. The bottom left panel is surveillance footage of the rat's behavior. In this frame the rat is showing clonic behavior including rearing and rhythmic shaking of the forelimbs.

Stage 4 is usually a brief and highly causal epoch where all areas intra and cross hemisphere are bi-directionally causal, shown in Figure 6-9. In the PGC movies, this stage consists of near saturation of causal effect with nearly the entire 32x32 frame shows strong causal interactions. Behaviorally, stage 4 marks the transition from
the tonic phase where the rat is motionless and appears tense to the clonic phase of the seizure where the rats appendages jerk rapidly and rhythmically. Immediately after stage 4, the pattern smoothly transitions into stage 5, which is made up of heavy spiking activity with a causality pattern similar to that observed during interictal activity.

Quantitative analysis between anatomical regions in hippocampus was conducted by creating an index from multiple electrodes common to that region, as described earlier. The 32 electrodes split between hemispheres were divided into those in the DG and those within the CA1/2 region. This results in four areas to compare using quantitative analysis. This index was calculated for each seizure at each Stage of the seizure (1-5) for all possible interactions including a scaled within area index. This allowed statistical comparison of the seizure stages across multiple seizures (n=15). The interactions between and within the 4 indexed areas for each seizure stage (16 interactions total) were compared sequentially with neighboring stages as well as to inter-ictal indexes.

All Stages were significantly different from inter-ictal baseline activity, $Fs(14,14) > 6.9$ $p < 0.01$. Figure 6-11 highlights the statistical comparisons between stages. Starting with stage 2 in panel C each of the 16 area indexes is compared with its analog in the previous stage using dots to indicate significance levels. One dot indicates a 80% confidence interval, $Fs(14,14) > 1.58$, two dots a 90% confidence interval, $Fs(14,14) > 2.02$, three dots a 95% confidence interval, $Fs(14,14) > 2.48$, while four dots indicates a 99% confidence interval, $Fs(14,14) > 3.70$.

The statistical analysis revealed gross changes between areas when transitions were made from one seizure stage to another as well as differentiated all seizure stages from inter-ictal baseline activity patterns. While the differences between seizure and baseline events are not unexpected, some interesting discoveries emerged from the analysis of the seizure progression. For instance, the transition between stages, such as from Stage 1 to Stage 2, is statistically distinct and discreet, as shown in Figure 6-11 panel C). These results also suggest that Stage 4 has only between-hemisphere activity in common with Stage three (no dots in top left and bottom right of Panel E) and within-hemisphere activity in common with Stage 5 (no dots in bottom left and top right of Panel F). This suggests that Stage 4 has elements of Stage 3 and Stage 5 within it, suggesting Stage 4 is a transition between 4 and 5. When comparing Stage 3 and Stage 5 there are no significant differences between within-hemisphere interactions (7 out of 8 $Fs(14,14) < 1.58$, $p=0.20$) while between-hemisphere interactions where significantly different (7 out of 8 $F(14,14) > 2.48$ $p=0.05$) indicating a decrease in between hemisphere interactions.

However, this analysis does little to capture the effects of short intense events such as the directional transfers shown in Stage 2. These transfers, while intense and obvious to discern in the causality movies used for quantification, are poorly reflected because of averaging over the analysis window. An example of one of these directional transfers was shown in Figure 6-7. Thus, Stage 2 and Stage 3 cross hemisphere indexes are not significantly different when compared to each other, see Figure 6-11 Panel D) (all $Fs(14,14) < 1.58$, $p=0.20$). However, CA1 to DG intra-hemispherical relationships between Stage 2 and Stage 3 were significantly different, $Fs(14,14) > 3.70$, $p=0.01$, an observation that was not made during qualitative analysis.

This analysis suggests that there is a large decrease in CA1 to DG intra-hemisphere interactions from Stage 2 to Stage 3. Qualitatively, a transition is observed in Stage 4 where the

dominant information flow from the CA1/2 to DG areas for both hemispheres reverses so that the dominant information flow becomes from the DG to CA1/2. This effect is highlighted by a comparison of Stage 2 (the highest magnitude instance of CA1 to DG interactions) to Stage 5 (the highest magnitude instance of CA1 to DG interactions) right and left CA1 to DG influences, $F(14,14) = 21.2$ and 13.3, respectively. This suggests that CA1 to DG influences are effectively eliminated by the start of Stage 5.

Discussion

Currently, synchronization is thought to be the dominant dynamic occurring across the limbic system during an epileptic seizure. Synchronization is defined as adjustment of rhythms of oscillating objects due to their interaction (123). Synchronization across a diffuse excitable network is thought to be a possible mechanism that initiates seizure in the limbic system (124). In contrast others suggest that a large amount of asynchrony is necessary to maintain seizure events once they have begun (125). The results from the Granger analysis do indeed find synchronization within the hippocampus prior to, during, and after the ictal event. However, the detailed interactions that occur during these seizures are largely unknown. *Hence, the detailed interactions illustrated in these results using Granger Causality analysis have never previously been described in the study of TLE*. These results provide a new picture of highly dynamic directional interactions among specific brain areas during a seizure that follow a common progression. For example, one of the distinct features in Stage 1 of nearly all seizures is an increase in local interactions within the CA1 area whose causal strength builds over time eventually influencing activity in DG. This is followed by a series of directional cross-hemisphere reverberations of Stage 2 in which the seizure appears to transfer back and forth from one hemisphere to the other. Together, these results suggest a hierarchical progression of

causation within the CA1 that spreads to the DG and finally crosses over into the neighboring hemisphere.

In contrast, if a coherence analysis were conducted over these data (a tool commonly used in this literature), it would suggest that these directional transfers were actually bidirectional phenomena because this method is non-directional. Non-directional measures such as coherence would also not be able to detect the reversal in directional connectivity between the dentate and CA1 during the Stage 4 transition. According to these measures the entire seizure would seem to be dominated by bidirectional synchronization across the entire network. However, Granger Causality analysis tells a very different story. The dominant directional influences in the beginning stage of the seizure are abnormal with the CA1 areas showing directional causation on the DG. This is the opposite of baseline interictal patterns that often show directional influences from the dentate to the CA1. Additionally, this abnormal pattern is time locked behaviorally with the tonic portion of the seizure. Interestingly, the flip of the directional connectivity to connectivity resembling baseline connectivity occurs during the transition from the tonic to clonic behavior. The implications of this directional flip are not completely clear, however.

One of the possibilities explaining the driving influence of CA1 to DG during the early seizure may be related to one of the weaknesses of the Granger Causality based methods. In this case the entorhinal cortex may be differentially driving both of these areas creating a false directed influence from CA1 to DG, instead of the influence of CA1 to DG being *mediated* through the entorhinal cortex. The entorhinal cortex has been implicated as a possible initiator of ictal events where disinhibited neurons in the entorhinal cortex may directly fire pyramidal cells in CA1 at least in a pilocarpine model (119). The entorhinal cortex is also anatomically connected to the DG. Hence, both of these situations are supported by the literature and may

even be happening simultaneously. It is unlikely based on the anatomical organization of the hippocampus that the effects of CA1 are mediated through CA2 and CA3 to the DG. Further experimental analysis using conditional granger causality with electrode coverage within the entorhinal cortex will be necessary to determine which of these possibilities is correct.

Nevertheless, these results provide strong support for the use of the Granger Causality metric as an important tool for seizure detection. The stage 4 transition from abnormal driving (CA1 to DG) to a normal driving pattern (DG to CA1) suggests that at some point prior to seizure the driving pattern became abnormal. The abnormal driving influence has been seen in the pre-ictal analysis at least a minute before seizure. An natural question to ask would be "When does this driving influence become abnormal?" Once identified, the transition from normal to abnormal driving influences could potentially be used as an indicator of an impending seizure. However, the role of the entorhinal cortex in this connectivity should be determined before this relationship is used for seizure detection. For example, if the entorhinal cortex turns out to be the source of the abnormal driving influence it may better aid detection if electrodes were placed in this area. Additionally, detection of this abnormal driving influence may increase the sensitivity of current seizure detection methods. This could be useful for detecting epochs during epileptigenesis that are not easily detected using behavioral or current electrographic seizure detection methods.

In conclusion, using Granger Causality to reveal effective connectivity has led to a new understanding of the interactions within the hippocampus during seizure. This understanding provides the opportunity to make new predictions about seizure detection and suggests new experiments that should expand our understanding of TLE. However, we have only used the

most basic of GC based tools in this analysis. Future work could make use of conditional and spectral GC analysis to paint a clearer picture of effective connectivity during seizure.

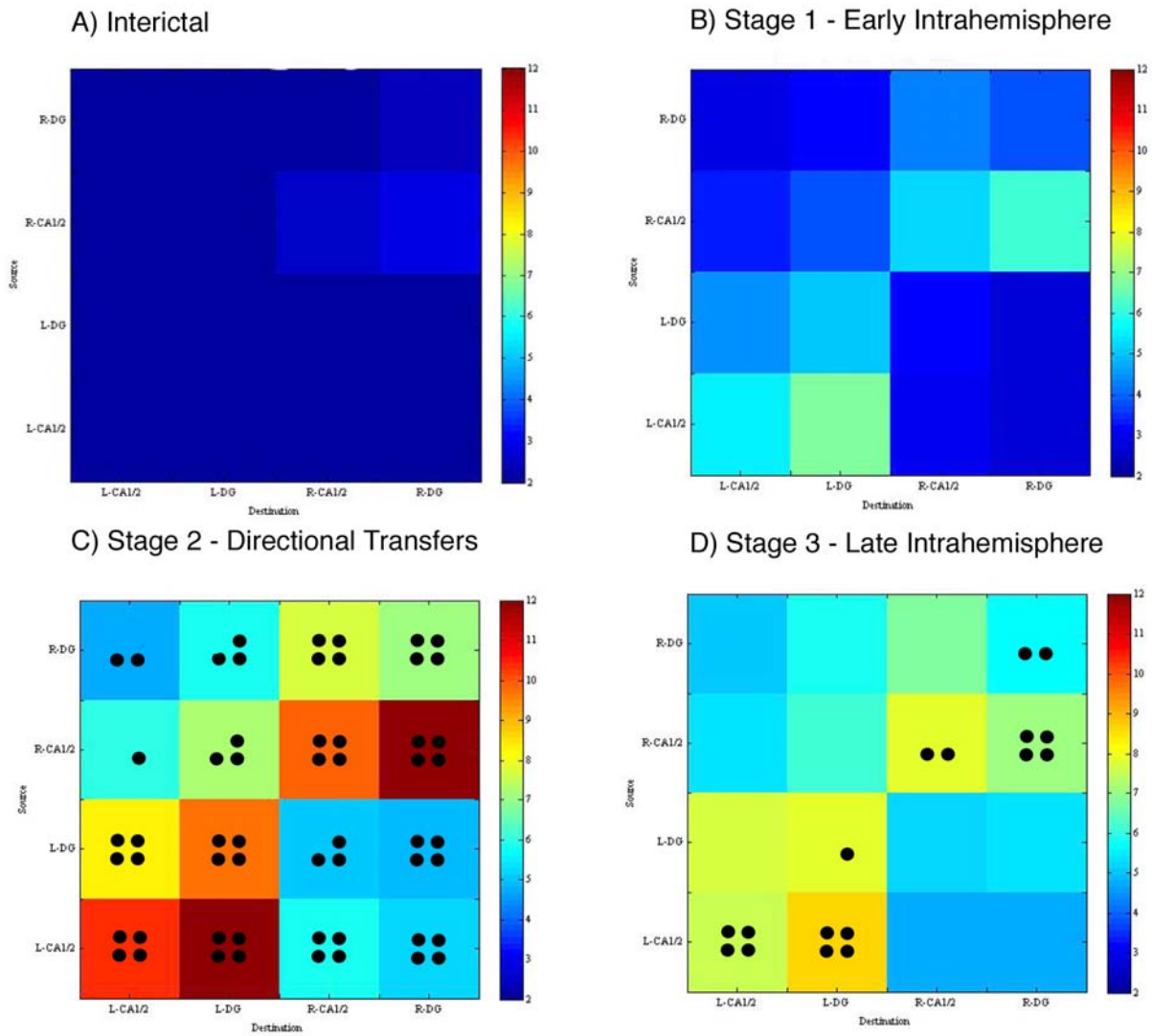

Figure 6-11 Quantitative analysis of the 5 seizure stages. Analysis was over 15 seizures from 3 subjects. A Granger Causality index was created for each of four areas: Left and Right DG, and Right and Left CA1. The effects for the electrodes in each of the four areas were summed and normalized to create these indices. The y-axis is the driving area and the x-axis is the receiving area, the magnitude of the interaction is described by the color ranging from blue (low interaction) to red (high interaction). Panel A) shows the pre-seizure interactions while the remaining five are during seizure. The black dots in panels C)-F) are used to indicate statistical difference for each interaction index from its corresponding index in the previous stage. The number of dots represent the significance level of that interaction ($p < 0.2$, $p < 0.10$, $p < 0.05$, $p < 0.01$, for 1-4 dots respectively).(Figure continued on next page)

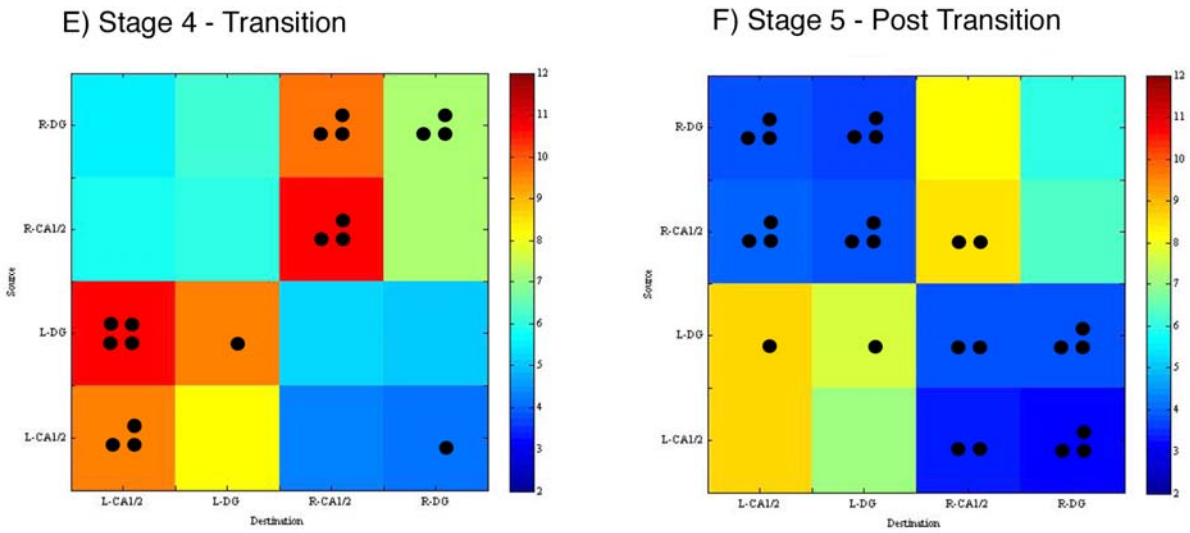

Figure 6-11. Continued

CHAPTER 7
SUMMARY OF RESULTS AND CONCLUSSIONS

Summary of Results

This research explored the use of Granger Causality and associated methods to reveal effective connectivity in a wide variety of neural systems. These include a neural network simulation in chapter 3, in-vitro dissociated cortical cultures in chapters 4 and 5, and finally in-vivo microelectrodes in the hippocampus of epileptic rats in Chapter 6. In each case, the goal was to reveal information about the actual connectivity underlying the system by using Granger Causality to calculate a measure of effective connectivity from the output of that system. The difficulty in recovering the actual connectivity increases as the complexity of the system increases. For example, increasing the number of modeling neurons in the simulated neural networks demonstrated this relationship. However, even in the extremely complex in-vitro and in-vivo systems Granger Causality was able to provide novel and useful insights into the workings of these neural systems.

The neural networks in Chapter 3 used a simple neural network model modified such that the input synaptic weights were known prior to simulation. The outputs from these simulations were used to recover the synaptic weights used to drive the network. In a simple network of two neurons the relationship between pre and post synaptic is a sigmoid with a linear section between 15mV and 45mV where Granger Causality increases from near zero to a little greater than 1. Granger Causality does not have an upper bound like that of coherence, thus the high end of the sigmoid being around 1 is merely coincidence. Increasing the complexity of this network to 100 neurons was shown to distort this simple relationship and requiring another tool, conditional granger causality, to recover the initial synaptic weights driving the network. CGC was needed to remove not only false direct influences but also to untangle mediated influences from direct

influences. Usually, untangling a mediated influence from a direct influence requires the use of conditional granger causality. However, it was found that under the special circumstance where a false direct influence was conditioned out (i.e. shown to be equal to zero and entirely mediated through the confounded pathway), the magnitude of the false connection could be simply subtracted from the confounded pathway. This shortcut relationship is from previous work by Geweke (126). The ability of both CGC and Geweke's shortcut to recover the direct influence from a confounded pathway were both evaluated and found to be effectively equivalent. However, as the complexity and length of the causal chain grew the ability of these methods decreased.

When the size of the network was increased to 100 neurons these methods consistently underestimated the original synaptic weights. This was likely due to the unknown effects of the network complexity on these pathways. These suggest that more work is needed to accurately recover synaptic weights from these networks. However, while the sigmoid curve equation shown in Chapter 3 does not always hold numerically, synaptic weight does scale linearly within the region where a presynaptic neuron begins to affect the firing rate of a postsynaptic neuron up the the point where it always causes the post synaptic neuron to fire. This relationship suggests that changes in effective connectivity calculated using Granger Causality observed in complex networks are likely linear changes that could relate to synaptic efficacy if the sigmoid relationship were know. This suggests that Granger Causality methods could be useful in revealing relationships in living neural networks.

In-vitro dissociated cortical neural networks grown on microelectrode arrays were used for the experiments in Chapters 4 and 5. Jimbo (4) used spike rate to describe simultaneous pathway specific potentiation and depression in these cultures. This was done with accomplished by

probing on each of the 60 channels 10 times and measuring the spike rates at all electrodes in the ensuing burst. The probe sequence and corresponding spike rates were used to establish a baseline spike rate response for every electrode and then used post treatment to assess possible changes. The treatment was a high frequency high amplitude pulse train or tetanus delivered to a single electrode that consistently responded to probing. This tetanus was designed to induce plasticity related changes in the culture and shown by Jimbo et al to potentiate or depress neural pathways. These results of Chapter 4 were consistent with Jimbo's finding identifying potential pathways within the dish using a comparison of changes in spike rate. PGC was then applied to the baseline and post-treatment probe data. The results were shown to agree with spike rate results, but PGC showed several marked improvements over Jimbo's analysis.

Admittedly spike rate is a computationally simpler method when compared to PGC. However, PGC showed many advantages over using spike rate for describing plasticity. First, it showed a higher contrast between baseline and post-treatment results. One of the difficulties in the use of spike rate as a measure is establishing the statistical significance of changes. The higher contrast PGC provides makes this task easier. Second, PGC has a significance threshold that can be obtained using a surrogate where the spike timings within the data are shuffled. This effectively destroys the spike timing relationships used to calculate PGC while maintaining the spike rate characteristics of this data. This analysis of this surrogate data demonstrated that the observed changes in the original data set were not simply due to changes in rate for if they were, the results would have been equivalent. Third, PGC gives a statistically relevant baseline measurement of effective connectivity establishing a baseline connectivity map. Spike rates from the baseline alone do not have any meaning without being used in conjunction with the

post-treatment spike rates. Thus, baseline spike rates provide no information about baseline effective connectivity.

Finally, PGC is a directional measure while spike rate is a non-directional non-causal measure. Results calculating using spike rate result in a 60x60 matrix with axes of probe channel and response channel. The use of PGC on the same data results in a 60x60x60 matrix with axes of probe channel, response channel, and source channel. Thus, in addition to giving similar results as spike rate, PGC provides 60 times more information. This extra information was exploited to learn more about the cultures. Comparison of probe/source plots to probe/response plots for potentiated pathways showed that some channel experienced an increase in output while others experienced and increase in input post-tetanus. This same relationship was shown in depressed channels except with decreases in output and input. This suggests that changes were not just global changes in rate and were likely reflected in their postsynaptic targets as well. The pre-tetanus effective connectivity calculated from PGC was also used to measure amplitude dependent plasticity by comparing the initial connectivity to changes in connectivity post-tetanus. Analysis of this data across 6 subjects showed that the amplitude dependent plasticity trends matched trends seen in work done by Bi & Poo (118), where potentiated pathways increase a lot if they are small and depressed pathways change by a constant percentage independent of initial strength.

A second experiment was developed based on the results shown from the analysis of the Jimbo protocol. This experiment made use of the ability of PGC to measure connectivity prior to tetanization. Once PGC was calculated from the pre-tetanus data sinks and sources of causal flow were identified within the culture. A sink was defined as a channel where the balance of causal information flow was inward, while a source was defined as a channel where the balance

of causal information flow was outward. The central hypothesis in this experiment was that tetanization on a sink would elicit depression at the sink while tetanization at a source would elicit potentiation. The experiment was carried out on 10 cultures. The results suggested that changes in plasticity did occur. However the direction of results did not match the predictions made prior to the experiment. Perhaps one reason this experiment was not successful was that the design and predictions underestimated the complexity of connectivity in the neural culture. One solution might be to reduce the complexity of the network by reducing the density of the neurons. Additionally, a paired pulse paradigm at pre and postsynaptic targets would likely increase the probability of plasticity induction only on targeted pathways.

In-vivo, PGC was used to explore effective connectivity of seizures in rats from the Evolution into Epilepsy project. While this analysis was mostly empirical, comparison of the effective connectivity during seizure and during interictal and baseline was conducted. Qualitative analysis of the results from PGC on 15 seizures from 3 subjects showed that there were 5 distinct stages of the seizure. Stage 1 consisted of the buildup of activity within the CA1 area and also of a directed influence from the CA1 to the dentate gyrus. This connectivity is already abnormal when compared to interictal and baseline results. Baseline connectivity often highlights a directed influence from the dentate gyrus to CA1, which is also the expected anatomical influence. Stage 2 consists of large reverberating directional transfers from one hemisphere to the other accompanied by large within hemisphere interactions mainly from CA1 to the dentate gyrus. Stage 3 shows a large decrease in the magnitude of directional transfers however the within and between hemisphere interactions continue. This stage often contains the largest observable waveforms in the ictal event. Stage 4 or the transition stage marks the time when the connectivity flips to a pattern more resembling that of baseline activity where the

dentate gyrus drives the activity of CA1. This stage is marked by a brief period of strong bidirectional causality between most electrodes in both hemispheres. Behaviorally, the surveillance video of the rat shows that Stage 4 also marks the transition from tonic to clonic behavior in the rat. Stage 5 or the post transition stage shows a strong causal influence from the dentate gyrus to the CA1 as the rat clonically seizes. Shortly after Stage 5, the seizure usually ends and the rat engages in normal exploratory behavior.

Quantitative analysis was also carried out by analysis of variance between granger causality indexes created for combinations of each of the four regions left and right CA1 and left and right dentate gyrus for each stage of the seizure. It served as no surprise that stages that were qualitatively different from each other were also quantitatively different. However, quantitative analysis confirmed that all seizure stages were different than interictal activity. Also, quantitative analysis confirmed that Stage 4 was likely a transition stage. It was shown that Stage 3 and Stage 5 had causal interactions in common with Stage 4 that they did not have with each other (i.e. Stage 4 contains aspects of Stage 3 and 5). Overall, the results from this analysis were quite instructive and suggest that a great deal of information can be gleaned using Granger Causality not only about causal bindings during seizure, but also about changes in effective connectivity during the period in which these seizures develop (epileptigenesis).

Overall Conclusions

The aims of this body of work were to exploit the ability of Granger Causality to reveal effective connectivity. Granger Causality tools were used to explore effective connectivity in simulated, in-vitro, and in-vivo neural systems. The simulated neural network models provided a means of evaluating the ability of granger causality to relate back to the initial structure of the neural network. The results from this model support the notion that linear changes in effective connectivity observed using PGC in a living system likely reflect actual linear changes in the

underlying connectivity. Further the models provided a change to test conditional granger causality's ability to identify false directed influences and to detangle direct and mediated influences in confounded pathways.

The in-vitro work with cortical cultures suggests that PGC is a useful tool in describing changes in plasticity. The advantage of using a statistically sound, directional, and causal method that yields a measure of effective connectivity allowed much more information to be extracted from Jimbo's protocol. This allowed phenomena such as amplitude dependent plasticity to be measured from spike timings. These results contribute more evidence that suggests the plasticity is being observed using Jimbo's protocol. These new measures also allowed new predictions to be made about the response of the culture to a differential tetanization on sink and sources. While the prediction that sinks would be depressed and sources would be enhanced proved to be too simplistic, the PGC analysis suggested that plasticity occurred as a result of tetanization. Future predictions that take this complexity into consideration may be successful by using Granger Causality to estimate effective connectivity prior to experimental treatment.

Finally, PGC was able to show previously unreported causal relationships during seizure that may be useful for efforts to prevent seizures from occurring. At some point prior to the ictal event the effective connectivity in the hippocampus appears to become abnormal with the CA1 driving activity in the dentate gyrus. If this flip to abnormality can be detected it may provide an opportunity to intervene at an opportune moment to prevent the immanent ictal event by correcting this abnormal activity pattern. Additionally, the use of PGC to analyze epileptigenesis could provide new insight that may lead to treatments for a condition that is notoriously hard to treat pharmacologically.

In each of these cases, using Granger Causality to reveal effective connectivity led to a new understanding of these systems. This understanding provided the opportunity to make new predictions about these systems and suggest new experiments that were previously not feasible. Overall, Granger Causality has proven to be a useful tool in exploring effective connectivity in a wide variety of neural systems and in the future, may become one of the traditional tools used in neuroscience.

LIST OF REFERENCES

1. Granger CWJ. Investigating Causal Relations by Econometric Models and Cross-spectral methods. Econometrica. 1969;3:424-38.

2. Ding M, Chen Y, Bressler SL. Granger Causality: Basic Theory and Application to Neuroscience. In: Timmer, Schelter, Winderhalder, editors. Handbook of Time Series Analysis. New York: Wiley; 2006.

3. Izhikevich EM. Simple Model of Spiking Neurons. IEEE Transactions on Neural Networks. 2003;14(6):1569-72.

4. Jimbo Y, Tateno T, Robinson HPC. Simultaneous Induction of Pathway-Specific Potentiation and Depression in Networks of Cortical Neurons. Biophysical Journal. 1999;76:670-8.

5. Brazier MA, Barlow JS, New Author. Some applications of correlation analysis to clinical problems in electroencephalography. Clin Neurophysiol Suppl. 1956;8:325-31.

6. Palm G, Aertsen A., Gerstein GL, New Author. On the significance of correlations among neuronal spike trains. Biological Cybernetics. 1988;59:1-11.

7. Brody CD. Correlations without synchrony. Neural Comput. 1999;11:1537-51.

8. Nowak L, Bullier J. Cross-correlograms for neuronal spike trains. Different typesof temporal correlation in neocortex, their origin and significance. Amsterdam: harwood Academic Publishers; 2000.

9. Pereda E, Quiroga RQ, Bhattacharya J. Nonlinear multivariate analysis of neurophysiological signals. Progress in Neurobiology. 2005;77:1-37.

10. Gerstein GL, Aertsen AM. Representation of cooperative firing activity among simultaneously recorded neurons. J Neurophysiol. 1985 December;54(6):1513-28.

11. Aertsen A, Gerstein GL. Evaluation of neuronal conectivity: sensitivity of cross-correlation. Brain Research. 1985;340:341-54.

12. Aertsen A, Gerstein GL, Habib MK, Plam G. Dynamics of neuronal firing correlation: modulation of effective connectivity. Journal of Neurophysiology. 1989;61:900-17.

13. Gerstein GL. Cross-correlation measures of unresolved multi-neuron recordings. J Neurosci Methods. 2000 July 7;100(1-2):41-51.

14. Segev R, Baruchi I, Hulata E, Ben-Jacob E. Hidden Neuronal Correlations in Cultured Networks. Physical Review Letters. 2004;92(11):118102.

15. Beggs JM, Plenz D. Neuronal avalanches in neocortical circuits. J Neurosci. 2003 December 12;23(35):11167-77.

16. Beggs JM, Plenz D. Neuronal avalanches are diverse and precise activity patterns that are stable for many hours in cortical slice cultures. J Neurosci. 2004 June 6;24(22):5216-29.

17. Brown EN, Kass RE, Mitra PP. Multiple neural spike train data analysis: state-of-the-art and future challenges. Nature Neuroscience. 2004;7(5):456-61.

18. Shahaf G, Marom S. Learning in Networks of Cortical Neurons. The Journal of Neuroscience. 2001 November 15, 2001;21(22):8782-8.

19. Tateno T, Jimbo Y, Robinson HP. Spatio-temporal cholinergic modulation in cultured networks of rat cortical neurons: spontaneous activity. Neuroscience. 2005;134(2):425-37.

20. Madhavan RA, Chao ZC, Potter SM. Plasticity of recurring spatiotemporal activity patterns in cortical networks. Physical Biology. 2007;4:181-93.

21. Tateno T, Jimbo Y. Activity-dependent enhancement in the reliability of correlated spike timings in cultured cortical neurons. Biological Cybernetics. 1999;80:45-55.

22. Zaveri H, Williams W, Sackellares J, Beydoun A, Duckrow R, Spencer S. Measuring the coherence of interacrania electroencephalograms. Clinical Neurophysiology. 1999;110:1717-25.

23. Albo Z, Di Prisco GV, Chen Y, Rangarajan G, Truccolo W, Feng J, et al. Is partial coherence a viable technique for identifying generators of neural oscillations? Biol Cybern. 2004 May;90(5):318-26.

24. Gersch W, Goddard GV. Epileptic Focus Location:spectral analysis method. Science. 1970;169(701-702).

25. Albo Z, Viana Di Prisco G, Chen Y, Rangarajan G, Truccolo WA, Feng J, et al. Is partial coherence a viable technique for identifying generators of neural oscillations? Biological Cybernetics. 2004;90:318-26.

26. Bressler S, Coppola R, Nakamura R. Episodic multiregional cortical coherence at multiple frequencies during visual task performance. Nature. 1993;366:153-6.

27. Dahlhaus R, Eichler M, Sandkuhler J. Identification of synaptic connections in neural ensembles by graphical models. Journal of Neuroscience Methods. 1997;77:93-107.

28. Liberati D, Cursi M, Locatelli T, Comi G, Cerutti S. Total and partial coherence analysis of spontansous and evoked EEG by means of multi-variable autoregressive processing. Med Biol Eng Comput. 1997;35:124-30.

29. Sun F, Miller L, D'Espisito M, New Author. Measuring interregional functional connectivity using coherence and partial coherence analyses of fMRI data. Neuroimage. 2004;21:647-58.

30. Rosenberg JR, Halliday DM, Breeze P, Conway BA. Identification of patterns of neuronal connectivity -- partial spectra, partial coherence, and neuronal interactions. Journal of Neuroscience Methods. 1998;83(1):57-72.

31. Ding M, Chen Y, Bressler SL, New Author, New Author. Handbook of Time Series Analysis. In: Timmer, Schelter, Winderhalder, editors. Granger Causality: Basic Theory and Application to Neuroscience. New York: Wiley; 2007.

32. Borst A, Theunissen F. Information theory and neural coding. Nature Neuroscience. 1999;2(11):947-57.

33. Buracas G, Zador A, DeWeese M, Albright T. Efficient Discrimination of Temporal Patterns by Motion Sensitive Neurons in the Primate Visual Cortex. Neuron. 1998;20:959-69.

34. London M, Schreibman A, Hausser M, Larkum M, Sevev I. The information efficacy of a synapse. Nature Neuroscience. 2002;5(4):332-40.

35. Rieke F, Warland D, de Ruyter van Steveninck R, Bialek W. Spikes: Exploring the Neural Code. Cambridge, Massachusetts: MIT Press; 1997.

36. Brillinger DR, Villa AEP. Assessing connections in networks of biological neurons. In: Brillinger DR, Fernholz LT, Morgenthaler S, editors. The Practice of Data Analysis: Essays in Honor of John W Tukey. Princeton, NJ: Princeton University Press; 1997. p. 77-92.

37. Brillinger DR. Nerve Cell Spike Train Data Analysis: A Progression of Technique. Journal of the American Statistical Association. 1992;87(418):260-1.

38. Okatan M, Wilson MA, Brown EN. Analysing Functional Conectivity Using a Network Likelihood Model of Ensemble Neural Spiking Activity. Neural Computation. 2005;17:1927-61.

39. Bernasconi C, von Stein A, Chiang C, Konig P. Bi-directional interactions between visual areas in the awake behaving cat. Neuroreport. 2000 March 3;11(4):689-92.

40. Sanchez JC, Mareci TH, Norman WM, Principe JC, Ditto WL, Carney PR. Evolving into epilepsy: Multiscale electrophysiological analysis and imaging in an animal model. Exp Neurol. 2006 March;198(1):31-47.

41. Kaminski M, Blinowska K, Szelenberger W. Topographic analysis of coherence and propogation of EEG activity during sleep and wakefulness. Electroencephalography and clinical neurophysiology. 1997;102:216-27.

42. Ginter J, Blinowska K, Kaminski M, Kus R. Propagation of brain electrical activity during real and imagined motor task by directed transfer function. Proceedings of the 2nd Internationals IEEE EMBS. 2005:5-8.

43. Schelter B, Winterhalder M, Eichler M, Peifer M, Hellwig B, Guschlbauer B, et al. Testing for directed influences among neural signals using partial directed coherence. Journal of Neuroscience Methods. 2006 April 4;152(1-2):210-9.

44. Kaminski M. Determination of transmission patterns in multichannel data. Philisophical Transactions of the Royal Society B. 2005;360:947-52.

45. Sameshima K, Baccala LA. Using partial directed coherence to describe neuronal ensemble interactions. J Neurosci Methods. 1999 December 12;94(1):93-103.

46. Fanselow EE, Sameshima K, Baccala LA, Nicolelis MAL. Thalamic bursting in rats during different awake behavioral states. Proceedings of the National Academy of Sciences. 2001 December 18, 2001;98(26):15330-5.

47. Eichler M. On the evaluation of information flow in multivariate systems by the directed transfer function. Biological Cybernetics. 2006;94:469-82.

48. Zhu L, Lai Y, Hoppensteadt FC, He J. Probing Changes in Neural Interaction During Adaptation. Neural Computation. 2003;15:2359-77.

49. Zhu L, Lai Y, Hoppensteadt FC, He J. Characterization of Neural Interaction During Learning and Adaptation from Spike-Train Data. Mathmatical Biosciences and Engineering. 2005;2(1):1-23.

50. Goebel R, Roebroeck A, Dae-Shik K, Formisano E. Investigating directed cortical interactions in time-resolved fMRI data using vector autoregressive modeling and Granger causality mapping. Magnetic Resonance Imaging. 2003;21:1251-61.

51. Sato JR, Junior EA, Takahashi DY, Felix MM, Brammer MJ, Morettin PA. A method to produce evolving functional connectivity maps during the course of an fMRI experiment using wavelet-based time-varying Granger causality. NeuroImage. 2006;31:187-96.

52. Kaminski M, Ding M, Truccolo WA, Bressler SL. Evaluating causal relations in neural systems: Granger causality directed transfer function and statistical assessment of significance. Biological Cybernetics. 2001 August;85(2):145-57.

53. Brovelli A, Ding M, Ledberg A, Chen Y, Nakamura R, Bressler SL. Beta Oscillations in a large-scale sersorimotor cortical network: Directional influences revealed by Granger Causality. Proceedings of the National Academy of Sciences. 2004;101(26):9849-54.

54. Chen Y, Bressler SL, Ding M. Frequency decomposition of conditional Granger causality and application to multivariate neural fielfd potential data. Journal of Neuroscience Methods. 2006;150:228-37.

55. Seth AK, Edelman GM. Distinguishing causal interactions in neural populations. Neural Comput. 2007 April;19(4):910-33.

56. Seth AK. Causal connectivity of evolved neural networks during behavior. Network-Computation in Neural Systems. 2005 March;16(1):35-54.

57. Wiener N. The Theory of Prediction. In: EF B, editor. Modern Mathmatics for Engineers, Series 1; 1956. p. Chapter 8.

58. Geweke JF. Measurement of Linear-Dependence and Feedback between Multiple Time-Series. Journal of the American Statistical Association. 1982;77(378):304-13.

59. Geweke JF. Measures of Conditional Linear Dependence and Feedback Between Time Series. Journal of the American Statistical Association. 1984;79(388):907-15.

60. Chen Y, Bressler SL, Ding M. Frequency decomposition of conditional Granger causality and application to multivariate neural field potential data. J Neurosci Methods. 2006 January 1;150(2):228-37.

61. Granger CWJ. Testing for Causality: A personal viewpoint. Journal of Economic Dynamics and Control 1980;2:329-52.

62. Seth AK, Granger CWJ. Granger Causality. Scholarpedia; 2007.

63. Jimbo Y, Kawana A, Parodi P, Torre V. The dynamics of neuronal culture of dissociated cortical neurons of neonatal rats. Biological Cybernetics. 2000;83:1-20.

64. Beggs JM, Plenz D. Neuronal Avalanches in Neocortical Circuits. The Journal of Neuroscience. 2003;23(35):11167-77.

65. Aertsen A, Gerstein GL, Habib MK, Plam G. Dynamics of neuronal firing correlation: modulation of "effective connectivity". Journal of Neurophysiology. 1989;61:900-17.

66. Chatfield C. The Analysis of Time Series an Introduction. 5 ed. Boca Raton, FL: Chapman & Hall; 1996.

67. Zhu L, Lai Y, Hoppensteadt FC, He J. Probing Changes in Neural Interaction During Adaptation. Neural Computation. 2003 October;15(10):2359-77.

68. Baccala LA, Sameshima K. Methods for Neural Ensemble Recordings. In: Nicolelis MAL, editor. Directed Coherence: A tool for exploring functional Interaction among brain structures: CRC Press; 1998.

69. Brovelli A, Ding MZ, Ledberg A, Chen YH, Nakamura R, Bressler SL. Beta oscillations in a large-scale sensorimotor cortical network: Directional influences revealed by Granger causality. Proceedings of the National Academy of Sciences of the United States of America. 2004 June 6;101(26):9849-54.

70. Sameshima K, Baccala LA, Ballester G, Valle AC, Timo-Iaria. Causality Analysis of rythmic activities of desynchronized sleep in the rat. Soc Neurosci Abstr. 1996;22(27).

71. Wolpaw JR, McFarland DJ. Control of a two-dimensional movement signal by a noninvasive brain-computer interface in humans. Proc Natl Acad Sci U S A. 2004;101(51):17849-54.

72. Hinrichs H, Heinze HJ, Schoenfeld MA. Causal visual interactions as revealed by an information theoretic measure and fMRI. NeuroImage. 2006 July 7;31(3):1051-60.

73. Sato JR, Amaro E, Takahashi DY, Felix MD, Brammer MJ, Morettin PA. A method to produce evolving functional connectivity maps during the course of an fMRI experiment using wavelet-based time-varying Granger causality. Neuroimage. 2006 May 5;31(1):187-96.

74. Brillinger DR, Villa AEP. The Practice of Data Analysis: Essays in Honor of John W. Tukey. In: Brillinger DR, Fernholz LT, Morgenthaler S, editors. Assessing connections in networks of biological neurons. Princeton, NJ: Princeton University Press; 1997. p. 77-92.

75. Izhikevich EM. Which Model to Use for Cortical Spiking Neurons? IEEE Transactions on Neural Networks. 2004;15(5):1063-70.

76. Kaminski M, Ding M, Truccolo WA, Bressler SL. Evaluating causal relations in neural systems: Granger causality directed transfer function and statistical assessment of significance. Biological Cybernetics. 2001;85:145-57.

77. Geweke JW. Measures of Conditional Linear Dependence and Feedback Between Time Series. Journal of the American Statistical Association. 1984;79(388):907-15.

78. Hodgkin AL, Huxley AF, Katz B. Ionic Currents underlying activity in the giant axon of the squid. Arch Sci Physiol. 1952;3(129-150).

79. Abeles M. Local Cortical Circuits. Berlin: Springer-Verlag; 1982.

80. Aertsen A, Diesmann M, Gewaltig MO, Grun S, Rotter S. Neural dynamics in cortical networks--precision of joint-spiking events. Novartis Found Symp. 2001;239:193-204; discussion -7, 34-40.

81. Wagenaar DA, Pine J, Potter SM. Searching for plasticity in dissociated cortical cultures on multi-electrode arrays. Journal of Negative Results in BioMedicine. 2006;5(16).

82. Natschlager T, Markram H, Maass W. Computer models and analysis tools for neural microcircuits. In: Kotter R, editor. Neurocience databases A practical Guide. Boston, MA: Kluwer Academic Publishers; 2003. p. 123-38.

83. Markram H, Lubke J, Frotscher M, Sakmann B. Regulation of synaptic efficacy by coincidence of postsynaptic APs and EPSPs. Science. 1997 Jan 10;275(5297):213-5.

84. Bi G, Poo M. Synaptic Modifications in ccultured hippocampal neurons: dependence on spike timing, synaptic strength, and postsynaptic cell type. Journal of Neuroscience. 1998;18:10464-72.

85. Gross GW, Rieske, E., Kreutzberg, G.W., and Meyer, A. A new fixed-array multielectrode system designed for long-term monitoring of extracellular single unit neuronal activity *in vitro*. Neuroscience Letters. 1977;6:101-5.

86. Pine J. Recording action potentials from cultured neurons with extracellular microcircuit electrodes. Journal of Neuroscience Methods. 1980:19-31.

87. Thomas CA, Springer PA, Loeb GE, Berwald-Netter Y, Okun LM. A miniature microelectrode array to monitor the bioelectric activity of cultured cells. Exp Cell Res. 1972;74:61-6.

88. Bi G, Poo M. Synaptic modification by correlated activity: Hebb's postulate revisited. Annu Rev Neurosci. 2001;24:139-66.

89. Marom S, Shahaf G. Development, learning and memory in large random networks of cortical neurons: lessons beyond anatomy. Q Rev Biophys. 2002;35(1):63-87.

90. Ruaro ME, Bonifazi P, Torre V. Toward the neurocomputer: image Processing and pattern recognition with neuronal cultures,. Biomedical Engineering, IEEE Transactions on. 2005;52(3):371-83.

91. Stenger DA, McKenna TM. Enabling Technologies for Cultured Neural Networks. San Diego, CA: Academic Press; 1994.

92. Advances in Network Electrophysiology: Using Multi-Electrode Arrays: Springer; 2006.

93. Hebb DO. The organization of behavior - a neuropsychological theory. New York: Wiley; 1949.

94. Eichler M, Dahlhaus R, Sandkuhler J. Partial correlation analysis for the identification of synaptic connections. Biol Cybern. 2003;89:289-302.

95. Schneidman E, Berry MJ, Segev R, Bialek W. Weak pairwise correlations imply strongly correlated network states in a neural population. Nature. 2006;440(7087):1007-12.

96. Schelter B, Winterhalder M, Eichler M, Peifer M, Hellwig B, Guschlbauer B, et al. Testing for directed influences among neural signals using partial directed coherence. Journal of Neuroscience Methods. 2005;152:210-9.

97. Sakurai Y. How do cell assemblies encode information in the brain? Neuroscience and Behavioral Reviews. 1999;23:785-96.

98. Lelong IH, Petegneif V, Rebel G. Neural Cells Mature Faster of Polyetyleneimine Coated Plates Than on Polylysine Coated Plates. Journal of Neuroscience Research. 1992;32:562-8.

99. Banker, Goslin. Culturing Nerve Cells: MIT Press Cambridge, Massachusetts; 1998.

100. Kamioka H, Maeda E, Jimbo Y, Robinson HP, Kawana A. Spontaneous periodic synchronized bursting during formation of mature patterns of connections in cortical cultures. Neurosci Lett. 1996 Mar 15;206(2-3):109-12.

101. Habets AM, Van Dongen AM, Van Huizen F, Corner MA. Spontaneous neuronal firing patterns in fetal rat cortical networks during development in vitro: a quantitative analysis. Exp Brain Res. 1987;69(1):43-52.

102. Ichikawa M, Muramoto K, Kobayashi K, Kawahara M, Kuroda Y. Formation and maturation of synapses in primary cultures of rat cerebral cortical cells: an electron microscopic study. Neurosci Res. 1993 Feb;16(2):95-103.

103. Muramoto K, Ichikawa M, Kawahara M, Kobayashi K, Kuroda Y. Frequency of synchronous oscillations of neuronal activity increases during development and is correlated to the number of synapses in cultured cortical neuron networks. Neurosci Lett. 1993 Dec 12;163(2):163-5.

104. Wagenaar DA, Pine J, Potter SM. A extremely rich repertoire of bursting paterns during the development of cortical cultures. BMC Neuroscience. 2006;7:11.

105. Claverol-Tinture E, Pine J. Extracellular potentials in low-density dissociated neuronal culture. Journal of Neuroscience Methods. 2002;117:13-21.

106. Bliss TVP, Lomo T. Long-lasting potentiation of synaptic transmissioni in the dentate are of anaesthetized rabbit following stimulation the perforant path. Journal of Physiology (London). 1973;232:331-56.

107. Turrigiano GG, Nelson SB. Homeostatic plasticity in the developing nervous system. Nature Reviews Neuroscience. 2004;5:97-107.

108. Froemke RC, Dan Y. Spike-timing-dependent synaptic modification induced by natural spike trains. Nature. 2002 March 3;416(6879):433-8.

109. Song S, Miller K, Abbott L. Competitive Hebbian Learning through Spike-Timing-Dependent Synaptic Plasticity. Nature Neuroscience. 2000(3):919-26.

110. Shimono K, Taketani M, Brucher F, Kubota D, Colgin L, Robertson S, et al. Continuous two-dimensional current source density analyses of electrophysiological activity in hippocampal slices. NEUROCOMPUTING. 2001 June;38:899-905.

111. Novak JL, Wheeler WC. Recording from the Aplysia Abdominal Ganglion with a Planar Microelectrode Array. IEEE Transactions on Biomedical Engineering. 1986;BME-33(2):196-202.

112. Ding L, Worrell G, Lagerlund T, He B. Ictal source analysis: Localization and imaging of causal interactions in humans. Neuroimage. 2007;34:575-86.

113. Franaszczuk P, Bergey G, Kaminski M. Analysis of mesial temporal seizure onset and propogation using the directed transfer function method. Electroencephalogr Clin Neurophysiol. 1994;91:413-27.

114. Franaszczuk P, Blinowska K, Kowalczyk M. Th application of parametric multichannel spectral estimates in the study of electrical brain activity. Biological Cybernetics. 1985;51:239-47.

115. Wagenaar DA, Nadasdy Z, Potter SM. Persistent dynamic attractors in activity patterns of cultured neuronal networks. Physical Review E. 2006;73:051907/1-8.

116. Cadotte AJ. Polymeric Drug Delivery of Antiepileptic Drugs to Neuronal Networks Cultured on Multielectrode Arrays. Gainesville, FL: University of Florida; 2004.

117. Wagenaar DA, Pine J, Potter SM. Effective parameters for stimulation of dissociated cultures using multi-electrode arrays. J Neurosci Methods. 2004 September 9;138(1-2):27-37.

118. Bi GQ, Poo MM. Distributed synaptic modification in neural networks induced by patterned stimulation. Nature. 1999;401(6755):792-6.

119. Avoli M, D'Antuono M, Louvel J, Köhling R, Biagini G, Pumain R, et al. Network and pharmacological mechanisms leading to epileptiform synchronization in the limbic system in vitro. Prog Neurobiol. 2002 October;68(3):167-207.

120. Ang CW, Carlson GC, Coulter DA. Massive and specific dysregulation of direct cortical input to the hippocampus in temporal lobe epilepsy. J Neurosci. 2006 November 11;26(46):11850-6.

121. Lothman EW, Bertram EH, Kapur J, Stringer JL. Recurrent spontaneous hippocampal seizures in the rat as a chronic sequela to limbic status epilepticus. Epilepsy Res. 1990 July;6(2):110-8.

122. Kaneda K, Fujiwara-Tsukamoto Y, Isomura Y, Takada M. Region-specific modulation of electrically induced synchronous oscillations in the rat hippocampus and cerebral cortex. Neurosci Res. 2005 May;52(1):83-94.

123. Pikovsky A, Rosenblum M. Synchronization. Scholarpedia.com; 2007.

124. Bertram E, Zhang D, Mangan P, Fountain N, Rempe D. Functional anatomy of limbic epilepsy: a proposal for central synchronization of a diffusely hyperexcitable network. Epilepsy Res. 1998;32.

125. Netoff T, Schiff S. Decreased neuronal synchronization during experimental seizures. The Journal of Neuroscience. 2002;22(16):7297-307.

126. Geweke J. Measurement of linear dependence and feedback between multiple time series. Journal of the American Statistical Association. 1982;77:304-13.

BIOGRAPHICAL SKETCH

Alex Cadotte was born in Glens Falls, New York in 1976. He grew up in Franklin, Virginia where he graduated with honors from Franklin High School in 1994. He received his B.S. in chemical engineering from Virginia Tech in 1999. He worked in industry from 1999 to 2002 at companies such as General Electric and Corning Optical Fiber in Wilmington, NC. Alex moved to Gainesville, FL, in August of 2002 and completed a Master of Science in August of 2004 at the University of Florida in biomedical engineering specializing in tissue and neural engineering. Alex began his PhD at the University of Florida in August of 2005, advanced to candidacy in April of 2006, and completed a Doctorate in Philosophy on November 20, 2007 specializing in neural computation and neural engineering. This dissertation is a summary of the work done by Alex under the mentorship of his doctoral committee consisting of Dr. Thomas DeMarse (chair), Dr. Mingzhou Ding, Dr. Paul Carney, Dr. William Ditto, and Dr. Jason Frazier (external) in this field of study.